COMPUTATION OF BREAST PTOSIS FROM 3D SCANS OF TORSO

A Thesis
Presented to
the Faculty of the Department of Electrical and Computer Engineering
University of Houston

In Partial Fulfillment
of the Requirements for the Degree
Master of Science
in Electrical Engineering

by
Danni Li
August 2013

COMPUTATION OF BREAST PTOSIS FROM 3D SCANS OF TORSO

Danni Li

Approved:

Chair of the Committee
Dr. Fatima Merchant, Assistant Professor,
Department of Engineering Technology

Committee Members:

Dr. Badrinath Roysam, Professor,
Electrical and Computer Engineering

Dr. Haluk Ogmen, Professor,
Electrical and Computer Engineering

Dr. Gregory P. Reece, M.D., Professor,
Department of Plastic Surgery
The University of Texas MD Anderson
Cancer Center

Dr. Suresh K. Khator, Associate Dean,
Cullen College of Engineering

Dr. Badrinath Roysam, Professor and Chair,
Electrical and Computer Engineering

Acknowledgements

First and foremost, I would like to express my deepest gratitude to my advisor, Dr. Fatima Merchant, for her excellent guidance and continual support during the course of my degree. Working with her was a wonderful experience and her wise knowledge, constructive advice, and constant encouragement that she shared during my stay at the University of Houston has been invaluable. She contributed signicantly to both my research and my professional development. I would also like to thank my thesis committee, Dr. Badrinath Roysam, Dr. Haluk Ogmen, and Dr. Gregory P. Reece, for their encouragement, insightful comments, valuable discussions, and accessibility.

During my graduate studies at the University of Houston, I have had the pleasure of meeting many students, who have helped me directly or indirectly in completing my studies and have made it a rewarding experience. I owe my thanks to them. In particular, I would like to thank my lab mates, Lijuan Zhao, Katrina Chan, and Johnny Andon. I appreciate all the helpful discussions that I had with them. I also thank my close friends, who have become an inseparable part of my life.

I am deeply indebted to my parents and my husband who have been a constant source of support and love throughout this degree and my life. Thank you for everything.

COMPUTATION OF BREAST PTOSIS FROM 3D SCANS OF TORSO

An Abstract
of a
Thesis
Presented to
the Faculty of the Department of Electrical and Computer Engineering
University of Houston

In Partial Fulfillment
of the Requirements for the Degree
Master of Science
in Electrical Engineering

by
Danni Li
August 2013

Abstract

Ptosis is an important morphological parameter for characterizing breast aesthetics and is frequently used for assessing the outcome of breast surgery. It refers to the extent to which the nipple is lower than the terminus of the inframammary fold (the contour along which the inferior part of the breast attaches to the chest wall). Current clinical assessment of ptosis involves qualitative visualization by observers which is subject to inter- and intra-observer variability. Alternatively, ptosis can be measured anthropometrically from the patient or from clinical photographs, but these methods are error prone. As stereophotography is now finding its niche in clinical breast surgery, in this study we investigated and evaluated the utility of three-dimensional (3D) features such as surface curvature, coronal projection and surface normal for the assessment of breast ptosis using 3D scans of the torso. Experimental results suggest that 3D features are successful for objectively categorizing breast ptosis with high accuracy and precision.

Table of Contents

List of Figures

List of Tables

Chapter 1

Introduction

Approximately 232,000 new cases of breast cancer are expected to be diagnosed among women in 2013 according to the National Cancer Institute (NCI) [1]. Presently, advances in screening technology enable the detection of breast cancer at an early stage, when treatment is more effective, and the cure more likely. Breast reconstruction (BR) surgery plays an important role in the breast cancer treatment process. Contemporary goals of breast treatment are not only limited to the cure, but also include maximizing the quality of life. Thus, BR surgery is critical to treatment, as it not only rebuilds the breast tissue that has been removed, but also aims to create a breast that is aesthetically satisfactory to the patient.

Breast aesthetics refer to the physical characteristics of the breast, such as shape, volume, ptosis, and symmetry [2] to name a few. The assessment of the cosmetic result, as an approach to evaluate one of the aspects of treatment quality, has become an essential part of breast cancer treatment. Nowadays, measures characterizing breast aesthetics are determined by (1) qualitative subjective assessment by human observers, (2) direct physical measurements (anthropometry), (3) computer aided measurements on clinical photographs (photogrammetry), and (4) computer aided measurements using three-dimensional (3D) images (stereophotogrammetry).

Subjective assessment of breast aesthetics is highly influenced by the observers' experience and may be biased based on his/her visual perception of breast aesthetics. This assessment is typically based on vaguely defined rating scales that are inherently subjective and qualitative. Substantial studies have reported low intra- and inter- observer agreement and reliability, primarily due to the lack of consistency in the manual perception and interpretation of aesthetic outcomes [3–5].

Anthropometry is a measurement performed directly on the patient's body using a measuring tape. Although it is a useful tool in quantifying the aesthetic outcomes, there are several pragmatic limitations. First of all, it is not only time consuming but also inconvenient for patients, making it impractical for routine use. More importantly, fundamental parameters such as breast projection is hard to evaluate because of the difficulty in making accurate measurements of curvature on the underlying chest wall, and the mobility of subcutaneous tissues. In addition, it is not feasible to make a large number of measurements on each subject. If a particular measurement does not prove valuable, one cannot retrospectively try a different one. To prove the validity of a specific measurement, studies across multiple institutions with multiple observers are needed, which are costly and labor intensive. Thus, direct anthropometry has limited utility in routine clinical practice and is not generally performed.

Photogrammetry is an alternative allowing indirect anthropometry on two-dimensional (2D) clinical photographs. In photogrammetry, digital images are typically displayed on a computer monitor, or conventional photographs are shown to observers for manually marking measurements. Photogrammetry is relatively more feasible and easy to implement since most medical institutions routinely take photographs for documentation purposes. However, photogrammetry has its drawbacks too. It cannot capture the 3D nature of the human torso. To get a complete view of the torso, a set of multiple photographs with the patient positioned at different angles have to be taken. Furthermore, accurate anatomic landmarks that are critical to obtaining reproducible assessment of aesthetic outcomes by photogrammetry may not be visible from 2D photographs. Some studies have also reported substantial observers' deviation for assessment from photographs, due to the lack of consistent guidelines for standard photography [6, 7].

To address limitations of photogrammetry, stereophotogrammetry, which involves measurements on 3D scans of torso, is being evaluated as an alternative method to assess breast aesthetics. 3D digital photography systems are capable of non-invasively generating precise images at high speeds. A single 3D image yields more information on breast appearance than multiple conventional 2D photographs. One 3D scan of the torso can be viewed from several different angles, which is impossible in 2D photogrammetry. They also enable objective determination of properties such as contour distance, surface area, volume, and surface curvature, which are not available from 2D images [8–10]. Thus, 3D imaging has tremendous potential for analysis of breast appearance.

Table 1.1: A preliminary comparison of measurements feasible for 2D and 3D photographs.

Features	**2D Photograph**	**3D Photograph**
Distance	Only straight-line distances can be measured from 2D photographs.	Contour/geodesic distances that follow the surface contour can be measured.
Area	Available with limited precision.	Can be accurately measured from a 3D torso image.
Volume	Can only be indirectly approximated with limited precision.	Can be accurately measured from a 3D torso image.
Surface curvature	2D radius of curvature measurements feasible.	3D surface curvature measurements available.
Surface normal	Planar surface normal measurements feasible.	3D surface normal available.

Ptosis is a measurement used for characterizing breast morphology that estimates the amount of sagging or drooping of the breast. It refers to the extent by which the nipple is lower than the inframammary fold (IMF), i.e., the lower breast contour along which the inferior part of the breast attaches to the chest wall. Regnault [11] was the first to classify ptosis into a four-grade scale based on qualitative criteria. Later, LaTrenta and Hoffman [12] added a quantitative strategy for measuring different grades. LaTrenta and Hoffman's classification facilitates objective analysis based on distance measurements on the patient. Kim *et al.* [13] proposed a quantitative and objective measurement of breast ptosis on 2D lateral and oblique views of clinical photographs.

Previous studies on breast ptosis measurements were all based either on subjective ratings, direct anthropometry or 2D photogrammetry. As discussed above, the intrinsic properties of a 2D image limits our ability to quantify 3D features, thereby affecting the analysis that can be performed. A simple comparison of the features available from 2D photographs with those from 3D stereophotographs is shown in Table 1.1, from which it is apparent that 3D stereophotogrammetry offers more features that can be potentially explored for quantitative assessment.

However, simply employing the techniques widely used on 2D ptosis assessment (e.g., based on vertical distance measurement) onto 3D images is suboptimal and many important features of 3D images will be under utilized. One important issue in measuring breast ptosis is that traditional ptosis ratings involves identification of fiducial points (such as the nipple and the terminus of the inframammary fold) on patients during anthropometry, or on photographs during 2D photogrammetry. However, the terminus of inframammary fold is often difficult to identify because it is vaguely defined and hard to distinguish [14]. Thus, an approach of measuring ptosis that excludes the identification of the terminus of the inframammary fold would provide robust performance and accurate results.

In this thesis, we explored features that can be computed from 3D images for measuring breast ptosis without predefining the terminus of inframammary fold. To achieve this, we first investigated Gaussian surface curvature, coronal projection and surface normal and generated template histograms for each feature. Second, we conducted leave-one-out cross-validation (LOOCV) on our data set to test the performance of each feature for classification. We evaluated the following 3D features, (1) Gaussian curvature of the surface mesh, (2) distribution of 3D points along coronal planes, (3) the Y component of the surface normal and, (4) all the combinations of these three features. Test results were compared to the ground truth (assessment of breast ptosis by an experienced surgeon). Our results show that the singular use of each of the three features, Gaussian surface curvature, coronal projection, and the Y component of the surface normal have an overall accuracy of 73%, 72%, and 77%, respectively. Whereas the combination of the three features has an overall accuracy of 78%.

This thesis is organized as follows: Chapter 2 presents background material on 3D surface imaging and existing commercial systems for the same. It also includes a brief description of the 3D Torso Image Database housing the images used in our study. In Chapter 3, related work on current assessment of breast aesthetics and breast ptosis is discussed. In Chapter 4, an algorithm for measuring ptosis using 3D features is described, and Chapter 5 presents the experimental results and discussion. Conclusion and some ideas for future work are presented in Chapter 6.

Chapter 2

Background

2.1 Image Acquisition

3D image acquisition systems are popular for clinical use since they provide minimal invasiveness, high capture speeds, good accuracy, and safety. 3D imaging provides accurate geometrical information on the human torso in conjunction with a 2D texture map overlaid on the surface for realistic rendering. Typically, data from 3D imaging systems consists of a point cloud from sampling the surface of the torso as shown in Figure 2.1. Each point has a x, y, and z position corresponding to the position in space obtained from a triangulation method, applied to images from multiple cameras with known geometries.

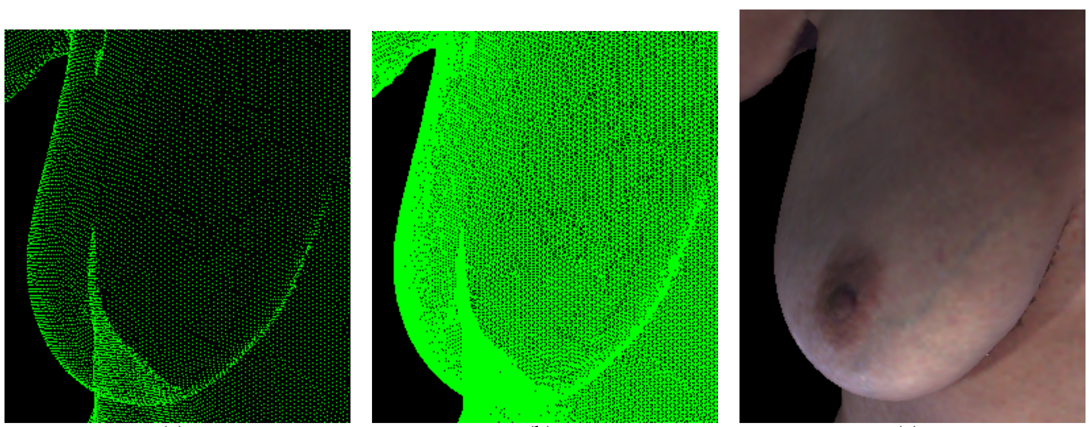

(a) (b) (c)

Figure 2.1: (a) Point cloud of 3D surface scan. (b) Triangular surface mesh. (c) 2D texture mapped onto the 3D triangular surface mesh.

2.2 Image Database

We have a database of 3D torso scans of patients, maintained by the Biomedical Informatics Laboratory (BMIL) at the University of Texas at Austin, TX. Each 3D image was captured at the University of Texas M. D. Anderson Cancer Center (MDACC), Houston ,TX. The database of images and related demographic information about each subject is hosted and managed by BMIL, and is accessible via a user-friendly web interface for data browsing, query and download. The number of images in the database is increasing as patients are enrolling into this study, and previously enrolled patients return for follow-up visits as the process of breast reconstruction procedure is implemented. An earlier model of the 3dMD imaging system, namely the DSP800; was used to capture the images of the first 40 patients, whereas the rest were acquired using the 3dMD Torso system (3dMD LLC, Atlanta, GA). The spatial resolution of scans from the DSP 800 is low ($\sim$15,000) when compared to that of the 3dMDTorso system ($\sim$75,000). The new system has improved geometrical accuracy and resolution.

2.3 Visualization Software

2.3.1 Commercial Software

Some of the popular commercial systems designed for plastic surgeons are Sulptor3D^{TM} from Canfield Clinical Systems (Fairfield, NJ), 3dMD Breast Analysis^{TM} and 3dMDVultus ^{TM} from 3dMD, LCC. (Atlanta, GA), and 3D Surgeon^{TM} from Genex Technologies Inc. (Kensington, MD). Most of these software packages enable a variety of surface path, angle, area and volume measurements.

2.3.2 University of Houston 3D Visualization Tool

Visualization is significant for image analysis, especially for quantitative analysis of 3D images, such as measurement of symmetry, ptosis, volume, etc. Various existing tools have been developed to perform different measurements. However, it is always beneficial to have a customized system according to our requirements and data. So we have developed a 3D visualization software for rendering, manipulation, alignment and analysis of 3D torso images. Our visualization tool i.e., BR software is shown in Figure 2.2.

The analysis modules allow computation of both distance (Euclidean and geodesic) and volume measurements. Currently the software supports the following features:

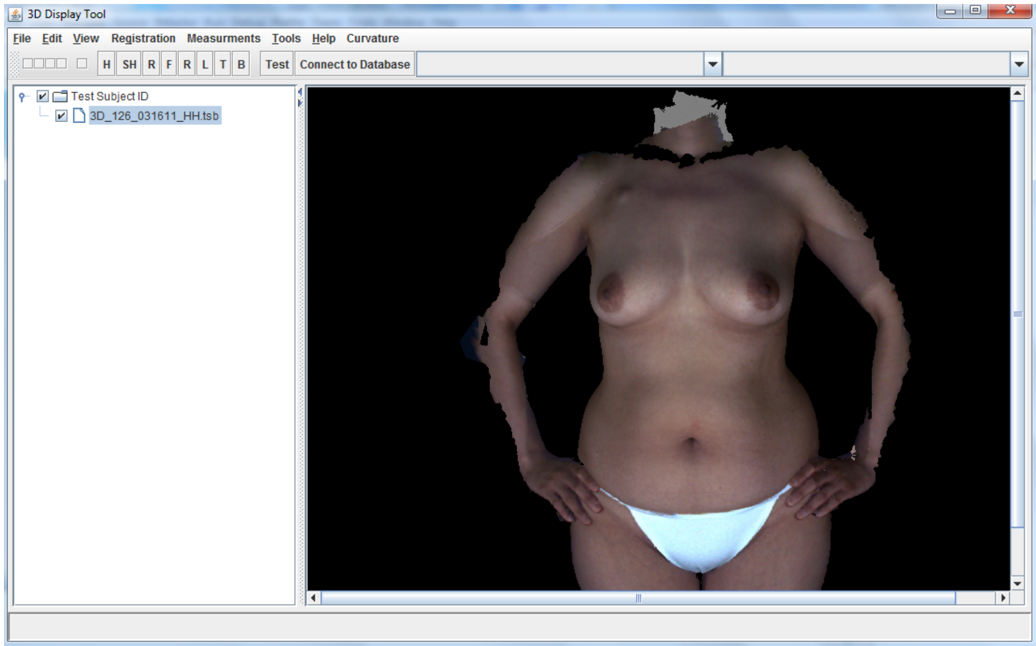

Figure 2.2: Screenshot of UH visualization tool.

- 3D image visualization and manipulation,
- Surface path measurements,
- Volume measurement,
- Curvature measurement,
- Recording and reporting of results,
- Connection to BMIL database of 3D Torso Images,
- 2D measurements.

The software was developed using Java, including JFC/Swing Application Program Interface (API) for dialogues, menus, and other basic user interface components. We have used XML configuration files for registration of functional code modules, which can be dynamically loaded by custom class loaders, yielding a very flexible plug-in capability. For 3D visualization we have used the Java 3D API, whereas the image representation and processing functionality is developed using the Java Advanced Imaging (JAI) API. Java 3D is a hierarchy of classes that serve as the interface to a sophisticated 3D graphics and sound-rendering system. It provides high-level constructs to create and manipulate 3D geometry, and to build the structure used to render that geometry.

Chapter 3

Related Work

In this chapter, relevant techniques for assessing breast aesthetics, especially for ptosis classification and measurement are discussed. We start with the description of a normal breast, and then define ptosis, its classification, and existing techniques for measuring ptosis. Two approaches are currently used for measuring ptosis: subjective and objective methods. We discuss both advantages and limitations of various approaches, with a focus on evaluation using two-dimensional (2D) versus three-dimensional (3D) data.

3.1 Normal Breast

Normally, the human breast is located between the second intercostal space and the sixth rib. In the primary or non-augmented breast, the ideal aesthetic nipple lies above the inframammary fold (IMF) and is located at the center of the breast gland in young females [11]. The IMF is defined as the natural boundary of the breast from below, i.e., the place where the breast and the chest meet. IMF is an important aesthetic landmark of the female breast, and plays an essential role in breast surgery, such as in ptosis classification [15–17].

When the volume of the breast is small and well supported by the skin envelope, no IMF is formed. As the breast volume increases and the breast is not supported well, the IMF can be visualized as the lower boundary of the breast, along the intersection of the breast with the chest wall. Normally, the nipple, skin, and breast gland follow the influence of gravity together. The distance of nipple to the IMF increases very little while the distance of the nipple to the clavicle elongates more.

3.2 Importance of Ptosis for Breast Reconstruction

Contemporary goals of surgery during breast cancer treatment are not only limited to cure, but also include restoration of breast aesthetics, to help patients improve body image and quality of life. Although current literature shows that the breast cancer survival is becoming more and more common, the aesthetic results of breast cancer treatment are poor in up to 15% of the cases [18]. Consequently, objective measurements of breast morphology are important for both surgeons and patients in setting up appropriate plans for pre-treatment and for evaluation of post-treatment outcomes.

Grewal *et al.* [19] followed up to a total number of 134 patients who underwent revisionary breast surgery in a 15-year period from 1994 to 2009. Their results suggest that ptosis is the most frequent reason (40% of the patients) for patients seeking revisionary surgery. Webster [20] also studied the relationship between patients' ptosis and their satisfactions after immediate partial breast reconstruction with local flaps and symmetrization of the contralateral breast. Strong correlations indicated that satisfaction was observed in patients with higher degree of ptosis who may better benefit from the combined techniques of immediate reconstruction and contralateral mammaplasty.

Ptosis plays an important role for surgeons evaluating breast surgical outcomes [3, 21, 22]. Bajaj *et al.* [23] used ptosis as a metric to facilitate the assessment of breast aesthetic changes during breast conservation therapy. Hauben [24] reported the relationship between breast ptosis, volume and size using the value of breast-areola-nipple proportion. Such analysis is important to plastic surgeons in planning breast reduction, augmentation, and reconstruction.

Ptosis is also an important factor in planning strategies of breast reconstruction surgery. Roehl *et al.* [25] showed that patients with different levels of ptosis require distinct strategies of breast reconstruction. For instance, youthful patients with round-shaped breast (without ptosis or with minor ptosis) may benefit from implant-based reconstructions, while breast rearrangement is usually ideal for large-breasted women with significant breast ptosis and/or asymmetry.

3.3 Classification of Breast Ptosis

Ptosis is a characteristic of breast morphology, which is routinely used to assess surgical outcomes in a variety of breast surgeries. It provides a measure for understanding patient requirements, informing consultants, and training future surgeons. Plastic surgeons use a classification system to categorize the degree of breast sagging, or ptosis. This classification system also helps surgeons determine what treatment option is the best for an individual based on the level of her breast ptosis.

A variety of classifications exist for ptosis, including Regnault (1976) [11], Lewis (1983) [26], Brink (1990) [27] and (1993) [28], LaTrenta and Hoffman (1994) [12], Kirwan (2002) [29], and de la Torre and Vasconez (2007) [30]. The classification of ptosis helps determine the type of surgery for mastopexy. The determination of whether to augment a breast, perform mastopexy, or to do a combination of both involves the physician discussing the pros and cons of each procedure with the patient and deciding on the most feasible procedure [31].

3.3.1 Regnault's Classification

Ptosis is usually classified according to the relative position of the nipple with respect to the IMF. Abnormal ptosis is identified when the nipple and inferior pole of the breast descend lower than the level of the terminus of the IMF [2]. Regnault [11] subjectively classified the ptosis grades, as shown in Figure 3.1.

- **Grade 0 (Normal breast)**: A normal breast has the nipple and parenchyma (glandular tissue and fat which compose the breast) sitting above the crease or the terminus of IMF.

- **Grade 1 (Minor ptosis)**: In first grade ptosis, the nipple lies at the level of the terminus of IMF and above the lowest contour of the breast.

- **Grade 2 (Moderate ptosis)**: In grade two ptosis, the breast exhibits sagging in which the nipple lies below the level of the terminus of IMF but remains above the lowest contour of the breast.

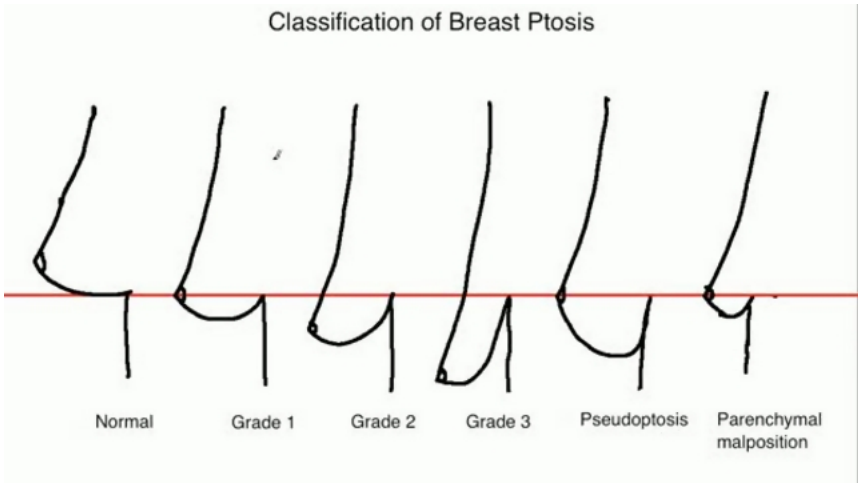

Figure 3.1: Regnault's classification of ptosis.

- **Grade 3 (Major ptosis)**: In grade three ptosis, the breast exhibits severe sagging in which the nipple lies well below the terminus of IMF and lies at the inferior contour of the breast.

In addition, Regnault also defined "Pseudoptosis" which is not true ptosis, or sagging, because the nipple lies above or at the level of the terminus of IMF. However, the majority of the breast parenchyma has descended below the level of the fold. Another condition is described as parenchymal maldistribution. The lower portion of the breast lacks fullness, and a higher terminus of the IMF is observed with a relatively short distance from the fold to the nipple. This is seen in conditions such as a tuberous breast. Pseudoptosis and parenchymal maldistribution are rare conditions and most clinical assessment systems typically only utilize the four-grade scale of ptosis (0-3).

3.3.2 Lewis's Classification

Lewis's [26] classification of breast ptosis is typically used for surgical classification as related to a pathological condition. It is defined as follows.

- Mildly ptotic breasts of adequate size, without hypertrophy.
- Mildly ptotic breast with atrophy.
- Mild to moderate ptosis with mild to moderate hypertrophy.

- Markedly ptotic breast with marked hypertrophy.
- Moderate or markedly ptotic breasts with adequate total breast bulk.
- Moderate or markedly ptotic breasts with inadequate total breast bulk.
- Mildly or moderately ptotic breasts with chronic cystic mastopathy.
- Breasts with marked ptosis or marked hypertrophy with cystic mastopathy.
- Asymmetry of the breasts (of significant degree).

3.3.3 Brink's Classification

Brink [27] classified ptosis similar to Regnault's classification as follows.

- **True ptosis**: The nipple-areola complex's relation to the IMF when the gland, skin, and nipple descend.
- **First-degree (minor) ptosis**: Nipple-areola complex at the IMF and above the breast contour (gland behind the nipple-areola complex).
- **Second-degree (moderate) ptosis**: Nipple-areola complex below the IMF but above the breast contour (gland behind the nipple-areola complex).
- **Third-degree (major) ptosis**: Nipple-areola complex below the IMF and below the breast contour (gland above the nipple-areola complex).

3.3.4 LaTrenta and Hoffman's Classification

In 1994, LaTrenta and Hoffman [12] presented a quantitative measurement on the vertical distance from the nipple to the terminus of IMF based on Regnault's classification. They quantified the classification using distance in centimeter metrics as follows.

- **First degree or minor ptosis**: nipple position lies within 1 cm of the level of the terminus of IMF.

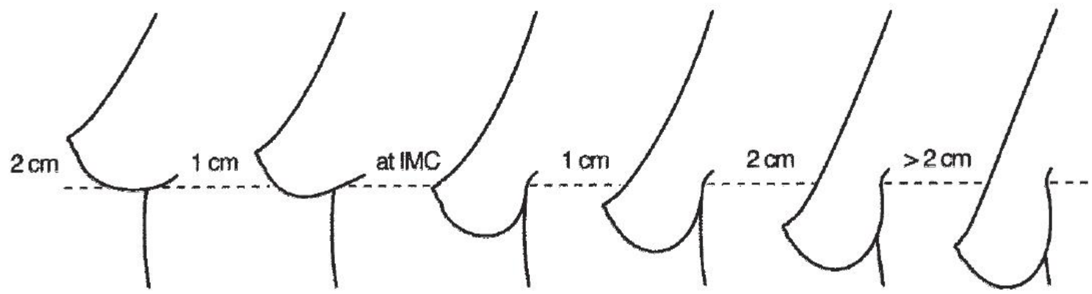

Figure 3.2: Kirwan's classification of ptosis from stage A to stage F.

- **Second degree or moderate ptosis**: nipple position lies 1-3 cm below the terminus of IMF.
- **Third degree or severe ptosis**: nipple position lies greater than 3 cm below the level of terminus of IMF and below the lower contour of the breast and skin envelope.
- **Pseudoptosis**: nipple position lies at or above the level of terminus of IMF with a loose "saggy" skin envelope, giving the impression of true ptosis.

3.3.5 Kirwan's Classification

Since the Regnault's classification is qualitative and subjective, it is ineffective for planning surgical strategies for different stages of ptosis. Kirwan [29] proposed a quantitative measurement based on the Regnault's classification. In a new system, 6 stages of breast ptosis covering a 5 cm distance are defined. Stages A to E progress in 1 cm increments as follows (Figure 3.2):

- **Stage A**: nipple position 2 cm above the IMF,
- **Stage B**: nipple position 1 cm above the IMF,
- **Stage C**: nipple position even with IMF,
- **Stage D**: nipple position 1 cm below the IMF,
- **Stage E**: nipple position 2 cm below the IMF.
- **Stage F**: nipple position greater than 2 cm below the IMF.

3.4 Subjective Assessment of Ptosis

Currently, subjective ptosis assessments are performed mainly via either patients self-evaluation, or by a single observer or a panel composed of observers and physicians based on printed photographs, digital images, or directly viewing patients [3, 4, 32, 33].

Although subjective ptosis assessment is still the most frequently used approach [34–36], it has been criticized for many limitations. First of all, the results are highly influenced by the observers' experience and may be biased based on his/her visual perception of breast aesthetics. Thus this approach has suffered from low reproducibility and variable internal and external consistency. For instance, Sneeuw *et al.* [5] reported higher intra-rater agreement between the nurse and the oncologist ($\kappa = 0.64$) but lower agreements between ratings by patients' and clinical observers' ratings ($\kappa < 0.10$) using the global 4-point scale. Sub-scales of the 4-point scale showed low to moderate reliability (κ = 0.24 - 0.40). In addition, Pezner *et al.* [3] also reported that experienced observers had higher agreements than novice observers. The scales showed low reliability ($\kappa = 0.31$). Consequently, data averaged from a panel rather than individual evaluator is often employed, but this approach is time and labor intensive. Oliveira *et al.* [37] reported this process can take months or even years when performed in a large number of patients with multiple observers.

Another major limitation of subjective ptosis assessment is that the lack of a standardized, explicit scale for analyzing cosmetic outcome also amortizes the precision of the process. A crude ordinal scale with four or five categories is imprecise for identifying individual aesthetic elements.

3.5 Objective Measurements of Ptosis

3.5.1 Anthropometry

As discussed before, anthropometry involves measurements made directly on the patient's body using a measuring tape. Penn's approach of defining nipple-to-sternal notch and mid-clavicle point distances based on 20 women with "aesthetically perfect" breasts has gained broad attention and has been adopted as normative [38]. Similarly, the distances between fiducial points were computed in 66 women in whom one-third had either breast hypertrophy, ptosis, or both [39]. Another study measured the symmetry of 40 patients by computing differences between the right and left breast and investigated the relationship between subjective rating and linear measurements [40]. A study of anthropometric breast measurement on 385 Turkish female students was also reported in [41].

“Aesthetically perfect breasts” was defined as a breast shape for which no aesthetic procedure would be indicated. The problem with this definition is that different surgeons have different notions when an aesthetic procedure is indicated. For example, in general, European Plastic Surgeons feel that what American Plastic Surgeons consider to be the “ideal breast” is really too large and they would recommend a breast reduction [42]. Typically, the outcomes of anthropometry analysis are highly correlated with other metrics of breasts. For instance, 22 linear measurements were designed and compared to the results of Penn [38] and Smith [39]. Nine of the measures were shown to have statistically significant correlation with breast volume [43]. Another study [24] computed the distances between the nipple and the border of the breast to calculate the nipple-areola-breast proportion and showed correlation of patient characteristics and breast proportions. Significant positive linear correlation between age and areola-breast proportion was reported and areola-nipple proportion was shown to be significantly larger in higher ptosis grades.

Furthermore, direct anthropometry is not only time consuming but inconvenient for patients, making it impractical for routine use. To prove the validity of a specific measurement, studies across multiple observers are needed, which are too costly. Also, the relationships between outcomes of anthropometry and subjective scales are unclear [44, 45]. For these reasons, anthropometry has limited utility in routine clinical practice.

3.5.2 2D Photogrammetry

Instead of direct measurement on a patient, 2D photogrammetry, wherein measures are made on a photograph (printed or digital), has shown great potential for quantifying breast ptosis. Photogrammetry is relatively more feasible and easy to implement since most medical institutions routinely take photographs for documentation purpose. In addition, it is also possible to make several measurements on the same photograph. Pezner *et al.* [3] reported an evaluation of a series of frontal views from 14 patients performed by 44 observers that challenged the value of subjective evaluations in terms of reproducibility. Prints produced from digital images, digital images displayed on a computer monitor, or conventional photographs are acceptable to observers for subjective assessment of breast aesthetics [46]. Furthermore, instead of obtaining subjective ratings based on photographs, several studies proposed objective measurements calculated on 2D photographs [13, 21, 47]. This approach has yielded encouraging results, but there are limitations to the reported studies.

Kim *et al.* [13] proposed an objective, quantitative measurement of breast ptosis based on the ratio of distances between fiducial points, such as nipple point, sternal notch, lateral terminus, and lowest visible point, manually identified in digitized/digital images of oblique and lateral clinical photographs (pre-operative). However, the automatic identification of fiducial points can be challenging to locate and manual interventions must be involved. Furthermore, outcomes of distance ratios which scale from 0 to 1 need to be accurately mapped on to the 4-point scale by Regnault to allow for easier interpretation of the outcome. The paper employed a simple linear regression approach to transform the distance ratios to subjective scales, based on two clinical groups of 52 patients and 10 patients, respectively. However, the distribution of the measurements in either group did not illustrate strong linear relationships between the 4-point Regnault's scale.

Lee *et al.* [48] proposed a novel quantitative measure of breast curvature based on catenary analysis. They compared the length, the area enclosed by the curve, and the curvature measure from the catenary curve to those from manual tracings of the breast contour. Likewise, the same procedure was applied to frontal photographs. This can be related with the difficulty of extracting robust features from lateral views. Studies [49] also showed that lateral and oblique views are difficult to standardize and the solution will be to move into 3D stereophotogrammetry. In our work, we employed curvature analysis to 3D photographs. since curvature is an intrinsic feature in 3D scans and is easy to extract and measure.

Furthermore, another limitation of 2D photogrammetry is that some anatomic landmarks may not be visible from the 2D photographs and the measurements cannot be obtained following the contours of the patient's body. To address this issue, clinical photographs of patients undergoing breast reconstruction are usually taken from five different views: anterior-posterior, right and left lateral, and right and left oblique views. An anteriorposterior (AP) view includes clavicles and shoulders above, pubis below, arms at side. An oblique view is taken with the patient turned 45 degree and with the distal arm back slightly. Lateral views are taken directly from the side such that only the proximal breast is visible [13]. Although there are lots of efforts on standardizing the procedure of the clinical photography [50–53], some studies continue to report substantial deviation for measurements on photographs, mainly due to the lack of consistency in the manual identification of anatomic landmarks [54]. Consistent guidelines for standard photography are critical to obtaining reproducible assessment of aesthetic outcomes by 2D photogrammetry.

3.5.3 3D Stereophotogrammetry

Compared with 2D photogrammetry, the advantage of 3D stereophotogrammetry is the ability to view the breast from a significant different number of angles in one photograph. Moreover, 3D images contain the geometric properties of the underlying surface, which enable objective quantitative measurements. Images obtained from 3D stereophotogrammetry techniques have more features such as surface area, volume and curvature, etc., which yield more information than traditional 2D photographs.

For breast surgery, 3D stereophotogrammetry is now being widely used in evaluation of differences in volume, surface area, shape, size, contour and symmetry [55–57]. Galdino *et al.* [57] investigated the use of clinical 3D imaging to determine quantitative information about the breast, such as volume or projection. They applied this approach to real cases, providing objective data on breast and surgical mammaplasty (especially augmentation mammaplasty). This helped surgeons better understand the factors that contribute to breast shape and influence surgical outcomes. A couple of limitations were also found, highlighted by patients with significant ptosis or suffering from obesity, which may introduce errors into the 3D data, making them unreliable.

Tepper *et al.* [58] used 3D images to enable an objective volumetric analysis of breasts prior to breast reconstruction. Surgeons are then capable of visualizing the size, shape, contour and symmetry of the breast with 3D breast models, as well as obtaining quantitative breast measurements and performing volumetric calculations. This application represents a significant advance from traditional approaches to aesthetic and reconstructive breast surgery.

Although 3D imaging has tremendous potentials for analysis of breast appearance, it does have limitations. High cost and the difficulty in using these methods on a daily basis prevents their widespread use. Additionally, it involves the long acquisition time needed to obtain the 3D model, which can result in time delay for the patient. During the period of acquisition any movement made by the patient can result in unreliable 3D models. Another important issue is related with automation of the existing commercial 3D software. Several features are still difficult to automatically identify thus manual interventions are needed. People still expect to have completely automated software with low cost, easily operated hardware and the public databases with which results can be compared.

Nevertheless, 3D stereophotogrammetry is evolving rapidly and may offer the most accurate way to quantify numerous elements of breast appearance and evaluate changes over time [59]. Further development of this technology might yield a variety of useful clinical tools to aid surgical planning, patient decision making, and outcomes analysis [60].

Chapter 4

Methodology

In this study, we first cropped the torso image into a single breast area as the region of interest (ROI), and then partitioned each breast into four quadrants according to the nipple position. We investigated a variety of 3D features and tested their feasibility for distinguishing the four-scale ptosis grades. 3D features including Gaussian surface curvature, distribution of points along coronal projection planes, and surface normal were evaluated and are discussed in detail in this chapter. We generated a histogram for each quadrant, and built template histograms for all the four grades for each feature to analyze their feasibility for classification. Finally, the Bhattacharyya distance for histogram matching was used to categorize the ptosis grade, followed by statistical measurements for analyzing the performance of the algorithm. Figure 4.1 shows the flowchart outlining the methods used to assess breast ptosis from 3D surface scans.

4.1 Image Cropping

As a first step, the torso data was cropped to remove the neck, arms, legs and belly, leaving only the upper portion of the torso encompassing the breast region as the ROI. The breast region was defined to enclose the whole breast area, as shown in Figure 4.2, with the height from sternal notch, which has the same level with mid-clavicle point, down to the lowest visible point of the breast. Horizontally, each breast was cropped individually from the mid-point of torso to the lateral point. The reason for cropping the torso image into individual breast regions is that the ptosis grade was determined individually for each breast, since a patient may either have asymmetric breasts, i.e., the two breasts may have different ptosis grades, or only one breast mount is intact due to whole or partial mastectomy.

Furthermore, each breast was divided into four quadrants with the nipple at the origin to capture any spatial morphological differences across four grades. The four quadrants were named

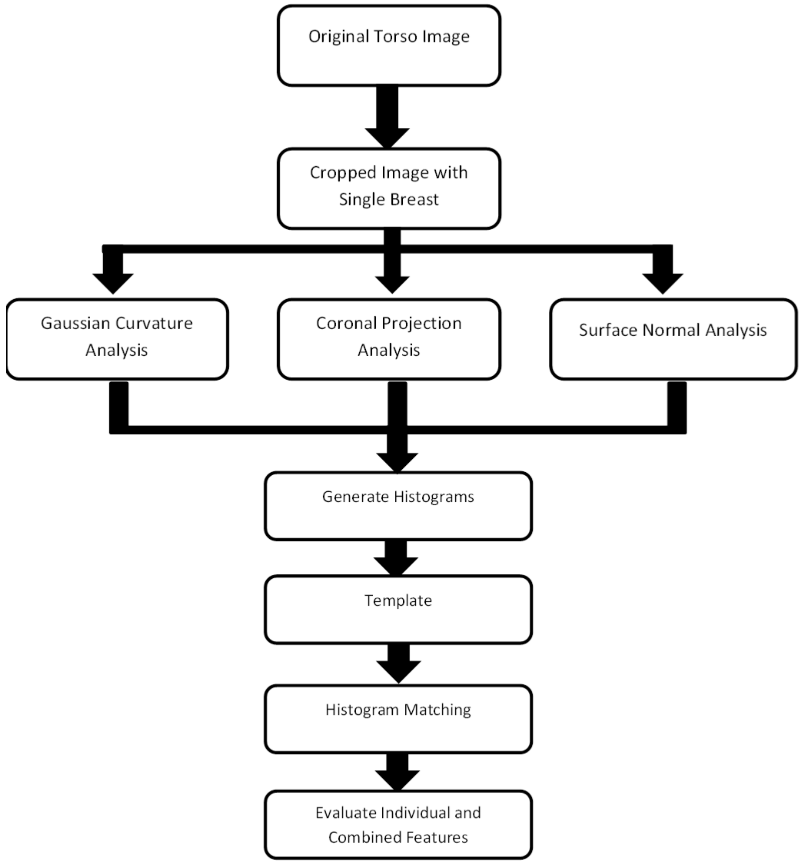

Figure 4.1: Flowchart of algorithm used to assess ptosis from 3D surface scans.

as *a*, *b*, *c*, and *d* clockwise as follows: the upper left quadrant *a*, the upper right quadrant *b*, the lower right quadrant *c*, and the lower left quadrant *d*. As ptosis grade increases, the nipple moves downward, and the shape of the breast within each quadrant as well as the distribution of points in each quadrant changes across the four grades.

4.2 Curvature Analysis

One major advantage of stereophotogrammetry is that it can represent the natural 3D morphology of the torso. Surface curvature measures how fast a curve is changing in direction for a given vertex in 3D space. Surface curvature analysis can be used to highlight the shape of the underlying 3D surface, thus it plays an important role in ptosis classification. We used a toolbox developed by Gabriel Peyre [61] based on the algorithms proposed by Cohen-Steiner et al. [62, 63]

(a) (b) (c)

Figure 4.2: A sample image with the neck and arms cropped, extending from the sternal notch to just below the IMF. (a) Cropped image with both breasts (b) Cropped image for right breast (c) Cropped image for left breast.

to calculate surface curvature, which can be calculated as

$$T(v) = \frac{1}{|B|} \sum_{edges \;\; e} \beta(e)|e \cap B|\bar{e}\bar{e}^t, \tag{4.1}$$

where v is an arbitrary vertex on the mesh, $|B|$ is the surface area around v over which the tensor is estimated, $\beta(e)$ is the signed angle between the normals to the two oriented triangles incident to edge e (positive if convex, negative if concave), $|e \cap B|$ is the length of e within B (always between 0 and $|e|$), and $\bar{e}$ is a unit vector in the same direction as e in Figure 4.3. The tensor is evaluated at every vertex location v, for a neighborhood B that approximates a geodesic disk around this vertex. The two principal eigenvalues, k_{min} and k_{max} calculated for this tensor vector, are the estimates of principal curvatures at v.

Generally curvature values are very small, and it is hard to visualize subtle differences in curvature. Thus, for visualization, we extend the range to enable a better partitioning of region depending on similar curvature values. In our curvature mapping, we linearly mapped the curvature value onto a color map.

In addition to principle curvatures (k_{min} and k_{max}), Gaussian (K) curvature can be computed

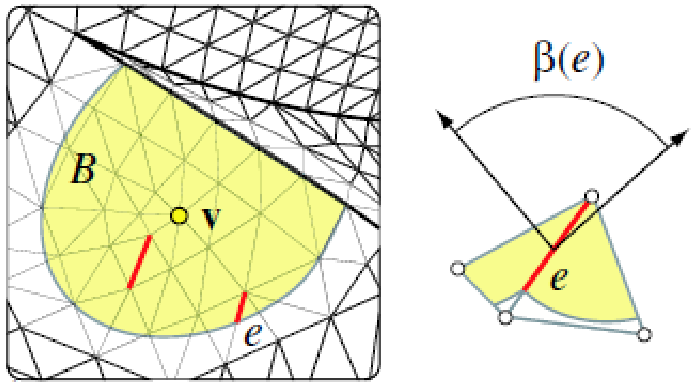

Figure 4.3: Estimation of curvature tensor.

by

$$K = k_{min} \cdot k_{max}. \tag{4.2}$$

The regions with $K>0$ are 'elliptic', while those with $K<0$ are 'hyperbolic', and those with $K = 0$ are either 'planar' or 'cylindrical'.

We partitioned each breast into four quadrants according to the nipple position as shown in Figure 4.4. Quadrants were named *a*, *b*, *c*, and *d* in the clockwise direction. The premise for using curvature analysis is that as the ptosis grade increases, the advanced drooping of the breast is reflected in the shape and consequently the curvature value of the surface. Differences in the curvature value are visually apparent on the superior and inferior parts of the breast, thus in this study our aim was to evaluate the feasibility of using curvature as a feature for distinguishing between different ptosis grades.

An ideal breast without ptosis is relatively symmetrical across the superior and inferior parts, whereas sagging of the breast gland with increasing ptosis results in a non-symmetric breast shape and consequent asymmetry in curvature is observed across the superior and inferior parts. When the ptosis grade increases, the underlying gland droops, leading to a larger area that is flatter (low curvature values) being observed within the regions of quadrant *a* and *b*. This indicates an increase in the number of points around curvature value equal to zero within these quadrants.

For inferior quadrants *c* and *d*, a reversal in the curvature value is observed. When the ptosis grade increases, the area of the lower two quadrants become smaller, and larger curvature values are

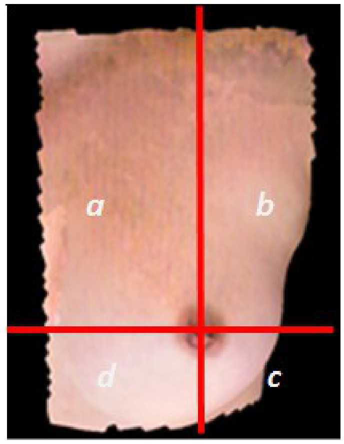

Figure 4.4: Breast divided into four quadrants: *a*, *b*, *c* and *d*.

apparent in the region below the IMF. Typically, a large portion of breast exhibits a convex shape, in other words positive curvature values, especially in the nipple-areola area, whereas below the IMF, the concave shape of the crease introduces negative curvature values. Thus over the inferior pole of the breast a smaller number of points with lower curvature values are observed. Figure 4.5 shows an example curvature map for both left and right breasts.

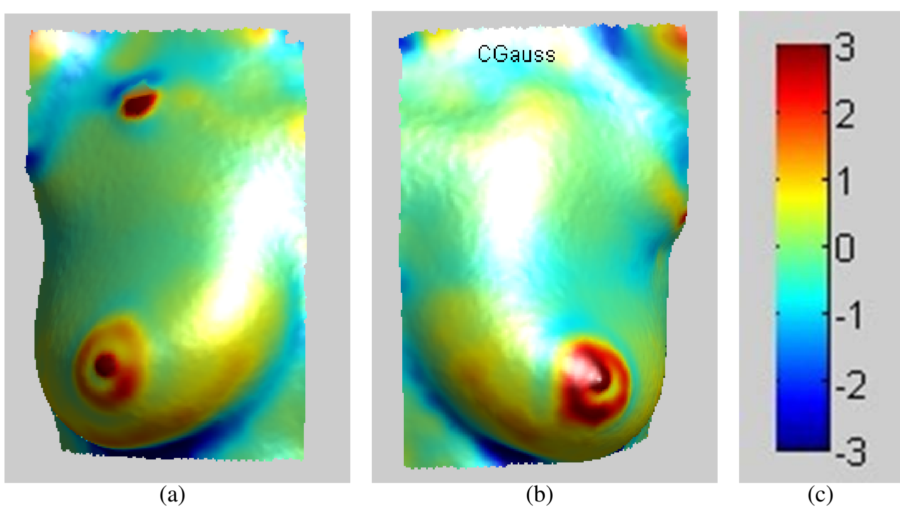

Figure 4.5: Gaussian curvature plot of the breasts exhibited in Figure 4.2.

In order to evaluate the feasibility of Gaussian curvature as a feature for classification, we generated histograms to visualize the distribution of curvature values in each of the 4 quadrants. Since the curvature values are very small and greater than 95% of the values are located within the range $\left[-6 \times 10^{-4}, 6 \times 10^{4}\right]$, we divided the range into 40 bins, with each bin holding a range of

1.5×10^{-5}, except that the first bin and the last bin are holding Gaussian curvatures smaller than -6×10^{-4} and greater than 6×10^{-4}, respectively. In order to standardize the size of the breast, the total number of points in each bin was normalized with respect to the total number of points in the ROI. Histograms of four quadrants were generated and concatenated in the order of *a*, *b*, *c*, and *d*. Finally, a histogram template for every grade was generated by taking the average of the histograms for all breasts within the specific grade, as shown in Figure 4.6 and Figure 4.7.

Figure 4.6 and Figure 4.7 shows the Gaussian curvature histogram templates for grade 0, 1, 2, and 3, respectively. Quadrant *a*, *b*, *c*, and *d* cover bins 1 - 40, 41 - 80, 81 - 120, and 121 - 160, respectively as shown in Table 4.1. Compared with grade 0 and grade 1, it is clear that the number of points acquired around curvature value zero (bin 19-20 and 69-70) are larger, indicating a flatter area. For quadrants *c* and *d*, the higher ptosis grade includes more low curvature values because of the drooping of the breast.

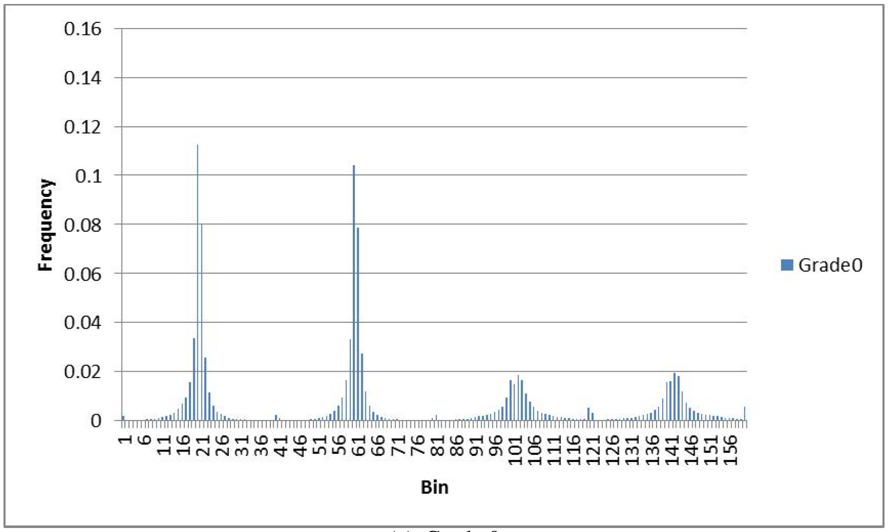

(a) Grade 0

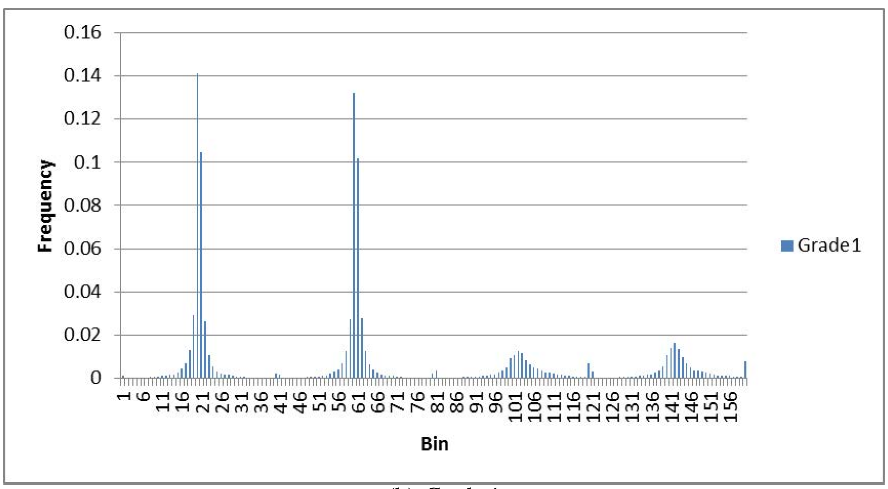

(b) Grade 1

Figure 4.6: Histogram templates of concatenated Gaussian curvature histograms including each of the four quadrants (*a*-*d*) for Grade 0 and Grade 1.

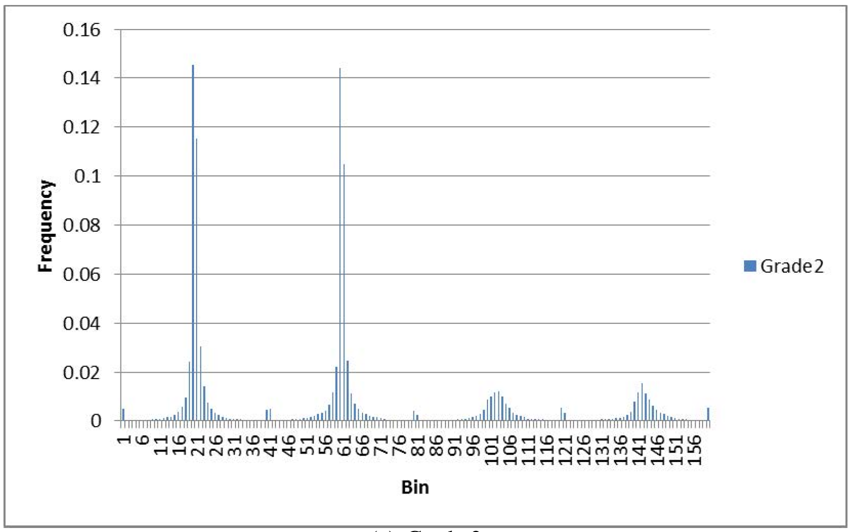

(a) Grade 2

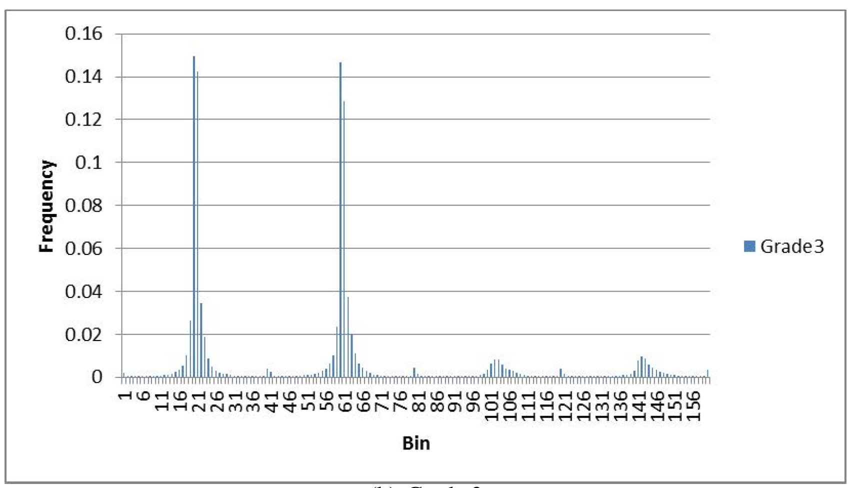

(b) Grade 3

Figure 4.7: Histogram templates of concatenated Gaussian curvature histograms including each of the four quadrants (*a*-*d*) for Grade 2 and Grade 3.

Table 4.1: The relationship between quadrants, bins, and the range of values for each bin for Gaussian curvature.

Quadrant *a*	**Quadrant *b***	**Quadrant *c***	**Quadrant *d***	**Range of Values**
1	41	81	121	$\left(-inf - 5.7 \times 10^{4}\right)$
2	42	82	122	$\left[-5.7 \times 10^{-4}, -5.4 \times 10^{4}\right)$
3	43	83	123	$\left[-5.4 \times 10^{-4}, -5.1 \times 10^{4}\right)$
4	44	84	124	$\left[-5.1 \times 10^{-4}, -4.8 \times 10^{4}\right)$
5	45	85	125	$\left[-4.8 \times 10^{-4}, -4.5 \times 10^{4}\right)$
6	46	86	126	$\left[-4.5 \times 10^{-4}, -4.2 \times 10^{4}\right)$
7	47	87	127	$\left[-4.2 \times 10^{-4}, -3.9 \times 10^{4}\right)$
8	48	88	128	$\left[-3.9 \times 10^{-4}, -3.6 \times 10^{4}\right)$
9	49	89	129	$\left[-3.6 \times 10^{-4}, -3.3 \times 10^{4}\right)$
10	50	90	130	$\left[-3.3 \times 10^{-4}, -3 \times 10^{4}\right)$
11	51	91	131	$\left[-3 \times 10^{-4}, -2.7 \times 10^{4}\right)$
12	52	92	132	$\left[-2.7 \times 10^{-4}, -2.4 \times 10^{4}\right)$
13	53	93	133	$\left[-2.4 \times 10^{-4}, -2.1 \times 10^{4}\right)$
14	54	94	134	$\left[-2.1 \times 10^{-4}, -1.8 \times 10^{4}\right)$
15	55	95	135	$\left[-1.8 \times 10^{-4}, -1.5 \times 10^{4}\right)$
16	56	96	136	$\left[-1.5 \times 10^{-4}, -1.2 \times 10^{4}\right)$
17	57	97	137	$\left[-1.2 \times 10^{-4}, -0.9 \times 10^{4}\right)$
18	58	98	138	$\left[-0.9 \times 10^{-4}, -0.6 \times 10^{4}\right)$
19	59	99	139	$\left[-0.6 \times 10^{-4}, -0.3 \times 10^{4}\right)$
20	60	100	140	$\left[-0.3 \times 10^{-4}, 0\right)$
21	61	101	141	$\left[0, 0.3 \times 10^{4}\right)$
22	62	102	142	$\left[0.3 \times 10^{-4}, 0.6 \times 10^{4}\right)$
23	63	103	143	$\left[0.6 \times 10^{-4}, 0.9 \times 10^{4}\right)$
24	64	104	144	$\left[0.9 \times 10^{-4}, 1.2 \times 10^{4}\right)$
25	65	105	145	$\left[1.2 \times 10^{-4}, 1.5 \times 10^{4}\right)$
26	66	106	146	$\left[1.5 \times 10^{-4}, 1.8 \times 10^{4}\right)$
27	67	107	147	$\left[1.8 \times 10^{-4}, 2.1 \times 10^{4}\right)$
28	68	108	148	$\left[2.1 \times 10^{-4}, 2.4 \times 10^{4}\right)$
29	69	109	149	$\left[2.4 \times 10^{-4}, 2.7 \times 10^{4}\right)$
30	70	110	150	$\left[2.7 \times 10^{-4}, 3 \times 10^{4}\right)$
31	71	111	151	$\left[3 \times 10^{-4}, 3.3 \times 10^{4}\right)$
32	72	112	152	$\left[3.3 \times 10^{-4}, 3.6 \times 10^{4}\right)$
33	73	113	153	$\left[3.6 \times 10^{-4}, 3.9 \times 10^{4}\right)$
34	74	114	154	$\left[3.9 \times 10^{-4}, 4.2 \times 10^{4}\right)$
35	75	115	155	$\left[4.2 \times 10^{-4}, 4.5 \times 10^{4}\right)$
36	76	116	156	$\left[4.5 \times 10^{-4}, 4.8 \times 10^{4}\right)$
37	77	117	157	$\left[4.8 \times 10^{-4}, 5.1 \times 10^{4}\right)$
38	78	118	158	$\left[5.1 \times 10^{-4}, 5.4 \times 10^{4}\right)$
39	79	119	159	$\left[5.4 \times 10^{-4}, 5.7 \times 10^{4}\right)$
40	80	120	160	$\left[5.7 \times 10^{-4}, inf\right)$

4.3 Coronal Projection Analysis

Coronal projection analysis is another feature which was evaluated in order to incorporate the effect of breast shape on ptosis grade. A coronal plane is a vertical plane that divides the breast into front and back sections. Coronal projection analysis includes the computation of the total number of points located on the surface mesh, between every two subsequent coronal planes, as shown is Figure 4.8.

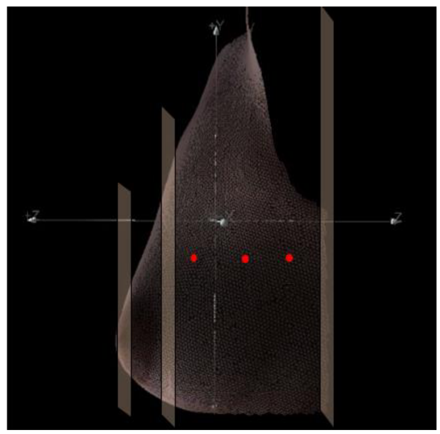

Figure 4.8: Coronal planes spaced at equal intervals placed depth-wise along the breast.

As mentioned before, each breast was divided into 4 quadrants according to the nipple position, the same set of coronal planes were applied on all the 4 quadrants. We put nine coronal planes spaced at equal intervals on the breast to cut it into ten vertical sections along the Z-axis. The depth of the breast was normalized along the Z-axis, such that the largest Z-coordinate is located at 1 and the smallest Z-coordinate is located at 0. Thus when we count the number of points within every two sequential coronal planes, each bin is collecting the same proportion of the whole breast for every breast. The number of points located on the surface mesh on or between every two sequential planes was counted and normalized by the total number of points in the ROI.

Because the point density for each subject is the same within ROI, we reasoned that the distribution of points on the torso represents the morphology of the breast. A coronal plane projection plot for each of the four grades is shown in Figure 4.9 to illustrate the idea. Contours shown in Figure 4.9 display points located on coronal planes with a interval of 6 mm. It is important to note

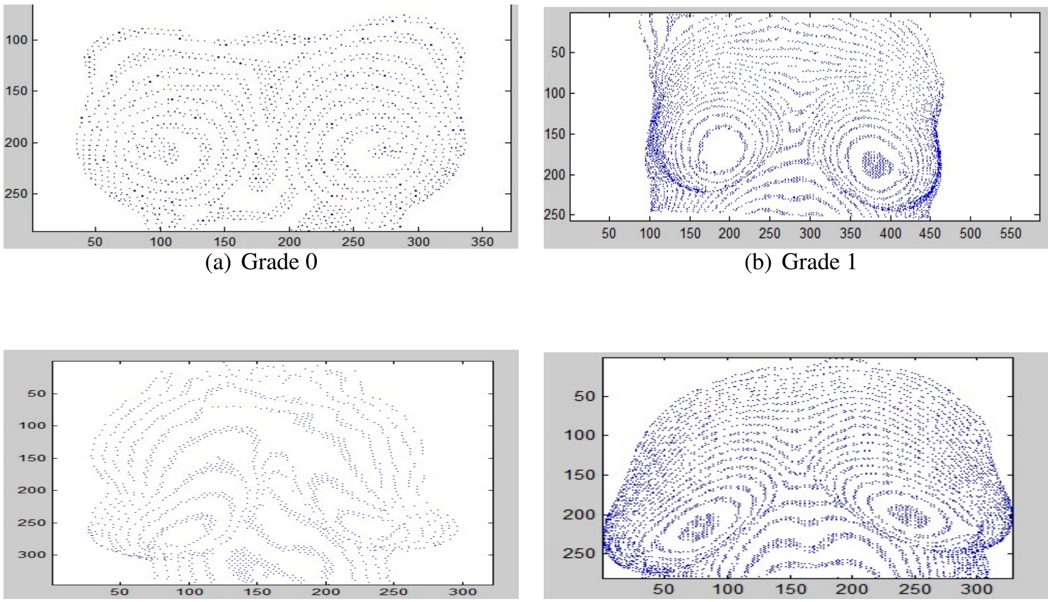

(a) Grade 0 (b) Grade 1

(c) Grade 2 (d) Grade 3

Figure 4.9: A simple coronal projection plot of Grade 0, 1, 2, and 3.

that nipple may or may not locate at the largest Z-value especially for highly ptotic breasts. For grade 0, which shows no ptosis, contours for superior and inferior part are circularly symmetric. With the ptosis grade increases, contours tend to be elliptical and non-symmetric.

Nine coronal planes cut the Z-axis into ten bins, with each bin representing a width of 0.1. Histograms for four quadrants were generated and concatenated in the order of *a*, *b*, *c*, and *d*. Histogram templates for each grade was generated by taking an average of all the breasts within each grade category.

Figure 4.10 and Figure 4.11 shows the coronal projection histogram templates of grade 0, 1, 2, and 3. Quadrant *a* covers bins 1 - 10, quadrant *b* covers bins 11 - 20, quadrant *c* covers bins 21 - 30, and quadrant *d* covers bins 31 - 40 as shown in Table 4.2. Within each quadrant, low bin numbers represent points closer to the chest, while higher bin numbers represent points closer to the nipple. With ptosis increases, nipple position moves downwards, the total number of point acquired in quadrants *a* and *b* increases, while that in quadrants *c* and *d* decreases.

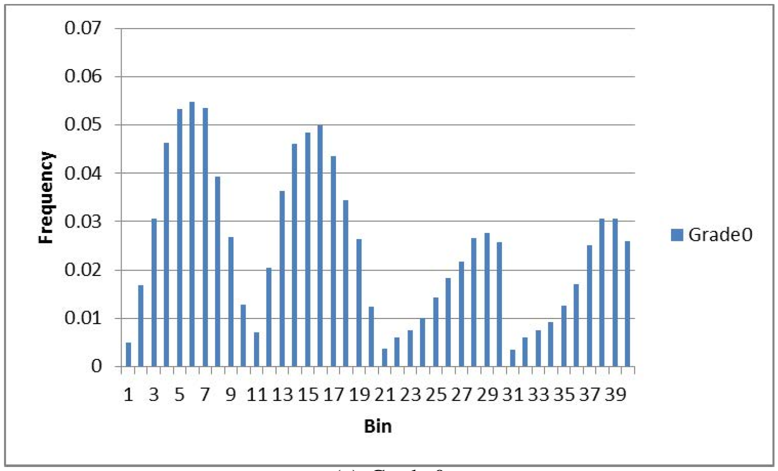

(a) Grade 0

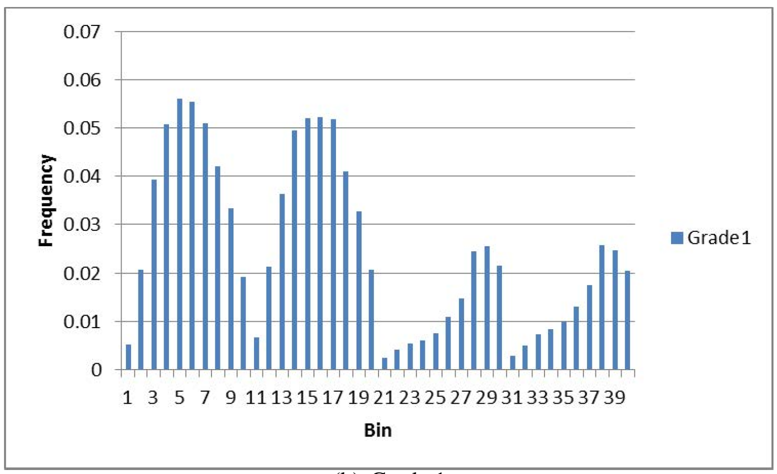

(b) Grade 1

Figure 4.10: Histogram templates for coronal plane analysis for grade 0 and grade 1. Four quadrants are concatenated in the order: a, b, c, and d.

Table 4.2: The relationship between quadrants, bins, and the range of values for each bin for coronal projection.

Quadrant *a*	**Quadrant *b***	**Quadrant *c***	**Quadrant *d***	**Range of Values**
1	11	21	31	$[0, 0.1)$
2	12	22	32	$[0.1, 0.2)$
3	13	23	33	$[0.2, 0.3)$
4	14	24	34	$[0.3, 0.4)$
5	15	25	35	$[0.4, 0.5)$
6	16	26	36	$[0.5, 0.6)$
7	17	27	37	$[0.6, 0.7)$
8	18	28	38	$[0.7, 0.8)$
9	19	29	39	$[0.8, 0.9)$
10	20	30	40	$[0.9, 1.0]$

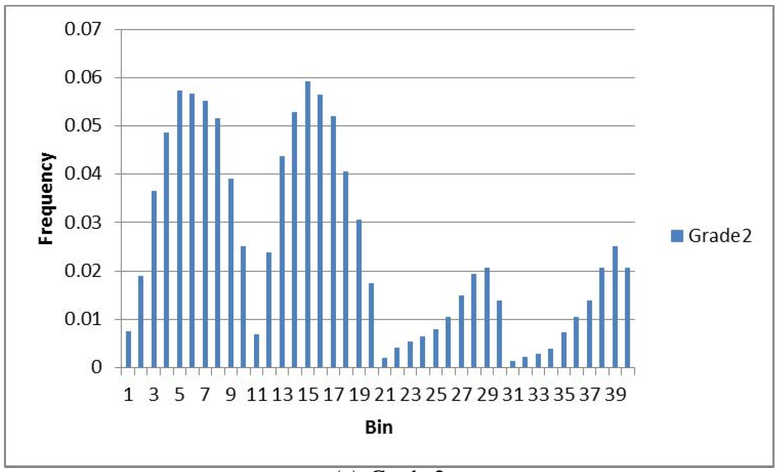

(a) Grade 2

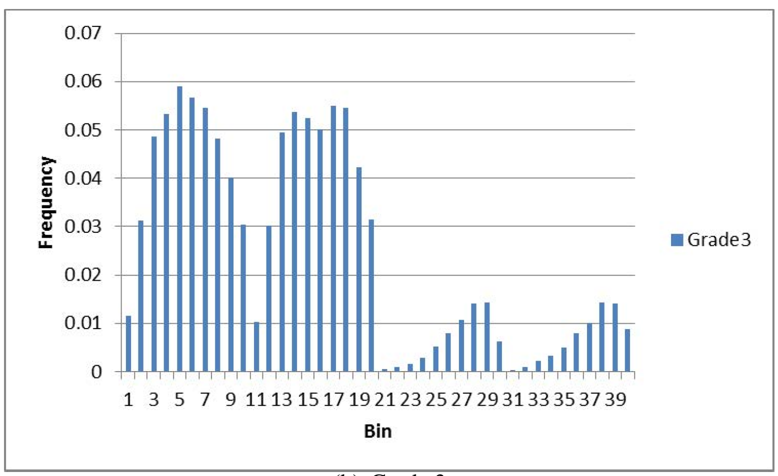

(b) Grade 3

Figure 4.11: Histogram templates for coronal plane analysis for grade 2 and grade 3. Four quadrants are concatenated in the order: *a*, *b*, *c*, and *d*.

4.4 Surface Normal Analysis

The 3D torso image is composed of the underlying triangular mesh, as shown in Figure 4.12(b). We calculated the surface normal for each triangle within the surface mesh.

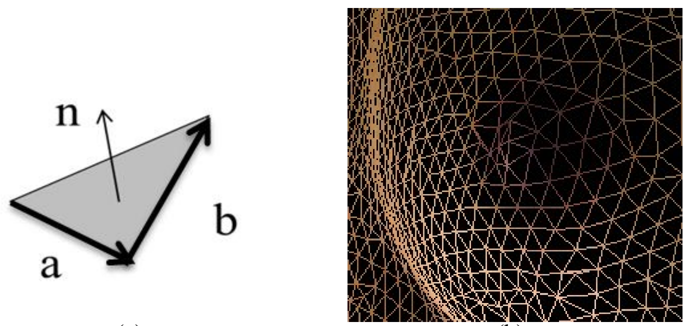

(a) (b)

Figure 4.12: (a) Calculation of surface normal (b) Triangular surface mesh.

Surface normal is computed as the cross product of two edges from the triangle, say $\vec{a}$ and $\vec{b}$, as shown in Figure 4.12(a). For each triangle, if $\vec{a}$ and $\vec{b}$ are two vectors denoting two sides of one triangle, the surface normal of this triangle is

$$\vec{n} = \vec{a} \cdot \vec{b}, \tag{4.3}$$

where $\vec{n}$ is the vector of surface normal including 3 components, n_x, n_y and n_z in the X, Y and Z directions, respectively. The surface normal is normalized so that the length is one, i.e., $|\vec{n}| = 1$.

n_x, which is the X component of the surface normal, represents the expanse of the breasts along X direction. n_z is the Z component of the surface normal, and it represents the degree of projection of the breast from the chest wall. n_x and n_z do not include information pertinent to breast ptosis. Thus, we eliminated these two components of the surface normal from further analysis.

n_y was estimated to be the most informative component among the three for the analysis of ptosis. It represents the orientation of a breast along the Y-axes, and hence indicates the amount of drooping of the breast. Since points on the superior part of the breast largely exhibit the positive values for n_y (corresponding to an upward orientation), while points on the inferior part are typically negative (downward orientation). The distribution of n_y can portray the orientation of the breast. Histograms for all quadrants were generated and concatenated in the order of *a*, *b*, *c*, and *d*. Histogram templates for each grade was generated by taking the average of all the breasts within the grade category. Figure 4.13 and Figure 4.14 show the histogram templates of the Y component of the surface normal for grades 0, 1, 2, and 3. Each quadrant covers 10 bins, in other words, quadrant *a*, *b*, *c*, and *d* covers bins 1 - 10, 11 - 20, 21 30, and 31 - 40, respectively as shown in Table 4.3. The Y component of the surface normal has a range of [-1, 1] so each bin possesses a range of 0.2. Within quadrant, lower bins represent negative surface normal values, while higher bins represent positive surface normal value.

Other than the difference in the number of points acquired in each quadrant, the histogram templates depict a transitional change in quadrant *c* and *d* across four grades. For grade 0, quadrants *c* and *d* have peaks in bin 25 and bin 35 respectively, which represents the range $[-0.2, 0]$. They were introduced by points around nipple area that were pointing straight forward rather than downward. As ptosis increase, points acquired in the range $[-0.2, 0]$ decrease because the nipple moves downward and the number of points acquired around nipple-areola area were pointing down, while lower negative y components becomes larger. For grade 3 patients, it is an extreme case with most of the points in quadrants *c* and *d* pointing downwards.

Table 4.3: The relationship between quadrants, bins, and the range of values for each bin for the Y component of the surface normal.

Quadrant *a*	**Quadrant *b***	**Quadrant *c***	**Quadrant *d***	**Range of Values**
1	11	21	31	$[-1.0, -0.8)$
2	12	22	32	$[-0.8, -0.6)$
3	13	23	33	$[-0.6, -0.4)$
4	14	24	34	$[-0.4, -0.2)$
5	15	25	35	$[-0.2, 0)$
6	16	26	36	$[0, 0.2)$
7	17	27	37	$[0.2, 0.4)$
8	18	28	38	$[0.4, 0.6)$
9	19	29	39	$[0.6, 0.8)$
10	20	30	40	$[0.8, 1.0]$

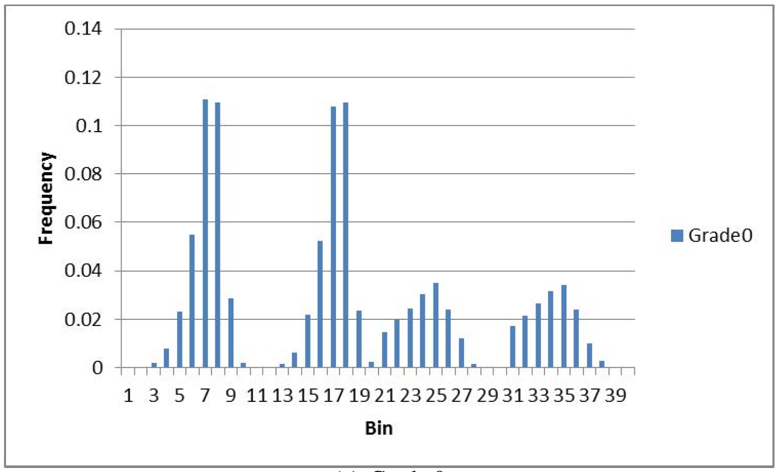

(a) Grade 0

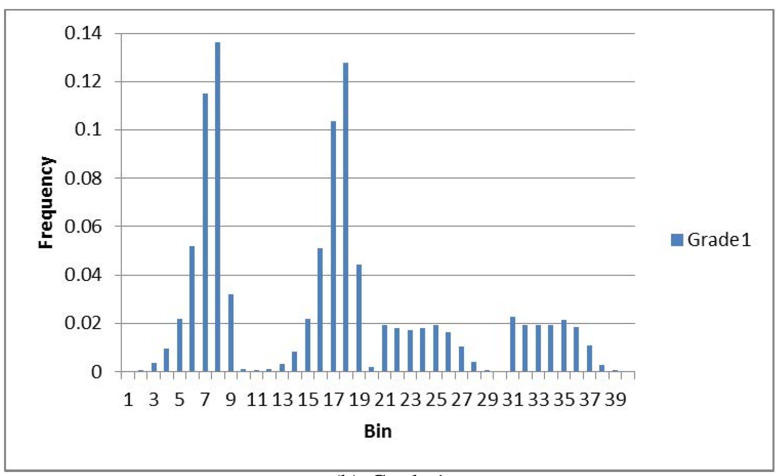

(b) Grade 1

Figure 4.13: Histogram templates for the Y component of the surface normal for grade 0 and grade 1. Four quadrants are concatenated in the order: *a*, *b*, *c*, and *d*.

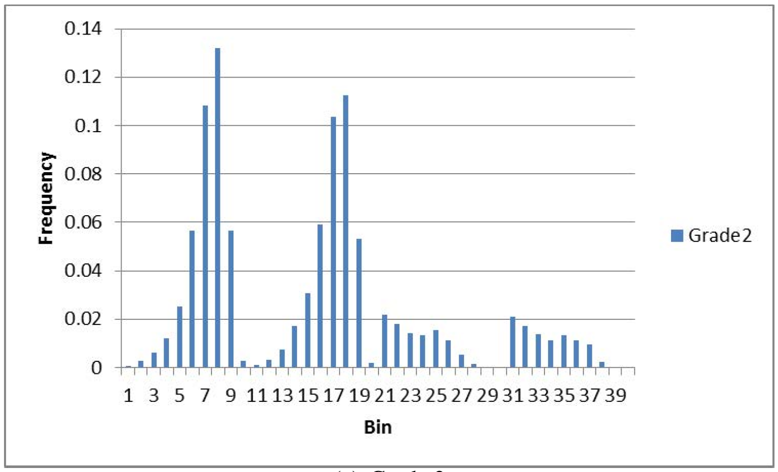

(a) Grade 2

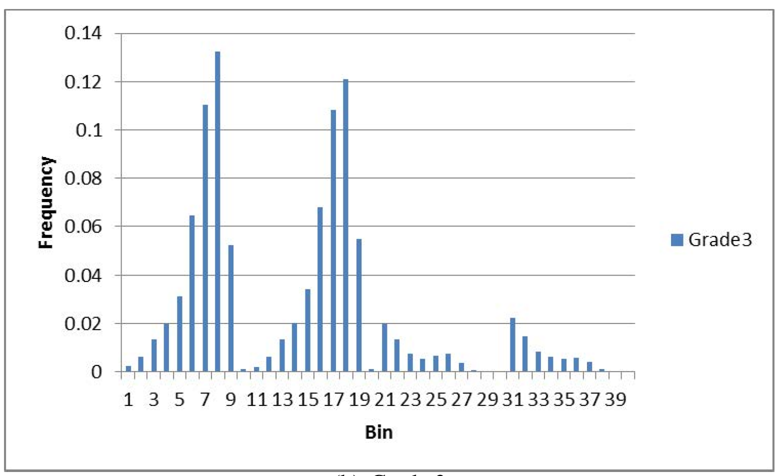

(b) Grade 3

Figure 4.14: Histogram templates for the Y component of the surface normal for grade 2 and grade 3. Four quadrants are concatenated in the order: *a*, *b*, *c*, and *d*.

4.5 Histogram Matching

The similarity of the histogram template and the test case was computed by measuring the Bhattacharyya distance [64]. The Bhattacharyya measure can be used to compare the similarity between two histograms as follows. H and R represent two normalized histograms such that

$$\sum_i H_i = 1, \tag{4.4}$$

and

$$\sum_i R_i = 1. \tag{4.5}$$

If we let H_i be the histogram value in bin i, and R_i the histogram value in the same bin. The Bhattacharyya distance can be computed using the following equation

$$d(H,R) = \sqrt{1 - \frac{1}{\sqrt{\bar{H}\bar{R}N^2}} \sum_i \sqrt{H_i \cdot R_i}}, \tag{4.6}$$

where

$$\bar{H} = \frac{1}{N} \sum_i H_i, \tag{4.7}$$

and N is the total number of bins in the histogram.

Bhattacharyya distance has the result in the scale of [0, 1]. $d(H,R) = 0$ or closer to 0 means a better match, whereas $d(H,R) = 1$ or closer to 1 means less similar. The rule of prediction is that by computing the Bhattacharyya distance between the test case's histogram and four template histograms, the grade with the smallest distance is set to be the predicted ptosis grade.

4.6 Statistical Measurement of Performance

In general, the result of classification can be characterized into four kinds: true positive (TP), false positive (FP), true negative (TN) and false negative (FN). Taking grade 0 for example:

- True positive means breasts of grade 0 were correctly identified as grade 0.

- False positive means breasts of other grades (grade1, 2, and 3) that were incorrectly identified as grade 0.

- True negative means breasts of other grades (grade1, 2, and 3) that were correctly rejected as not grade 0.

- False negative means breasts of grade 0 that were incorrectly identified as other grades (grade1, 2, or 3).

Several statistical analyses are made based on the following formula

- **Sensitivity** is defined as the proportion of actual positives which are correctly identified, with the formula,

$$Sensitivity = \frac{TP}{TP + FN}. \tag{4.8}$$

- **Specificity** is defined as the proportion of negatives which are correctly identified, with the formula,

$$Specificity = \frac{TN}{TN + FP}. \tag{4.9}$$

- **Accuracy** measures the proportion of true result, with the formula,

$$Accuracy = \frac{TP + TN}{TP + FP + TN + FN}. \tag{4.10}$$

- **Precision or Positive Prediction Value (PPV)** is defined as the proportion of the true positives against all the positive results, with the formula,

$$Precision = \frac{TP}{TP + FP}. \tag{4.11}$$

- **F score** is a measure of accuracy and can be defined as the harmonic mean of precision and sensitivity, with the formula,

$$FScore = \frac{2 \times precision \times sensitivity}{precision + sensitivity}. \tag{4.12}$$

Chapter 5

Results

In this chapter we evaluated the potential of different 3D features for categorizing breast ptosis from 3D scans of female torso. The performance of our algorithm on predicting ptosis grade is compared with the performance of subjective rating and the the performance of 2D photogrammetric measurement. The inter-observer variability between two surgeons' rating is also assessed.

5.1 Experimental Setup

In this study, we used patient images captured using the 3dMD Torso^{TM} system from 3dMD LLC, Atlanta Georgia. 3D torso images were taken from female patients undergoing breast reconstruction surgery at The University of Texas M. D. Anderson Cancer Center, Houston, TX. For this study, we selected subjects with the breast mount intact and the nipple clearly visible, This criteria was established because a clearly visible nipple was necessary for subjective rating which is visually estimated based on the level of nipple with respect to the terminus of the IMF. The data included a total of 247 breasts, from 170 patients and 5 commissioned volunteers. The sample subject population is a reflection of the distribution of the various grades observed in general population. Table 5.1 shows the number of breast for each grade in our data set. All subjects were chosen to have a complete torso image without holes or other artifacts such as missing data on the surface mesh, specifically over the region of interest encompassing the breast gland.

5.2 Evaluation of Objective Measurements on 3D Images

Cross-validation is a validation technique typically used to estimate the performance of a predictive model. For each round of cross-validation, the data set is partitioned into two complementary subsets, a training set and a test set. The training set is used to perform the analysis, while the test set is used to validate the analysis. Usually multiple rounds of cross-validation are performed on

Table 5.1: Distribution of the number of left and right breast for every grade.

Grade	**Left**	**Right**	**Total**
Grade 0	44	43	87
Grade 1	39	52	91
Grade 2	28	18	46
Grade 3	12	11	23

different partitions of the data set and the validation result is averaged over rounds. In leave-one-out cross-validation (LOOCV), as its name suggests, the data set is partitioned into two subsets: one sample data in the test set and the remaining samples in the training set. It is repeated such that all samples are used once as a test set.

We performed LOOCV on 203 breasts randomly chosen from the 247 breasts as the data set, including 71 breasts of grade 0, 75 breast of grade 1, 35 breasts of grade 2 and 22 breasts of grade 3. For each test, we picked one breast out of the data set as the test case, and the remaining 202 breasts formed the training set. Template histograms were generated for each grade by taking average of all the individual histograms for each breast image in the training data set. The cross-validation analysis was repeated for 203 times so that each subject image in the data set was used once as the validation data.

5.2.1 Gaussian Curvature

We evaluated the performance of using Gaussian curvature as a feature by conducting LOOCV on the 203 breast images. Table 5.2 and Table 5.3 show the cumulative and averaged confusion matrix for the LOOCV result. We used an experienced surgeon's rating as the ground truth. Table 5.4 shows the statistical measurements of the performance of Gaussian curvature. The statistical measures include sensitivity, specificity, accuracy, precision, F score and PPV for each grade. An overall performance was computed by averaging the values over all grades. Figure 5.1 shows the measurements for all grades and the overall performance.

Gaussian curvature provided a high accuracy on grade 3 of 83%. The accuracy of grade 0, grade 1 and grade 2 were 75%, 60% and 76%, which leads to an overall accuracy of 73%. Grade 3

Table 5.2: Cumulative confusion matrix for the result of LOOCV using Gaussian curvature as a feature.

	Predicted Grade			
Ground Truth	0	1	2	3
0	40	29	2	0
1	17	34	11	13
2	3	11	2	19
3	0	1	2	19

Table 5.3: Averaged confusion matrix for the result of LOOCV using Gaussian curvature as a feature.

	Predicted Grade			
Ground Truth	0	1	2	3
0	0.1970	0.1429	0.0099	0.0000
1	0.0837	0.1675	0.0542	0.0640
2	0.0148	0.0542	0.0099	0.0936
3	0.0000	0.0049	0.0099	0.0936

Table 5.4: Statistical measurements for the performance of Gaussian curvature as a feature.

	Grade 0	**Grade 1**	**Grade 2**	**Grade 3**	**Average**
Sensitivity	0.6667	0.4533	0.1176	0.3725	0.4025
Specificity	0.7832	0.6797	0.8226	0.9803	0.8165
Accuracy	0.7488	0.5961	0.7635	0.8276	0.7345
Precision	0.5634	0.4533	0.0571	0.8636	0.4845
F score	0.6107	0.4533	0.0769	0.5205	0.4155
PPV	0.5634	0.4533	0.0571	0.8636	0.4845

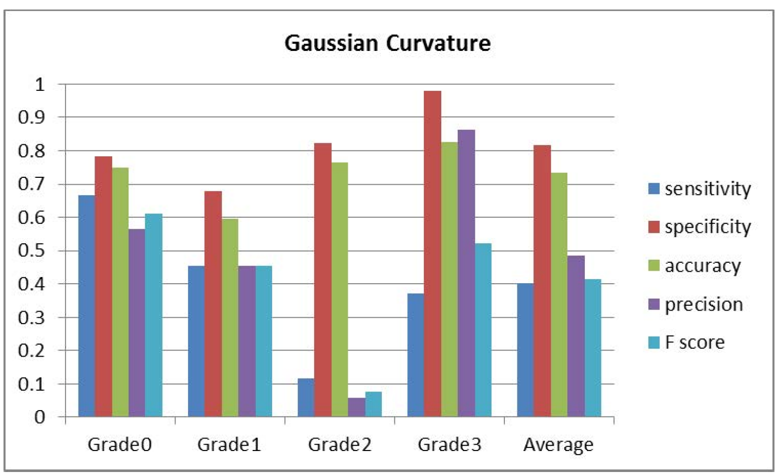

Figure 5.1: Statistical measurements for the performance of Gaussian curvature as a feature.

also showed a high precision rate of 86%, indicating that the performance of Gaussian curvature for predicting grade 3 is relatively good.

5.2.2 Coronal Projection

We evaluated the performance of using coronal projection as a feature by conducting LOOCV on the same 203 breast images. Table 5.5 and Table 5.6 show the cumulative and averaged confusion matrix, respectively for the LOOCV result. We used an experienced surgeon's rating as the ground truth. Table 5.7 shows the statistical measurements of the performance of coronal projection. An overall performance was computed by averaging the values over all grades. Figure 5.2 shows the statistical measurements for all grades and the overall performance.

Table 5.5: Cumulative confusion matrix for the result of LOOCV using coronal projection as a feature.

	Predicted Grade			
Ground Truth	0	1	2	3
0	25	23	23	0
1	4	35	32	4
2	1	7	19	8
3	0	2	8	12

Table 5.6: Averaged confusion matrix for the result of LOOCV using coronal projection as a feature.

	Predicted Grade			
Ground Truth	0	1	2	3
0	0.1232	0.1133	0.1133	0.0000
1	0.0197	0.1724	0.1576	0.0197
2	0.0049	0.0345	0.0936	0.0394
3	0.0000	0.0099	0.0394	0.0591

Table 5.7: Statistical measurements for the performance of coronal projection as a feature.

	Grade 0	**Grade 1**	**Grade 2**	**Grade 3**	**Average**
Sensitivity	0.8333	0.5224	0.2317	0.5000	0.5219
Specificity	0.7341	0.7059	0.8678	0.9441	0.8130
Accuracy	0.7488	0.6453	0.6108	0.8916	0.7241
Precision	0.3521	0.4667	0.5429	0.5455	0.4768
F score	0.4950	0.4930	0.3248	0.5217	0.4586
PPV	0.3521	0.4667	0.5429	0.5455	0.4768

Coronal projection provided a high accuracy on grade 3 of 89% and precision rate of 55%, with the accuracy for other grades falling in the range of 60%-75%. The overall accuracy was determined to be 72% with a precision of 48%.

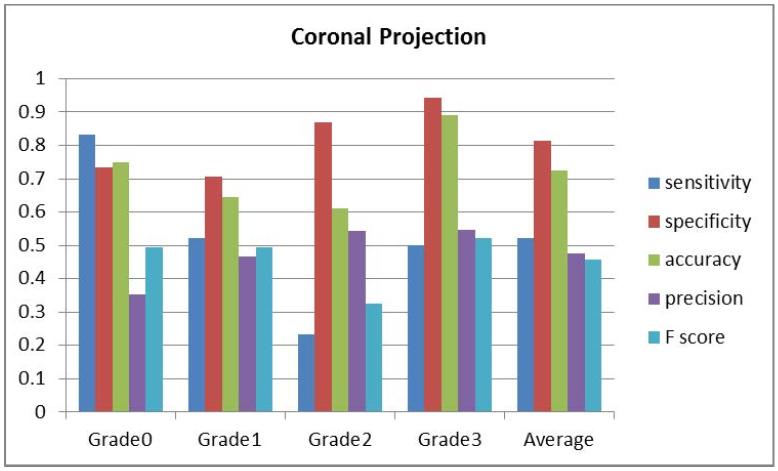

Figure 5.2: Statistical measurements for the performance of coronal projection as a feature.

5.2.3 Surface Normal

We evaluated the performance of using the Y component of the surface normal as a feature by conducting LOOCV on the same 203 breast images. Table 5.8 and Table 5.9 show the cumulative and averaged confusion matrix, respectively for the result. Table 5.10 shows the statistical measurements of the performance of the Y component of the surface normal. An overall performance was computed by averaging the values over all the grades. Figure 5.3 shows the statistical measurements for all grades and the overall performance.

Table 5.8: Cumulated confusion matrix for the result of LOOCV using the Y component of the surface normal as a feature.

	Predicted Grade			
Ground Truth	0	1	2	3
0	57	9	5	0
1	29	32	10	4
2	2	18	6	9
3	0	0	8	14

Table 5.9: Averaged confusion matrix for the result of LOOCV using the Y component of the surface normal as a feature.

	Predicted Grade			
Ground Truth	0	1	2	3
0	0.2808	0.0443	0.0246	0.0000
1	0.1429	0.1576	0.0493	0.0197
2	0.0099	0.0887	0.0296	0.0443
3	0.0000	0.0000	0.0394	0.0690

Table 5.10: Statistical measurements for the performance of the Y component of the surface normal as a feature.

	Grade 0	**Grade 1**	**Grade 2**	**Grade 3**	**Average**
Sensitivity	0.6477	0.5424	0.2069	0.5185	0.4789
Specificity	0.8783	0.7014	0.8333	0.9545	0.8419
Accuracy	0.7783	0.6552	0.7438	0.8966	0.7685
Precision	0.8028	0.4267	0.1714	0.6364	0.5093
F score	0.7170	0.4776	0.1875	0.5714	0.4884
PPV	0.8028	0.4267	0.1714	0.6364	0.5093

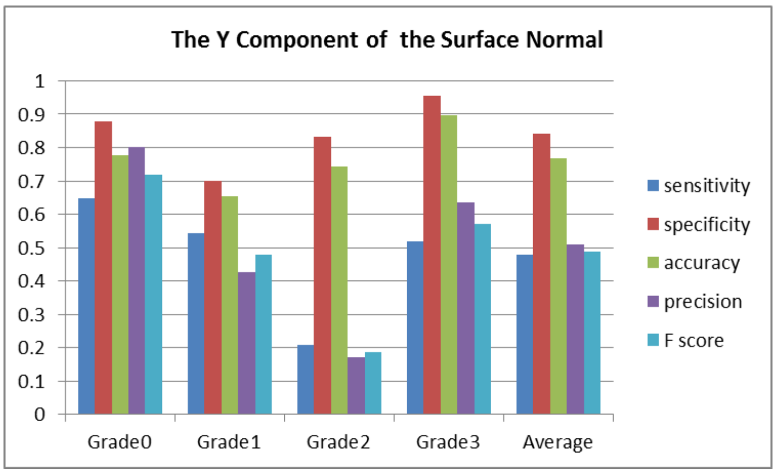

Figure 5.3: Statistical measurements for the performance of the Y component of the surface normal as a feature.

The Y component of the surface normal provided a good accuracy of 77% on grade 0, 65% on grade 1, 74% on grade 2 and 90% on grade 3, and had an overall accuracy of 77%. Grade 0 and grade 3 also had a high precision rate of 80% and 64%. This suggests that the Y component of surface normal is a relatively strong feature for predicting grade 0 and 3.

5.2.4 Combination of Features

We next evaluated the potential of different combinations of features to determine which combination, if any, allows improved classification. Gaussian curvature, coronal projection, or surface normal, independently do not provide high accuracy and precision for all four grades, but have the potential of identify ptosis on specific grades, i.e. Gaussian curvature and the Y component of the surface normal have a good performance on predicting Grade 0 and grade 3, while coronal projection provided the best performance on predicting grade 2. Thus, we evaluated the effect of combining features for prediction of the ptosis grade. Concatenation of individual templates was done to facilitate the evaluation of various combinations of features.

5.2.4.1 Gaussian Curvature and Coronal Projection

We evaluated the combination of Gaussian curvature and coronal projection as features. A normalized and concatenated template of Gaussian curvature and coronal projection was generated for each grade. LOOCV was performed on the same 203 breast images. Table 5.11 and Table 5.12 show the cumulative and average confusion matrix, respectively for the result. Table 5.13 shows the statistical measurements of the performance. An overall performance was computed by averaging all four grades. Figure 5.4 shows the statistical measurements for all grades and the overall performance.

Table 5.11: Cumulative confusion matrix for the result of LOOCV using Gaussian curvature and coronal projection as features.

	Predicted Grade			
Ground Truth	0	1	2	3
0	33	22	16	0
1	13	29	25	8
2	2	7	16	10
3	0	0	3	19

Table 5.12: Averaged confusion matrix for the result of LOOCV using Gaussian curvature and coronal projection as features.

	Predicted Grade			
Ground Truth	0	1	2	3
0	0.1626	0.1084	0.0788	0.0000
1	0.0640	0.1429	0.1232	0.0394
2	0.0099	0.0345	0.0788	0.0493
3	0.0000	0.0000	0.0148	0.0936

5.2.4.2 Gaussian Curvature and the Y Component of the Surface Normal

We evaluated the combination of Gaussian curvature and the Y component of surface normal as features. A normalized and concatenated template of Gaussian curvature and the Y component

Table 5.13: Statistical measurements for the performance of Gaussian curvature and Coronal projection as features.

	Grade 0	**Grade 1**	**Grade 2**	**Grade 3**	**Average**
Sensitivity	0.6875	0.5000	0.2667	0.5135	0.4919
Specificity	0.7548	0.6828	0.8671	0.9819	0.8217
Accuracy	0.7389	0.6305	0.6897	0.8966	0.7389
Precision	0.4648	0.3867	0.4571	0.8636	0.5431
F score	0.5546	0.4361	0.3368	0.6441	0.4929
PPV	0.4648	0.3867	0.4571	0.8636	0.5431

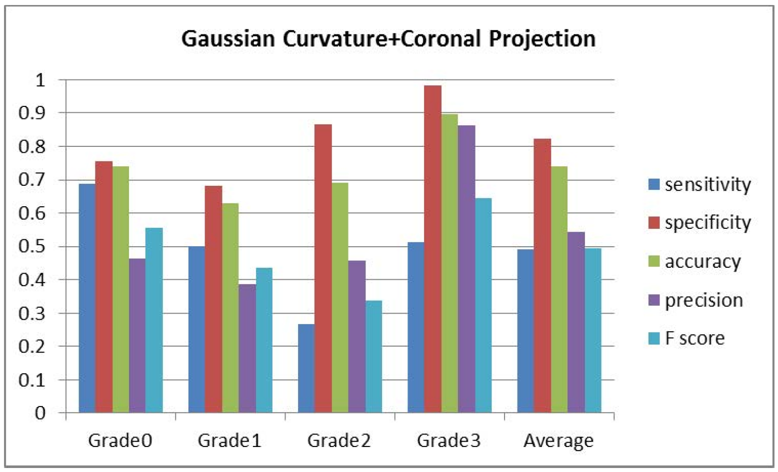

Figure 5.4: Statistical measurements for the performance of Gaussian curvature and Coronal Projection as features.

of surface normal was generated for each grade. LOOCV was performed on the same 203 breast images. Table 5.14 and Table 5.15 show the cumulative and averaged confusion matrix, respectively for the result. The statistical measurements are presented in Table 5.16 and plotted in Figure 5.5.

Table 5.14: Cumulative confusion matrix for the result of LOOCV using Gaussian curvature and the Y component of the surface normal as features.

	Predicted Grade			
Ground Truth	0	1	2	3
0	54	15	2	0
1	21	36	11	7
2	3	14	6	12
3	0	0	7	15

Table 5.15: Averaged confusion matrix for the result of LOOCV using Gaussian curvature and the Y component of the surface normal as features.

	Predicted Grade			
Ground Truth	0	1	2	3
0	0.2660	0.0739	0.0099	0.0000
1	0.1034	0.1773	0.0542	0.0345
2	0.0148	0.0690	0.0296	0.0591
3	0.0000	0.0000	0.0345	0.0739

Table 5.16: Statistical measurements for the performance of Gaussian curvature and the Y component of the surface normal as features.

	Grade 0	**Grade 1**	**Grade 2**	**Grade 3**	**Average**
Sensitivity	0.6923	0.5538	0.2308	0.4412	0.4795
Specificity	0.8640	0.7174	0.8362	0.9586	0.8440
Accuracy	0.7980	0.6650	0.7586	0.8719	0.7734
Precision	0.7606	0.4800	0.1714	0.6818	0.5235
F score	0.7248	0.5143	0.1967	0.5357	0.4929
PPV	0.7606	0.4800	0.1714	0.6818	0.5235

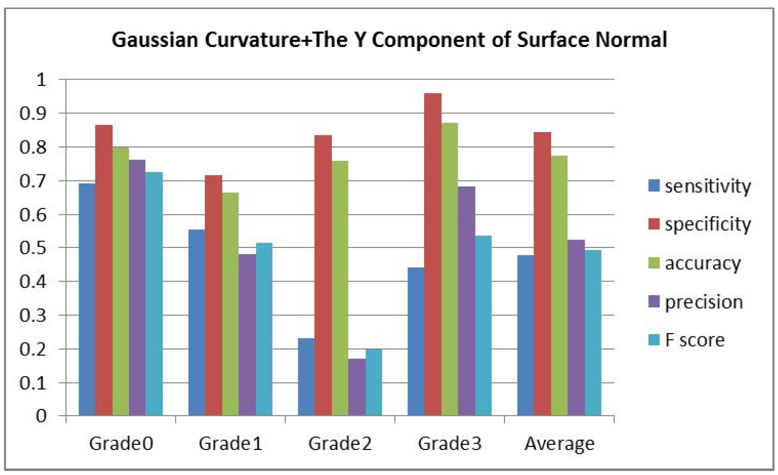

Figure 5.5: Statistical measurements for the performance Gaussian curvature and the Y component of the surface normal as features.

5.2.4.3 Coronal Projection and the Y component of surface normal

We evaluated the combination of coronal projection and the Y component of the surface normal. A normalized and concatenated template of coronal projection and Y component of surface normal was generated for each grade. LOOCV was performed on the same 203 breast images. Table 5.17 and Table 5.18 show the cumulative and averaged confusion matrix, respectively for the result. The statistical measurements are presented in Table 5.19 and plotted in Figure 5.6.

Table 5.17: Cumulative confusion matrix for the result of LOOCV using coronal projection and the Y component of the surface normal as features.

	Predicted Grade			
Ground Truth	0	1	2	3
0	49	14	8	0
1	23	31	18	3
2	2	11	14	8
3	0	1	6	15

Table 5.18: Averaged confusion matrix for the result of LOOCV using coronal projection and the Y component of the surface normal as features.

	Predicted Grade			
Ground Truth	0	1	2	3
0	0.2414	0.0690	0.0394	0.0000
1	0.1133	0.1527	0.0887	0.0148
2	0.0099	0.0542	0.0690	0.0394
3	0.0000	0.0049	0.0296	0.0739

Table 5.19: Statistical measurements for the performance of coronal projection and the Y component of the surface normal as features.

	Grade 0	**Grade 1**	**Grade 2**	**Grade 3**	**Average**
Sensitivity	0.6622	0.5439	0.3043	0.5769	0.5218
Specificity	0.8295	0.6986	0.8662	0.9605	0.8387
Accuracy	0.7685	0.6552	0.7389	0.9113	0.7685
Precision	0.6901	0.4133	0.4000	0.6818	0.5463
F score	0.6759	0.4697	0.3457	0.6250	0.5291
PPV	0.6901	0.4133	0.4000	0.6818	0.5463

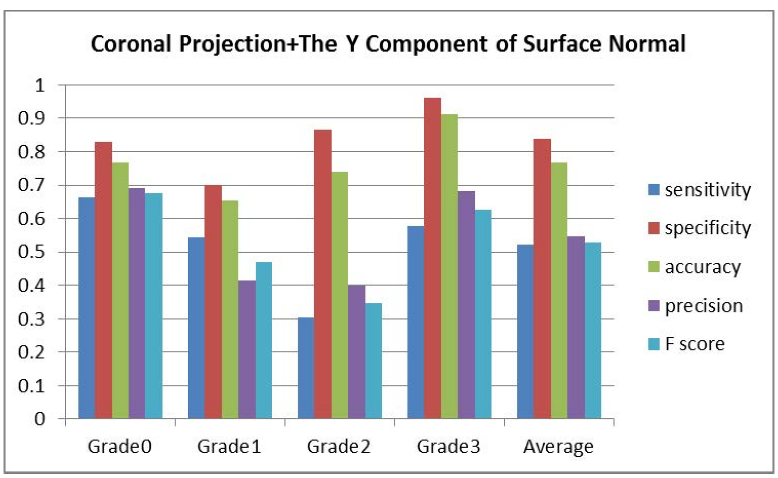

Figure 5.6: Statistical measurements for the performance of coronal projection and the Y component of the surface normal as features.

5.2.4.4 All Features Combined

Finally, we combined all the three features together, by concatenating and normalizing all three templates. We evaluated the template by conducting LOOCV on the same 203 breast images. Table 5.20 and Table 5.21 show the cumulative and averaged confusion matrix, respectively for the result. The statistical measurements are presented in Table 5.22 and plotted in Figure 5.7.

Table 5.20: Cumulative confusion matrix for the result of LOOCV using all the three 3D measures as features.

	Predicted Grade			
Ground Truth	0	1	2	3
0	50	13	8	0
1	16	36	20	3
2	3	11	12	9
3	0	0	5	17

Table 5.21: Averaged confusion matrix for the result of LOOCV using all the three 3D measures as features.

	Predicted Grade			
Ground Truth	0	1	2	3
0	0.2463	0.0640	0.0394	0.0000
1	0.0788	0.1773	0.0985	0.0148
2	0.0148	0.0542	0.0591	0.0443
3	0.0000	0.0000	0.0246	0.0837

Table 5.22: Statistical measurements for the performance of all the three 3D measures as features.

	Grade 0	**Grade 1**	**Grade 2**	**Grade 3**	**Average**
Sensitivity	0.7246	0.6000	0.2667	0.5862	0.5444
Specificity	0.8433	0.7273	0.8544	0.9713	0.8491
Accuracy	0.8030	0.6897	0.7241	0.9163	0.7833
Precision	0.7042	0.4800	0.3429	0.7727	0.5750
F score	0.7143	0.5333	0.3000	0.6667	0.5536
PPV	0.7042	0.4800	0.3429	0.7727	0.5750

5.3 Evaluation of Subjective Rating

We had a team of two surgeons with experience in breast reconstruction who subjectively rated the ptosis grade using the Regnault's classification scale for the 203 breasts randomly chosen

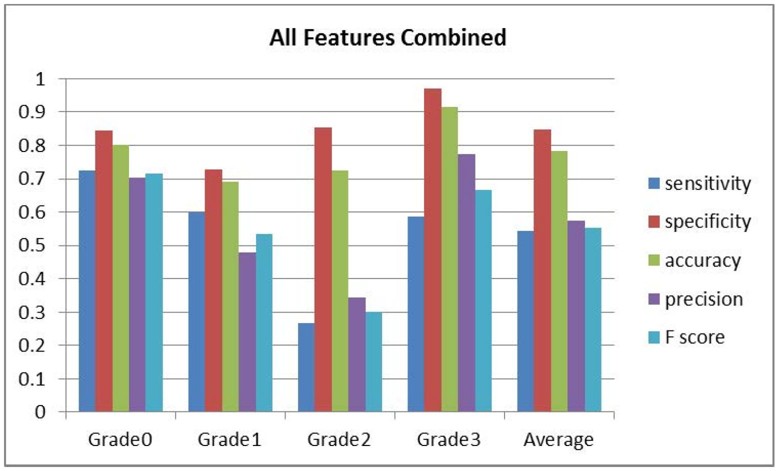

Figure 5.7: Statistical measurements for the performance of the combination of all the three 3D features.

from the 247 breasts. We used the rating of the experienced senior surgeon (in terms of number of years in clinical practice) as the golden standard (i.e., ground truth) in our study. All the results were evaluated based on this surgeon's rating as the ground truth to maintain consistency.

We evaluated the result of ptosis graded by the other surgeon by comparing with the result from the senior surgeon which we used as ground truth. Table 5.23 shows the confusion matrix for subjective rating. From the table, we can see that the most disagreement amongst the two surgeons exists for grade 1 and grade 2.

Table 5.23: Confusion matrix for subjective rating of ptosis.

	Predicted Grade			
Ground Truth	0	1	2	3
0	41	21	9	0
1	4	19	47	5
2	0	5	16	15
3	0	0	0	22

Table 5.24 (Figure 5.8) shows the statistical measures on the performance of subjective rating. Subjective rating had an relatively high accuracy of 84% on grade 0, and 91% on grade 3, but low accuracy of 60% on grade1 and 63% on grade 2, leading to an overall average accuracy of 74%. Grade 3 had a high precision rate of 1.0. Because grade 3 ptosis is an extreme case of breast ptosis so visually it can be easily identified . Whereas grade 1 and 2 had a lower precision rate of 25% and

44%, respectively, leading to an averaged precision of 57%.

Table 5.24: Statistical measures of the performance of subjective rating of ptosis.

	Grade 0	**Grade 1**	**Grade 2**	**Grade 3**	**Average**
Sensitivity	0.9111	0.4222	0.2222	0.5238	0.5198
Specificity	0.8113	0.6478	0.8485	1.0000	0.8269
Accuracy	0.8374	0.6010	0.6305	0.9064	0.7438
Precision/PPV	0.5775	0.2533	0.4444	1.0000	0.5688
F score	0.7069	0.3167	0.2963	0.6875	0.5018

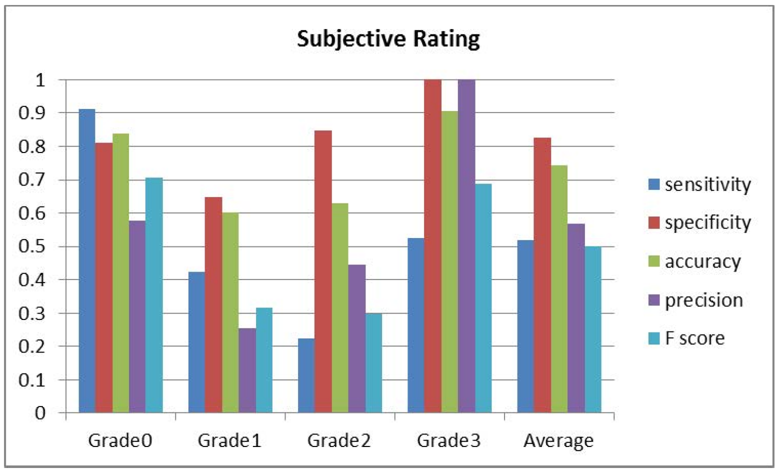

Figure 5.8: Statistical measurements for the performance of subjective rating of ptosis.

5.4 Evaluation of LaTrenta and Hoffman's Classification

We performed the LaTrenta and Hoffman's quantitative classification [12] on the same data set (203 breasts), by computing the distance of the nipple from the terminus of IMF using our customized BR software [14]. An observer manually recorded the height of nipple level and that of the terminus of the IMF, and computed the vertical distance between nipple and the terminus of IMF. Grading was assessed according to LaTrenta and Hoffman's quantitative classification scheme as described earlier in Section 3.3.4. Table 5.25 presents the confusion matrix of the result. The ground truth was the ptosis grade determined by the experienced senior surgeon. Predicted ptosis grade was the result using LaTrenta and Hoffman's classification.

Table 5.26 (Figure 5.9) shows the statistical measurements of the performance of LaTrenta

Table 5.25: Cumulative confusion matrix for LaTrenta and Hoffman's classification using photogrammetry.

	Predicted Grade			
Ground Truth	0	1	2	3
0	51	8	12	0
1	37	3	33	2
2	11	2	17	5
3	2	5	7	8

and Hoffmans classification. Grade 3 holds a relatively high accuracy of 90%, while grade 0, 1, and 2 exhibit a relatively lower accuracy at 65%, 57% and 66%, respectively. Also grade 0 has a relatively high precision of 72%, while grade 1, 2, and 3 have a low precision of 4%, 49% and 36% respectively, leading to an average precision of 40%.

Table 5.26: Statistical measures for the performance of LaTrenta and Hoffman's classification.

	Grade 0	**Grade 1**	**Grade 2**	**Grade 3**	**Average**
Sensitivity	0.5050	0.1667	0.2464	0.5333	0.3628
Specificity	0.8039	0.6108	0.8657	0.9255	0.8015
Accuracy	0.6552	0.5714	0.6552	0.8966	0.6946
Precision	0.7183	0.0400	0.4857	0.3636	0.4019
F score	0.5930	0.0645	0.3269	0.4324	0.3542
PPV	0.7183	0.0400	0.4857	0.3636	0.4019

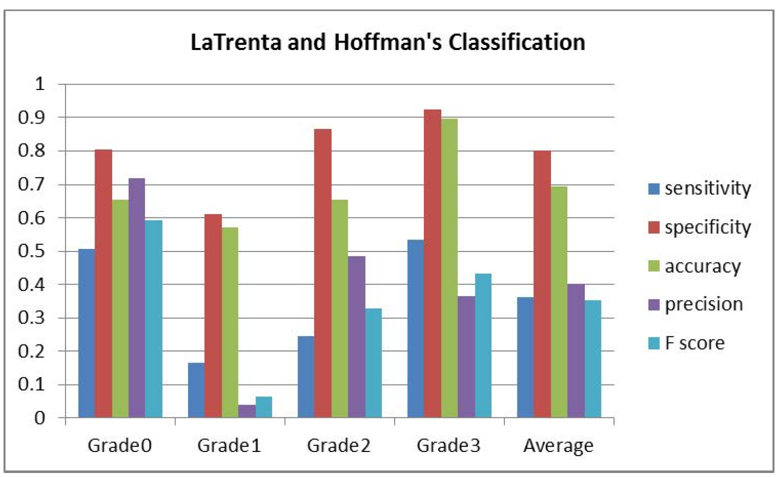

Figure 5.9: Statistical measurements for performance of LaTrenta and Hoffman's classification.

5.5 Evaluation of Kim's Distance Ratio Methods

We evaluated Kim's objective methods using distance ratios [13] for assessing ptosis on 3D images. We randomly picked 64 breasts, with 16 breasts per grade out of the 247 as the training data set and made simple linear regressions on both methods. We evaluated the performance of the linear regression by testing on the same 203 breasts. We computed two distance ratios: measure 1: $(s-i)/(s-n)$, measure 2: $(n-v)/(i-v)$, where $s-i$ represents vertical distance between sternal notch and lateral terminus, $s-n$ is the vertical distance between sternal notch and nipple, $n-v$ is the vertical distance between nipple and the lowest visible point, $i-v$ is the vertical distance between lateral terminus and the lowest visible point. Based on the ground truth, linear regressions between the two distance ratios and the ground truth were determined. Figure 5.10 shows the simple linear regressions.

Based on the linear regressions of the two measurements, we evaluated the test set by mapping the distance ratios into a scale of [0, 3]. We set the nearest integer as the predicted grade. Table 5.27 and Table 5.28 show the confusion matrices for the result using measure 1 and measure 2. Figure 5.11 shows the average performance of Kim's distance ratio methods. Measure 1 has an accuracy of 65%, 46%, 64% and 90% for grade 0, 1, 2, and 3 respectively, leading to an average accuracy of 66%. Measure 2 has an accuracy of 65%, 40%, 62% and 88% for grade0, 1, 2, and 3 respectively, leading to an average accuracy of 64%.

Table 5.27: Confusion matrix for the result using distance ratios (measure 1).

	Predicted Grade			
Ground Truth	0	1	2	3
0	0	52	19	0
1	0	38	35	2
2	0	11	24	0
3	0	9	9	4

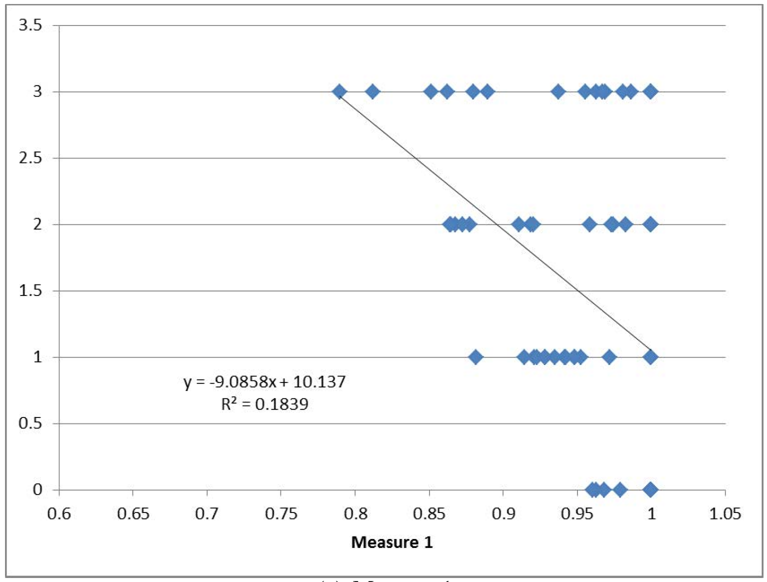

(a) Measure 1

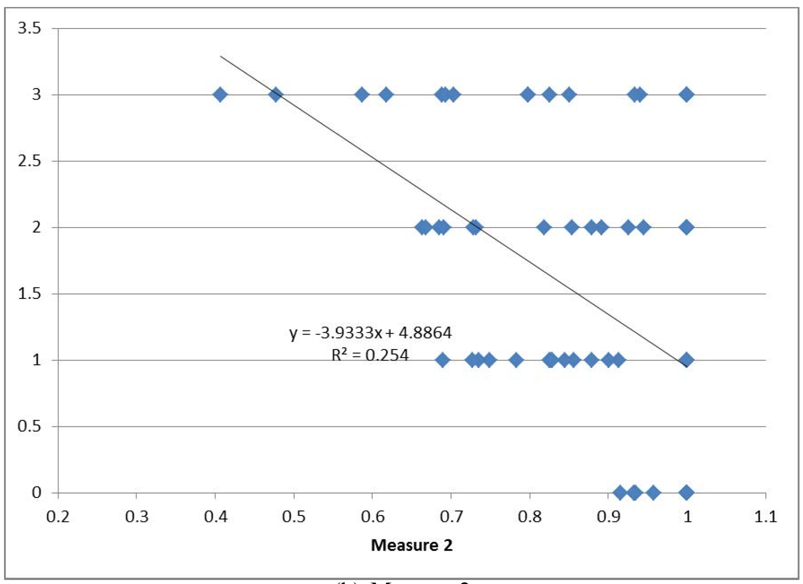

(b) Measure 2

Figure 5.10: Linear regression of distance ratios with subjective scores.

Table 5.28: Confusion matrix for the result using distance ratios (measure 2).

	Predicted Grade			
Ground Truth	0	1	2	3
0	0	62	9	0
1	0	34	41	0
2	0	11	18	6
3	0	7	11	4

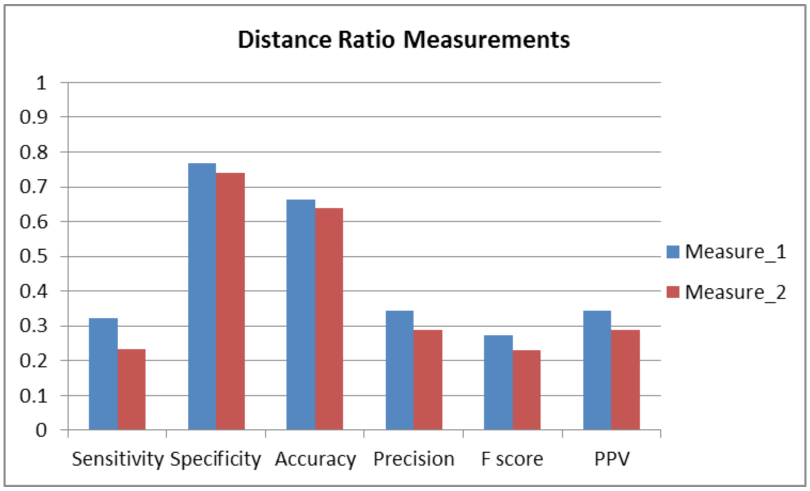

Figure 5.11: Statistical measurements for the performance of Kim's distance ratio method.

5.6 Discussion

So far, we evaluated the performance of our 3D measurements, as well as subjective rating, LaTrenta and Hoffman's classification and Kim's distance ratio methods based on the same 203 breast images. Figure 5.12 shows a comparison of statistical result over all the measurements on grade 0. In the following figures, LaTrenta and Hoffman's classification is abbreviated as LH, G represents Gaussian curvature, P represents coronal projection, and Ny indicates the Y component of the surface normal. According to Figure 5.12, subjective measurement provided the highest accuracy (84%) but relative low precision rate (58%). All the 3D features and their combinations provided higher accuracy over LaTrenta and Hoffman's classification and Kim's distance ratio measurements. The combination of all three features provided the highest accuracy of 80% and precision rate of 70% among all the 3D features. Moreover, Ny provided the highest precision rate of 80% as well as a high accuracy of 78%.

Figure 5.13 shows a comparison of statistical result over the subjective measurement, LaTrenta and Hoffman's classification, Kim's distance ratios, and all the 3D measurements on grade 1. As seen in Figure 5.13, the overall performance of 3D features is better than that of subjective measurement, and 2D photogrammetry (LaTrenta and Hoffman's classification, and Kim's measurements). The combination of all the three features provided the best performance on grade 1

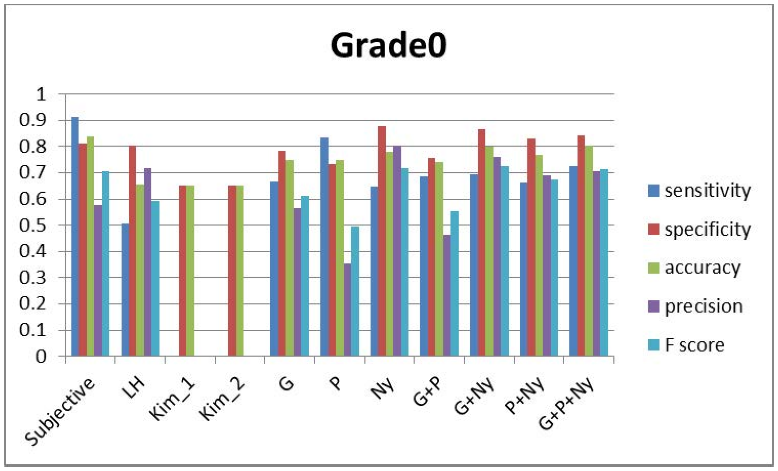

Figure 5.12: A comparison of the performance of subjective measurement, 2D photogrammetry, and 3D stereophotogrammetry for assessing grade 0.

with the accuracy of 69% and precision rate of 48%.

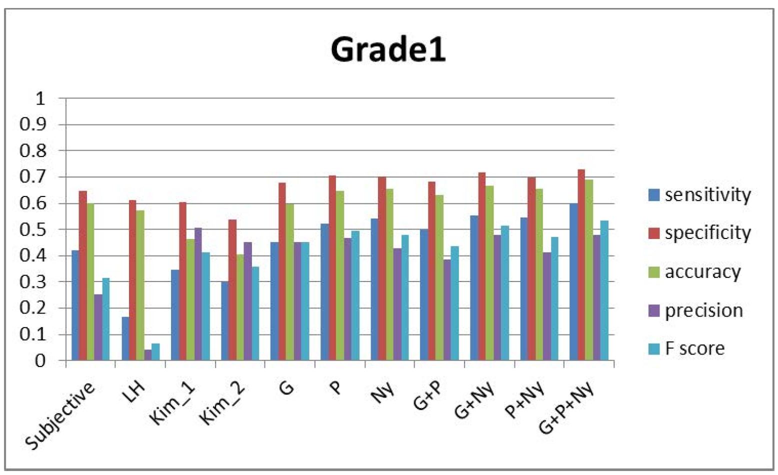

Figure 5.13: A comparison of the performance of subjective measurement, 2D photogrammetry, and 3D stereophotogrammetry for assessing grade 1.

Figure 5.14 shows a comparison of the performance of subjective rating, photogrammetry and stereophotogrammetry for grade 2. According to Figure 5.14, all the 3D measurements provided a higher accuracy over the other methods. The combination of all three features provided the best performance by having an accuracy of 76% and precision rate of 34% among all the 3D features.

Figure 5.15 shows a comparison of the performance of statistical result all the measurements for grade 3. As seen in Figure 5.15, subjective rating provided the highest accuracy of 91% and precision rate of 100%. Because grade 3 is the extreme case of ptosis, it is easy to visually identify.

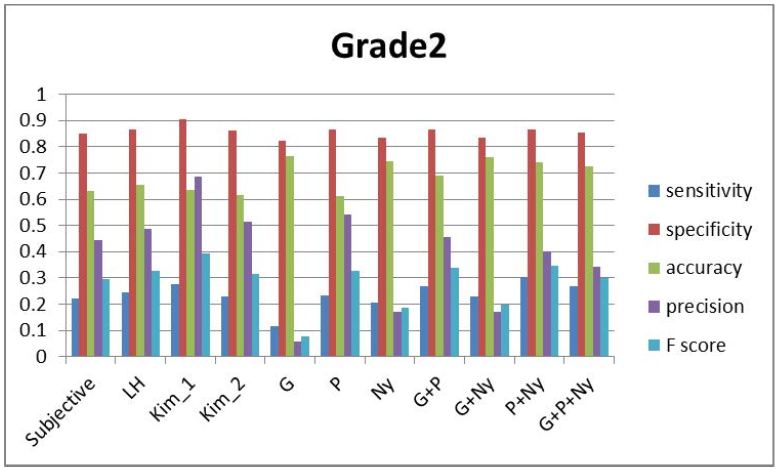

Figure 5.14: A comparison of the performance of subjective measurement, 2D photogrammetry, and 3D stereophotogrammetry for assessing grade 2.

All the 3D measurements provided a better performance than LaTrenta and Hoffman's classification and Kim's measurements by having higher precision rate. The best feature for identifying grade 3 is G+P, with an accuracy of 90% and precision rate of 86%.

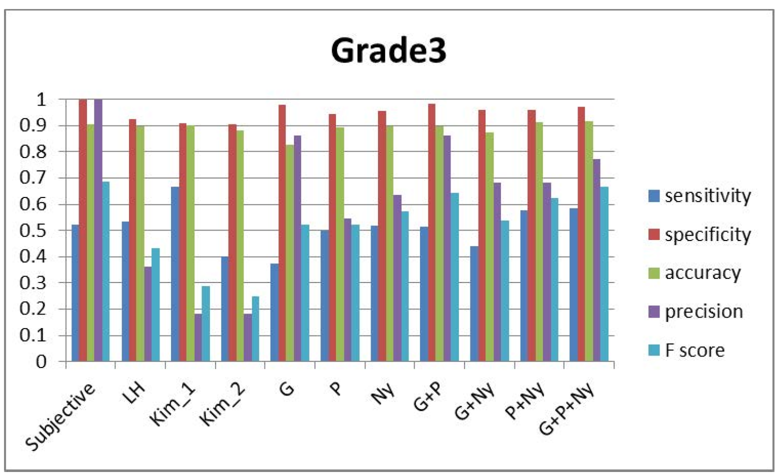

Figure 5.15: A comparison of the performance of subjective measurement, 2D photogrammetry, and 3D stereophotogrammetry for assessing grade 3.

Table 5.29 and Figure 5.16 shows a comparison of the average performance over all the approaches evaluated. Subjective rating of breast ptosis provided a good performance with an accuracy of 74% and precision rate of 57%. LaTrenta and Hoffman's classification and Kim's distance ratio measurements provided a lower accuracy of around 60%-70% and precision rate of around 29%-40%. This indicated that the LaTrenta and Hoffman's classification and Kim's measurement used on

3D image were suboptimal. All the 3D measurements exhibited good performance with accuracy in the range of 73%-78% and precision rate of 48%-57%. The best feature for the overall performance was G+P+Ny, which was the combination of all three 3D features. It provided an accuracy of 78% and precision rate 57%.

Table 5.29: A comparison of the overall performance of subjective rating, 2D photogrammetry, and 3D stereophotogrammetry.

Average	Sub	LH	Kim_1	Kim_2	G	P	Ny	G+P	G+Ny	P+Ny	G+P+Ny
Sensitivity	0.52	0.36	0.32	0.23	0.40	0.52	0.48	0.49	0.48	0.52	0.54
Specificity	0.83	0.80	0.77	0.74	0.82	0.81	0.84	0.82	0.84	0.84	0.85
Accuracy	0.74	0.69	0.66	0.64	0.73	0.72	0.77	0.74	0.77	0.77	0.78
Precision	0.57	0.40	0.34	0.29	0.48	0.48	0.51	0.54	0.52	0.55	0.57
F score	0.50	0.35	0.27	0.23	0.42	0.46	0.49	0.49	0.49	0.53	0.55
PPV	0.57	0.40	0.34	0.29	0.48	0.48	0.51	0.54	0.52	0.55	0.57

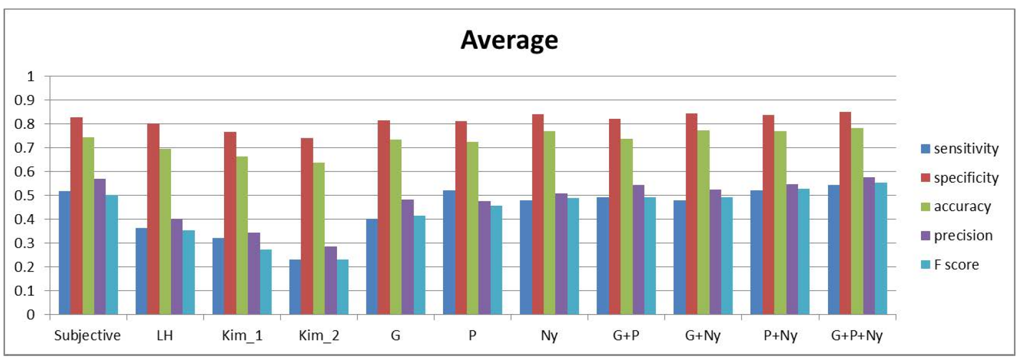

Figure 5.16: A comparison of the overall performance of subjective measurement, 2D photogrammetry, and 3D stereophotogrammetry for assessing grades 0-3.

In conclusion, all the 3D features and their combinations provided a good performance compared to subjective measurement, LaTrenta and Hoffman's classification and Kim's distance ratio methods by having a higher accuracy and higher precision rate. The best feature is the combination of Gaussian curvature, the coronal projection and the Y component of surface normal since it provides the highest accuracy of 78% and precision rate of 57% on the average performance.

Chapter 6

Conclusion

Development of an objective and quantitative method for measuring ptosis from 3D images is an important yet challenging task. Prior work mainly focused on either subjective rating, anthropometry or 2D photogrammetry. In this study, we proposed a new approach for measuring breast ptosis using 3D torso scans. We explored unique 3D morphological features from stereophotogrammetry that surpass the need of predefining the terminus of IMF. We investigated Gaussian curvature, coronal projection and the Y component of surface normal as features and built a 3D ptosis classification model. The results demonstrate that our new approach on 3D images yielded better performance compared to both subjective measurements and 2D photogrammetry.

Currently we employ three feature sets in training the model. However, the margin of each decision boundary is relatively small, which results in a higher rate of false positives and negatives. In future work, we will explore additional 3D features. Furthermore, the current features we chose are linearly combined together and assumed to be mutually exclusive from each other for simplicity. In real world, however, features may be correlated. Thus a more sophisticated multi-variant discriminant model needs to be explored.

We used the native histogram estimator where the feature space is divided into equal-sized bins. In addition, we used the Bhattacharyya distance to calculate the distance between histograms. More powerful machine learning approaches can be employed in future work. For instance, the k-means clustering method can be used where images are partitioned into k clusters in which the ones with same grade belong to one cluster with the nearest mean distance.

Last but not least, an important direction of the future work is to automating the assessment procedure. Currently our method is semi-automated where the 3D images need to be manually cropped before the following processes can be adopted. However, it would be desirable to have a completely automated algorithm, that incorporates computerized cropping and fiducial point detection to achieve robust and speedy prediction of breast ptosis.

Bibliography

[1] A. C. Society, "Cancer facts and figures," 2013. [Online]. Available: http://www.cancer.org.

[2] J. Bostwick, "Plastic and reconstructive breast surgery," 2000.

[3] R. D. Pezner, J. A. Lipsett, N. L. Vora, and K. R. Desai, "Limited usefulness of observer-based cosmesis scales employed to evaluate patients treated conservatively for breast cancer," *International Journal of Radiation Oncology* Biology* Physics*, vol. 11, no. 6, pp. 1117–1119, 1985.

[4] J. C. Lowery, E. G. Wilkins, W. M. Kuzon, and J. A. Davis, "Evaluations of aesthetic results in breast reconstruction: an analysis of reliability," *Annals of plastic surgery*, vol. 36, no. 6, pp. 601–607, 1996.

[5] K. Sneeuw, N. Aaronson, J. Yarnold, M. Broderick, J. Regan, G. Ross, and A. Goddard, "Cosmetic and functional outcomes of breast conserving treatment for early stage breast cancer. 1. comparison of patients' ratings, observers' ratings and objective assessments," *Radiotherapy and oncology*, vol. 25, no. 3, pp. 153–159, 1992.

[6] C. Vrieling, L. Collette, E. Bartelink, J. H. Borger, S. J. Brenninkmeyer, J.-C. Horiot, M. Pierart, P. M. Poortmans, H. Struikmans, E. Van der Schueren *et al.*, "Validation of the methods of cosmetic assessment after breast-conserving therapy in the eortc boost versus no boost trial," *International Journal of Radiation Oncology* Biology* Physics*, vol. 45, no. 3, pp. 667–676, 1999.

[7] R. Yavuzer, S. Smirnes, and I. T. Jackson, "Guidelines for standard photography in plastic surgery," *Annals of plastic surgery*, vol. 46, no. 3, pp. 293–300, 2001.

[8] C. P. Honrado and W. F. Larrabee Jr, "Update in three-dimensional imaging in facial plastic surgery," *Current opinion in otolaryngology & head and neck surgery*, vol. 12, no. 4, pp. 327–331, 2004.

[9] V. F. Ferrario, C. Sforza, C. Dellavia, G. M. Tartaglia, A. Colombo, and A. Carù, “A quantitative three-dimensional assessment of soft tissue facial asymmetry of cleft lip and palate adult patients,” *Journal of Craniofacial Surgery*, vol. 14, no. 5, pp. 739–746, 2003.

[10] S. Lee, “Three-dimensional photography and its application to facial plastic surgery,” *Archives of Facial Plastic Surgery*, vol. 6, no. 6, pp. 410–414, 2004.

[11] P. Regnault, “Breast ptosis. definition and treatment.” *Clinics in plastic surgery*, vol. 3, no. 2, p. 193, 1976.

[12] G. S. LaTrenta and L. A. Hoffman, “Breast reduction,” *Aesthetic plastic surgery. WB Saunders, Philadelphia*, pp. 932–933, 1994.

[13] M. S. Kim, G. P. Reece, E. K. Beahm, M. J. Miller, and M. K. Neely Atkinson, E andMarkey, “Objective assessment of aesthetic outcomes of breast cancer treatment: measuring ptosis from clinical photographs,” *Computers in Biology and Medicine*, vol. 37, no. 1, pp. 49–59, 2007.

[14] M. Kawale, “Automated identification of fiducial points on three-dimensional torso images,” *M.S. thesis, Dept. Comp.Sc., University of Houston, Houston, TX*, 2010.

[15] J. Fan, E. Raposio, J. Wang, and R. E. Nordström, “Development of the inframammary fold and ptosis in breast reconstruction with textured tissue expanders,” *Aesthetic plastic surgery*, vol. 26, no. 3, pp. 219–222, 2002.

[16] S. Boutros, M. Kattash, A. Wienfeld, E. Yuksel, S. Baer, and S. Shenaq, “The intradermal anatomy of the inframammary fold,” *Plastic and reconstructive surgery*, vol. 102, no. 4, pp. 1030–1033, 1998.

[17] J. Gibney, “The long-term results of tissue expansion for breast reconstruction.” *Clinics in plastic surgery*, vol. 14, no. 3, pp. 509–518, 1987.

[18] K. Asgeirsson, T. Rasheed, S. McCulley, and R. Macmillan, “Oncological and cosmetic outcomes of oncoplastic breast conserving surgery,” *European Journal of Surgical Oncology (EJSO)*, vol. 31, no. 8, pp. 817–823, 2005.

[19] N. S. Grewal and J. Fisher, "Why do patients seek revisionary breast surgery?" *Aesthetic Surgery Journal*, vol. 33, no. 2, pp. 237–244, 2013.

[20] R. Webster, "How does ptosis affect satisfaction after immediate reconstruction plus contralateral mammaplasty?" *Annals of plastic surgery*, vol. 65, no. 3, pp. 294–299, 2010.

[21] E. Van Limbergen, A. Rijnders, E. Van der Schueren, T. Lerut, and R. Christiaens, "Cosmetic evaluation of breast conserving treatment for mammary cancer. 2. a quantitative analysis of the influence of radiation dose, fractionation schedules and surgical treatment techniques on cosmetic results," *Radiotherapy and oncology*, vol. 16, no. 4, pp. 253–267, 1989.

[22] V. Sacchini, A. Luini, S. Tana, L. Lozza, V. Galimberti, M. Merson, R. Agresti, P. Veronesi, and M. Greco, "Quantitative and qualitative cosmetic evaluation after conservative treatment for breast cancer," *European Journal of Cancer and Clinical Oncology*, vol. 27, no. 11, pp. 1395–1400, 1991.

[23] A. K. Bajaj, P. S. Kon, K. C. Oberg, and D. A. Miles, "Aesthetic outcomes in patients undergoing breast conservation therapy for the treatment of localized breast cancer," *Plastic and reconstructive surgery*, vol. 114, no. 6, pp. 1442–1449, 2004.

[24] D. J. Hauben, N. Adler, R. Silfen, and D. Regev, "Breast-areola-nipple proportion," *Annals of plastic surgery*, vol. 50, no. 5, pp. 510–513, 2003.

[25] K. R. Roehl, B. Wilhelmi, and L. Phillips, "Breast reconstruction," *Sabiston Textbook of Surgery. The Biological Basis of Modern Surgical Practice. 19th ed. St. Louis, MO: WB Saunders Company*, 2012.

[26] J. Lewis Jr, "Mammary ptosis," *Aesthetic Breast Surgery. Baltimore, Williams & Wilkins*, pp. 130–145, 1983.

[27] R. R. Brink, "Evaluating breast parenchymal maldistribution with regard to mastopexy and augmentation mammaplasty," *Plastic and reconstructive surgery*, vol. 86, no. 4, pp. 715–719, 1990.

[28] R. Brink, "Management of true ptosis of the breast," *Plastic and reconstructive surgery*, vol. 91, no. 4, pp. 657–662, 1993.

[29] L. Kirwan, "A classification and algorithm for treatment of breast ptosis," *Aesthetic Surgery Journal*, vol. 22, no. 4, pp. 355–363, 2002.

[30] V. L. de la Torre J, "Breast mastopexy," 2007. [Online]. Available: http://www.emedicine.com/plastic/topic128.htm.

[31] M. A. Shiffman, "Classification of breast ptosis," in *Breast Augmentation*, M. A. Shiffman, Ed. Springer Berlin Heidelberg, 2009, pp. 251–255. [Online]. Available: http://dx.doi.org/10.1007/978-3-540-78948-2_31.

[32] D. Christie, M. O'brien, J. Christie, T. Kron, S. Ferguson, C. Hamilton, and J. Denham, "A comparison of methods of cosmetic assessment in breast conservation treatment," *The Breast*, vol. 5, no. 5, pp. 358–367, 1996.

[33] M. H. Brown, J. L. Semple, and P. C. Neligan, "Variables affecting symmetry of the nipple-areola complex," *Plastic and reconstructive surgery*, vol. 96, no. 4, pp. 846–851, 1995.

[34] A. L. Abner, A. Recht, F. A. Vicini, B. Silver, D. Hayes, S. Come, and J. R. Harris, "Cosmetic results after surgery, chemotherapy, and radiation therapy for early breast cancer," *International Journal of Radiation Oncology* Biology* Physics*, vol. 21, no. 2, pp. 331–338, 1991.

[35] A. de la Rochefordière, A. L. Abner, B. Silver, F. Vicini, A. Recht, and J. R. Harris, "Are cosmetic results following conservative surgery and radiation therapy for early breast cancer dependent on technique?" *International Journal of Radiation Oncology* Biology* Physics*, vol. 23, no. 5, pp. 925–931, 1992.

[36] I. Lindsey, J. Serpell, W. Johnson, and A. Rodger, "Cosmesis following complete local excision of breast cancer," *Australian and New Zealand journal of surgery*, vol. 67, no. 7, pp. 428–432, 1997.

[37] H. P. Oliveira, J. S. Cardoso, A. Magalhães, and M. J. Cardoso, “Methods for the aesthetic evaluation of breast cancer conservation treatment: A technological review,” *Current Medical Imaging Reviews*, vol. 9, no. 1, pp. 32–46, 2013.

[38] J. Penn, “Breast reduction,” *British journal of plastic surgery*, vol. 7, pp. 357–371, 1955.

[39] D. J. Smith Jr, W. E. Palin Jr, V. L. Katch, and J. E. Bennett, “Breast volume and anthropomorphic measurements: normal values,” *Plastic and reconstructive surgery*, vol. 78, no. 3, pp. 331–335, 1986.

[40] D. J. Smith Jr, W. E. Palin Jr, V. Katch, and J. E. Bennett, “Surgical treatment of congenital breast asymmetry,” *Annals of plastic surgery*, vol. 17, no. 2, pp. 92–101, 1986.

[41] D. K. Avşar, A. C. Aygıt, E. Benlier, H. Top, and O. Taşkınalp, “Anthropometric breast measurement a study of 385 turkish female students,” *Aesthetic Surgery Journal*, vol. 30, no. 1, pp. 44–50, 2010.

[42] M. S. Kim, J. C. Sbalchiero, G. P. Reece, M. J. Miller, E. K. Beahm, and M. K. Markey, “Assessment of breast aesthetics,” *Plastic and reconstructive surgery*, vol. 121, no. 4, p. 186e, 2008.

[43] M. Westreich, “Anthropomorphic breast measurement: protocol and results in 50 women with aesthetically perfect breasts and clinical application,” *Plastic and reconstructive surgery*, vol. 100, no. 2, pp. 468–479, 1997.

[44] L. Tsouskas and I. Fentiman, “Breast compliance: a new method for evaluation of cosmetic outcome after conservative treatment of early breast cancer,” *Breast cancer research and treatment*, vol. 15, no. 3, pp. 185–190, 1990.

[45] B. Stark and N. Olivari, “Breast asymmetry: an objective analysis of postoperative results,” *European Journal of Plastic Surgery*, vol. 14, no. 4, pp. 173–176, 1991.

[46] “An investigation into digital imaging in assessing cosmetic outcome after breast surgery,” *Journal of Visual Communication in Medicine*, vol. 23, no. 1, pp. 12–16, 2000.

[47] R. D. Pezner, M. P. Patterson, L. R. Hill, N. Vora, K. R. Desai, J. O. Archambeau, and J. A. Lipsett, “Breast retraction assessment: an objective evaluation of cosmetic results of patients treated conservatively for breast cancer,” *International Journal of Radiation Oncology* Biology* Physics*, vol. 11, no. 3, pp. 575–578, 1985.

[48] J. Lee, S. Chen, G. P. Reece, M. A. Crosby, E. K. Beahm, and M. K. Markey, “A novel quantitative measure of breast curvature based on catenary,” *Biomedical Engineering, IEEE Transactions on*, vol. 59, no. 4, pp. 1115–1124, 2012.

[49] F. Fitzal, W. Krois, H. Trischler, L. Wutzel, O. Riedl, U. Kühbelböck, B. Wintersteiner, M. Cardoso, P. Dubsky, M. Gnant *et al.*, “The use of a breast symmetry index for objective evaluation of breast cosmesis,” *The Breast*, vol. 16, no. 4, pp. 429–435, 2007.

[50] B. E. DiBernardo, R. L. Adams, J. Krause, M. A. Fiorillo, and G. Gheradini, “Photographic standards in plastic surgery,” *Plastic and reconstructive surgery*, vol. 102, no. 2, pp. 559–568, 1998.

[51] R. Ellenbogen, S. Jankauskas, and F. J. Collini, “Achieving standardized photographs in aesthetic surgery,” *Plastic and reconstructive surgery*, vol. 86, no. 5, pp. 955–961, 1990.

[52] J. P. DiSaia, J. J. Ptak, and B. M. Achauer, “Digital photography for the plastic surgeon,” *Plastic and reconstructive surgery*, vol. 102, no. 2, pp. 569–573, 1998.

[53] G. Gherardini, A. Matarasso, A. S. Serure, L. S. Toledo, and B. E. DiBernardo, “Standardization in photography for body contour surgery and suction-assisted lipectomy,” *Plastic and reconstructive surgery*, vol. 100, no. 1, pp. 227–237, 1997.

[54] J. R. Harris, M. B. Levene, G. Svensson, and S. Hellman, “Analysis of cosmetic results following primary radiation therapy for stages i and ii carcinoma of the breast,” *International Journal of Radiation Oncology* Biology* Physics*, vol. 5, no. 2, pp. 257–261, 1979.

[55] J. Boot, A. Naftel, and A. Ramli, “Bodymap: an image processing system for the measurement of body surface profiles encountered in skin expansion surgery,” *International journal of bio-medical computing*, vol. 31, no. 3, pp. 189–204, 1992.

[56] C. Malata, J. Boot, E. Bradbury, A. Ramli, and D. Sharpe, “Congenital breast asymmetry: subjective and objective assessment,” *British journal of plastic surgery*, vol. 47, no. 2, pp. 95–102, 1994.

[57] G. M. Galdino, M. Nahabedian, M. Chiaramonte, J. Z. Geng, S. Klatsky, and P. Manson, “Clinical applications of three-dimensional photography in breast surgery,” *Plastic and Reconstructive Surgery*, vol. 110, no. 1, pp. 58–70, 2002.

[58] O. M. Tepper, N. S. Karp, K. Small, J. Unger, L. Rudolph, A. Pritchard, and M. Choi, “Three-dimensional imaging provides valuable clinical data to aid in unilateral tissue expander-implant breast reconstruction,” *The breast journal*, vol. 14, no. 6, pp. 543–550, 2008.

[59] A. Losken, H. Seify, D. D. Denson, A. A. Paredes Jr, and G. W. Carlson, “Validating three-dimensional imaging of the breast,” *Annals of plastic surgery*, vol. 54, no. 5, pp. 471–476, 2005.

[60] R. A. Jacobs *et al.*, “Three-dimensional photography,” *Plastic and reconstructive surgery*, vol. 107, no. 1, pp. 276–277, 2001.

[61] A. Bose, S. Shah, G. Reece, M. Crosby, E. Beahm, M. Fingeret, M. Markey, and F. Merchant, “Automated spatial alignment of 3d torso images,” in *Engineering in Medicine and Biology Society,EMBC, 2011 Annual International Conference of the IEEE*, 2011, pp. 8455–8458.

[62] J. J. Koenderink and A. J. van Doorn, “Surface shape and curvature scales,” *Image and vision computing*, vol. 10, no. 8, pp. 557–564, 1992.

[63] D. Cohen-Steiner and J.-M. Morvan, “Restricted delaunay triangulations and normal cycle,” in *Proceedings of the nineteenth annual symposium on Computational geometry*. ACM, 2003, pp. 312–321.

[64] S.-H. Cha and S. N. Srihari, “On measuring the distance between histograms,” *Pattern Recognition*, vol. 35, no. 6, pp. 1355–1370, 2002.

Appendix A

Objective Measurements on 3D Images

A.1 LOOCV Results for Gaussian Curvature Analysis

Table A.1: LOOCV results for Gaussian curvature analysis.

Subjects	Patient	Truth	Predicted	Distance G0	Distance G1	Distance G2	Distance G3
1	003L	0	C	0.29916	0.30966	0.33343	0.36380
2	003R	0	C	0.29837	0.33013	0.35388	0.40316
3	005R	0	C	0.34447	0.34695	0.36428	0.37918
4	007L	0	1	0.41064	0.40211	0.41260	0.42019
5	007R	0	1	0.39904	0.39369	0.40562	0.41396
6	008R	0	C	0.29619	0.31656	0.34022	0.36932
7	009L	0	C	0.50018	0.51879	0.53310	0.57613
8	013R	0	C	0.35243	0.37436	0.39705	0.42723
9	016R	0	C	0.32645	0.36588	0.38100	0.41192
10	025L	0	C	0.34518	0.37850	0.39695	0.43935
11	029R	0	C	0.42413	0.44488	0.47157	0.50747
12	037L	0	C	0.32176	0.33129	0.33971	0.36786
13	037R	0	C	0.35342	0.37035	0.38490	0.41795
14	046L	0	1	0.25794	0.24753	0.25624	0.28043
15	046R	0	1	0.27530	0.27443	0.29077	0.32497
16	049L	0	C	0.24041	0.24499	0.27305	0.32016
17	053L	0	C	0.26496	0.30646	0.32768	0.37252
18	053R	0	C	0.29683	0.35471	0.35551	0.41694
19	055L	0	C	0.26636	0.30035	0.30336	0.33334
20	055R	0	C	0.34894	0.38657	0.40222	0.43085
21	067R	0	C	0.24930	0.28365	0.29883	0.34283
22	073R	0	C	0.25085	0.25655	0.27499	0.31292
23	076L	0	C	0.39989	0.45721	0.45437	0.51058
24	078L	0	C	0.33857	0.37666	0.39214	0.42931
25	079R	0	C	0.20375	0.24329	0.25791	0.31334
26	084L	0	1	0.29684	0.29151	0.29977	0.31840
27	084R	0	1	0.33204	0.32450	0.34066	0.36421
28	088R	0	C	0.32066	0.33705	0.35302	0.38812
29	089R	0	C	0.22995	0.24177	0.26390	0.28789
30	093L	0	C	0.22275	0.26130	0.28456	0.33294
31	096L	0	C	0.23445	0.24607	0.26932	0.29406
32	113R	0	C	0.22509	0.24068	0.25901	0.29031
33	131R	0	C	0.27729	0.33767	0.35432	0.39922
34	135R	0	C	0.29444	0.33829	0.36039	0.40229
35	154R	0	C	0.21507	0.22758	0.25033	0.29832
36	160L	0	1	0.22495	0.21431	0.23679	0.24737
37	175L	0	C	0.27359	0.28841	0.28800	0.31690
38	183L	0	C	0.19472	0.21785	0.23683	0.29615
39	186R	0	C	0.29132	0.31311	0.32624	0.35287
40	188R	0	1	0.24266	0.21325	0.25583	0.26918
41	192L	0	C	0.24031	0.25993	0.27794	0.31176
42	200L	0	1	0.19849	0.17950	0.19749	0.21450
43	201R	0	C	0.21785	0.22491	0.23927	0.27714
44	203L	0	1	0.25131	0.23593	0.23633	0.25745
45	204L	0	2	0.24748	0.21771	0.20761	0.22039

Table A.1: LOOCV results for Gaussian curvature analysis (continuted).

Subjects	Patient	Truth	Predicted	Distance G0	Distance G1	Distance G2	Distance G3
46	205L	0	1	0.24795	0.24070	0.25027	0.27829
47	205R	0	1	0.22714	0.21550	0.23654	0.26209
48	211R	0	2	0.26831	0.25313	0.24484	0.24976
49	217L	0	1	0.21101	0.17106	0.17680	0.18720
50	220L	0	C	0.20916	0.24558	0.24970	0.29677
51	220R	0	C	0.21727	0.25015	0.27103	0.30998
52	505L	0	C	0.27044	0.28260	0.29600	0.32372
53	505R	0	C	0.26951	0.29508	0.32407	0.36117
54	508R	0	1	0.26905	0.21762	0.23712	0.24505
55	511L	0	1	0.26962	0.21500	0.22143	0.23174
56	523L	0	1	0.24116	0.20208	0.21731	0.22837
57	528R	0	1	0.23989	0.20955	0.23061	0.24448
58	529L	0	C	0.29148	0.30523	0.31691	0.36334
59	529R	0	C	0.25475	0.28124	0.30025	0.33182
60	535L	0	1	0.22902	0.20396	0.21732	0.23475
61	535R	0	1	0.22214	0.18505	0.21078	0.22388
62	542L	0	1	0.23291	0.20876	0.22952	0.23117
63	542R	0	1	0.23852	0.23213	0.26225	0.28797
64	554L	0	1	0.26035	0.25611	0.26009	0.26899
65	554R	0	1	0.26895	0.25626	0.26216	0.26597
66	700R	0	1	0.25316	0.21445	0.24512	0.25391
67	702L	0	1	0.22831	0.21178	0.23742	0.25460
68	702R	0	1	0.23802	0.22403	0.24861	0.25554
69	704R	0	1	0.25220	0.22568	0.24084	0.25579
70	705L	0	1	0.25256	0.23403	0.24846	0.25877
71	710L	0	1	0.27012	0.20431	0.21937	0.21635
72	006L	1	0	0.32103	0.32679	0.33277	0.35696
73	012L	1	0	0.38616	0.39313	0.39304	0.41444
74	012R	1	0	0.36726	0.37457	0.38296	0.40062
75	018L	1	0	0.37260	0.39590	0.40486	0.44056
76	018R	1	0	0.37706	0.40441	0.42551	0.44663
77	022L	1	0	0.38783	0.40178	0.41946	0.44279
78	022R	1	0	0.37390	0.39463	0.41414	0.44612
79	023L	1	0	0.37297	0.38629	0.40350	0.43099
80	023R	1	0	0.35539	0.38735	0.40305	0.44875
81	027R	1	2	0.45790	0.46702	0.45000	0.45337
82	047L	1	C	0.21731	0.19808	0.20970	0.20947
83	047R	1	C	0.26153	0.24483	0.26020	0.29528
84	049R	1	0	0.24807	0.26242	0.28793	0.33605
85	056L	1	C	0.17169	0.14833	0.15126	0.18748
86	057R	1	2	0.20440	0.17803	0.17765	0.20383
87	060L	1	0	0.23225	0.24567	0.26492	0.28566
88	069R	1	0	0.22761	0.23166	0.24950	0.27541
89	070R	1	C	0.21216	0.18901	0.20218	0.22355
90	075R	1	0	0.20386	0.20693	0.22223	0.24496
91	082L	1	C	0.21128	0.19374	0.20778	0.23312
92	086L	1	C	0.20409	0.18749	0.19515	0.23358
93	094R	1	C	0.20081	0.19498	0.20603	0.24238
94	095R	1	C	0.26335	0.25114	0.25143	0.25119
95	098R	1	C	0.22892	0.21965	0.23785	0.25301
96	124R	1	0	0.27046	0.28082	0.29992	0.33704
97	133L	1	C	0.18721	0.15824	0.16626	0.17330
98	133R	1	C	0.21454	0.21259	0.22407	0.23102
99	163R	1	C	0.28373	0.27333	0.28247	0.30668
100	181L	1	0	0.26839	0.26900	0.28062	0.30897

Table A.1: LOOCV results for Gaussian curvature analysis (continuted).

Subjects	Patient	Truth	Predicted	Distance G0	Distance G1	Distance G2	Distance G3
101	184L	1	0	0.20083	0.20393	0.21584	0.26539
102	190L	1	0	0.22563	0.23387	0.25225	0.26470
103	197R	1	C	0.26089	0.23241	0.23854	0.26278
104	199L	1	C	0.21452	0.19644	0.20661	0.23227
105	200R	1	C	0.21264	0.20235	0.20934	0.21785
106	203R	1	C	0.21921	0.21821	0.23662	0.27411
107	204R	1	2	0.24475	0.21923	0.21651	0.21844
108	209R	1	3	0.23614	0.17771	0.16716	0.15713
109	210L	1	3	0.28592	0.23029	0.22262	0.19509
110	219L	1	C	0.25741	0.23562	0.23943	0.25347
111	507L	1	2	0.26660	0.21786	0.20407	0.20743
112	507R	1	3	0.28835	0.23264	0.23114	0.22162
113	509R	1	2	0.31547	0.26670	0.25052	0.25952
114	511R	1	C	0.26846	0.20740	0.21643	0.20750
115	512R	1	C	0.23671	0.20460	0.21384	0.23581
116	514L	1	C	0.27567	0.23471	0.23536	0.23971
117	515L	1	C	0.27760	0.23640	0.24738	0.24579
118	515R	1	C	0.29948	0.24953	0.25708	0.25015
119	516L	1	3	0.31091	0.25248	0.22728	0.20862
120	516R	1	2	0.31361	0.25966	0.25460	0.25463
121	517L	1	3	0.32959	0.27292	0.25139	0.23890
122	517R	1	3	0.32320	0.26459	0.25614	0.25385
123	521L	1	C	0.23155	0.20113	0.21127	0.23529
124	522R	1	C	0.20801	0.18990	0.20318	0.21934
125	523R	1	3	0.27482	0.21409	0.21135	0.19453
126	527L	1	2	0.27619	0.24328	0.23756	0.25359
127	527R	1	C	0.23516	0.19808	0.20690	0.22558
128	534L	1	3	0.26878	0.23058	0.21409	0.20520
129	539R	1	C	0.22115	0.19390	0.21302	0.24065
130	540L	1	3	0.26006	0.21971	0.21338	0.19834
131	541L	1	3	0.27164	0.23380	0.23320	0.22304
132	541R	1	2	0.27691	0.23305	0.22939	0.24092
133	543L	1	3	0.26329	0.22089	0.20934	0.19534
134	543R	1	3	0.26443	0.23054	0.22802	0.22314
135	574R	1	C	0.23680	0.20687	0.22578	0.21913
136	691L	1	C	0.26347	0.24553	0.26281	0.29274
137	691R	1	2	0.25892	0.20628	0.20368	0.20420
138	699R	1	C	0.21772	0.18971	0.20527	0.21168
139	700L	1	C	0.25895	0.22252	0.23007	0.23744
140	703R	1	2	0.26728	0.22662	0.22521	0.23093
141	704L	1	2	0.25467	0.22801	0.22399	0.23860
142	710R	1	C	0.24942	0.19420	0.20814	0.21237
143	711L	1	3	0.32638	0.27548	0.26925	0.26148
144	713L	1	C	0.21475	0.17837	0.20000	0.22005
145	713R	1	C	0.22959	0.18613	0.20309	0.21170
146	717R	1	C	0.27264	0.24530	0.27317	0.27539
147	002L	2	0	0.40474	0.40955	0.41010	0.41360
148	010L	2	3	0.43068	0.43290	0.43238	0.41812
149	026L	2	1	0.30743	0.30052	0.30827	0.30470
150	029L	2	0	0.40198	0.45933	0.48630	0.54338
151	065L	2	1	0.21395	0.20592	0.22059	0.24020
152	066L	2	0	0.42383	0.43828	0.44287	0.45984
153	189L	2	1	0.25435	0.24053	0.25728	0.25038
154	208L	2	3	0.31454	0.24920	0.23135	0.18305
155	214R	2	C	0.24250	0.20494	0.20058	0.21340

Table A.1: LOOCV results for Gaussian curvature analysis (continuted).

Subjects	Patient	Truth	Predicted	Distance G0	Distance G1	Distance G2	Distance G3
156	216L	2	1	0.25352	0.23775	0.24587	0.27090
157	219R	2	1	0.22435	0.18489	0.19146	0.19079
158	506L	2	3	0.29393	0.24526	0.23690	0.22739
159	509L	2	3	0.32725	0.29854	0.29347	0.29334
160	518L	2	3	0.30804	0.26433	0.26413	0.26308
161	518R	2	3	0.28040	0.21581	0.19629	0.17232
162	520L	2	3	0.26525	0.22087	0.20796	0.19904
163	520R	2	C	0.27034	0.22333	0.22015	0.23021
164	522L	2	3	0.24657	0.20565	0.20988	0.19253
165	525L	2	3	0.32373	0.25450	0.23767	0.20165
166	526R	2	3	0.26309	0.21252	0.19573	0.18817
167	530R	2	3	0.26459	0.22802	0.21010	0.19419
168	532L	2	1	0.21792	0.16882	0.18083	0.19046
169	532R	2	3	0.31381	0.24645	0.23819	0.19971
170	533L	2	3	0.28737	0.22928	0.21295	0.20745
171	533R	2	3	0.31562	0.26557	0.25893	0.24981
172	536L	2	1	0.26479	0.23912	0.25175	0.26095
173	536R	2	3	0.29095	0.23886	0.24026	0.22283
174	537R	2	1	0.22582	0.18231	0.18721	0.19324
175	539L	2	1	0.24586	0.20693	0.20759	0.22180
176	546L	2	1	0.23657	0.21161	0.21945	0.23763
177	546R	2	1	0.22645	0.19158	0.19704	0.19668
178	689R	2	3	0.29043	0.23762	0.23850	0.20754
179	692L	2	3	0.29620	0.24361	0.24691	0.23191
180	694L	2	3	0.26521	0.22306	0.22549	0.22212
181	701R	2	3	0.30270	0.23371	0.21511	0.17443
182	177L	3	C	0.25729	0.21228	0.18725	0.17570
183	177R	3	C	0.32818	0.26673	0.25909	0.20382
184	206L	3	C	0.32612	0.26953	0.23399	0.19633
185	207R	3	2	0.27965	0.24248	0.22802	0.22893
186	212L	3	C	0.30255	0.24259	0.21905	0.18392
187	215L	3	C	0.27519	0.21544	0.19303	0.15362
188	215R	3	C	0.27466	0.21115	0.17884	0.14286
189	513L	3	C	0.29927	0.23768	0.21212	0.17753
190	513R	3	C	0.33445	0.28457	0.25687	0.24472
191	519L	3	2	0.24047	0.22533	0.21959	0.22027
192	519R	3	1	0.20825	0.17987	0.18371	0.18523
193	526L	3	C	0.29132	0.24159	0.21560	0.18841
194	52R	3	C	0.27449	0.22462	0.20762	0.19080
195	534R	3	C	0.27833	0.22748	0.20538	0.18952
196	538L	3	C	0.27088	0.21238	0.19998	0.19880
197	538R	3	C	0.24470	0.17480	0.16751	0.16740
198	547L	3	C	0.30102	0.24496	0.23037	0.21473
199	547R	3	C	0.30152	0.24089	0.21175	0.17029
200	549R	3	C	0.25815	0.18249	0.16886	0.14366
201	62R	3	C	0.34331	0.29481	0.26841	0.21338
202	697L	3	C	0.40985	0.35370	0.32872	0.27043
203	712L	3	C	0.28228	0.22778	0.21265	0.19510

A.2 LOOCV Results for Coronal Projection Analysis

Table A.2: LOOCV results for coronal projection analysis.

Subjects	Patient	Truth	Predicted	Distance G0	Distance G1	Distance G2	Distance G3
1	003L	0	2	0.28086	0.28439	0.25920	0.32155
2	003R	0	1	0.33514	0.31113	0.34970	0.36781
3	005R	0	1	0.24242	0.21696	0.22325	0.22788
4	007L	0	1	0.22502	0.21643	0.22076	0.25810
5	007R	0	C	0.21799	0.22162	0.23072	0.25367
6	008R	0	C	0.32382	0.32547	0.34115	0.38194
7	009L	0	C	0.24479	0.27100	0.26864	0.31855
8	013R	0	1	0.22203	0.21448	0.24455	0.26029
9	016R	0	C	0.32814	0.34039	0.35061	0.37993
10	025L	0	C	0.31490	0.34688	0.34538	0.40852
11	029R	0	C	0.24596	0.26042	0.28721	0.32329
12	037L	0	2	0.31360	0.30858	0.27402	0.32656
13	037R	0	1	0.35607	0.33013	0.35703	0.36682
14	046L	0	2	0.25394	0.26263	0.24311	0.29939
15	046R	0	1	0.26213	0.25521	0.28845	0.30333
16	049L	0	2	0.28726	0.29742	0.26956	0.33768
17	053L	0	C	0.27676	0.30441	0.29630	0.36990
18	053R	0	C	0.26989	0.30212	0.32394	0.37937
19	055L	0	C	0.24572	0.26949	0.26504	0.32110
20	055R	0	C	0.24783	0.26653	0.29939	0.34627
21	067R	0	C	0.17856	0.19622	0.22319	0.27701
22	073R	0	1	0.44296	0.42542	0.45640	0.46221
23	076L	0	C	0.39375	0.42060	0.42292	0.47830
24	078L	0	C	0.29280	0.31764	0.31921	0.37313
25	079R	0	1	0.29376	0.27539	0.31981	0.33398
26	084L	0	2	0.22150	0.23242	0.21114	0.26703
27	084R	0	1	0.19840	0.19524	0.21982	0.25266
28	088R	0	C	0.24116	0.24626	0.28521	0.32312
29	089R	0	1	0.33426	0.30917	0.34079	0.32874
30	093L	0	C	0.24550	0.28162	0.27299	0.34955
31	096L	0	2	0.26523	0.27923	0.25728	0.31603
32	113R	0	1	0.20672	0.19730	0.22465	0.24904
33	131R	0	1	0.32313	0.31859	0.36156	0.38452
34	135R	0	1	0.31727	0.31118	0.35549	0.37986
35	154R	0	1	0.27311	0.26224	0.30730	0.33841
36	160L	0	2	0.25838	0.24471	0.22051	0.26762
37	175L	0	2	0.24694	0.26594	0.24490	0.30665
38	183L	0	C	0.29717	0.32242	0.32054	0.38887
39	186R	0	C	0.20570	0.22666	0.25687	0.30085
40	188R	0	1	0.22134	0.19729	0.22972	0.23588
41	192L	0	C	0.24237	0.25799	0.24282	0.29337
42	200L	0	2	0.38473	0.39224	0.37850	0.41708
43	201R	0	1	0.43631	0.41716	0.43954	0.44326
44	203L	0	2	0.38789	0.39301	0.37638	0.42234
45	204L	0	2	0.24885	0.25013	0.22121	0.26180
46	205L	0	2	0.24300	0.25542	0.23767	0.30016
47	205R	0	1	0.24846	0.22889	0.25989	0.28707
48	211R	0	1	0.34600	0.31603	0.32949	0.33692
49	217L	0	2	0.32315	0.32010	0.29344	0.33976
50	220L	0	C	0.23287	0.24103	0.24075	0.28240
51	220R	0	1	0.36151	0.35387	0.38814	0.42305

Table A.2: LOOCV results for coronal projection analysis (continuted).

Subjects	Patient	Truth	Predicted	Distance G0	Distance G1	Distance G2	Distance G3
52	505L	0	C	0.32317	0.33844	0.32506	0.38423
53	505R	0	C	0.21846	0.23640	0.27092	0.31477
54	508R	0	1	0.22887	0.19400	0.21724	0.21221
55	511L	0	2	0.27978	0.26842	0.23985	0.25410
56	523L	0	2	0.26159	0.26803	0.23495	0.30105
57	528R	0	C	0.24703	0.24897	0.25697	0.29199
58	529L	0	C	0.24719	0.27896	0.27012	0.34938
59	529R	0	C	0.20489	0.23472	0.25887	0.31725
60	535L	0	2	0.32675	0.32926	0.30070	0.35562
61	535R	0	1	0.24428	0.21377	0.23537	0.24278
62	542L	0	2	0.26189	0.26812	0.24027	0.28154
63	542R	0	C	0.22516	0.23048	0.22830	0.27530
64	554L	0	2	0.26319	0.26216	0.24876	0.29894
65	554R	0	1	0.20857	0.18984	0.21376	0.21292
66	700R	0	2	0.20695	0.18858	0.18463	0.20137
67	702L	0	2	0.24747	0.25772	0.23559	0.28825
68	702R	0	2	0.21681	0.21015	0.19978	0.22245
69	704R	0	1	0.20812	0.17519	0.20549	0.21471
70	705L	0	2	0.24122	0.21871	0.19146	0.21031
71	710L	0	2	0.23095	0.21500	0.18634	0.20098
72	006L	1	2	0.19745	0.20183	0.18682	0.24161
73	012L	1	2	0.24314	0.24130	0.21528	0.26197
74	012R	1	C	0.22559	0.20003	0.22728	0.23639
75	018L	1	2	0.34892	0.36863	0.34067	0.39808
76	018R	1	C	0.31824	0.31258	0.33773	0.35382
77	022L	1	2	0.34737	0.36318	0.34221	0.40541
78	022R	1	0	0.24860	0.26482	0.28890	0.33734
79	023L	1	2	0.36278	0.38352	0.35565	0.41839
80	023R	1	C	0.38418	0.37496	0.41095	0.42263
81	027R	1	3	0.30901	0.25967	0.26712	0.21245
82	047L	1	2	0.37979	0.37800	0.35963	0.38821
83	047R	1	C	0.33986	0.33188	0.36748	0.39257
84	049R	1	C	0.26801	0.26243	0.29819	0.31934
85	056L	1	2	0.20209	0.20482	0.18038	0.24056
86	057R	1	C	0.25413	0.21608	0.23854	0.23371
87	060L	1	2	0.21162	0.21451	0.19617	0.24128
88	069R	1	C	0.34921	0.33355	0.36413	0.37959
89	070R	1	C	0.24639	0.21802	0.25235	0.25381
90	075R	1	C	0.23346	0.20087	0.22644	0.22623
91	082L	1	0	0.19505	0.21276	0.19965	0.24446
92	086L	1	2	0.28036	0.28626	0.25660	0.30964
93	094R	1	C	0.25115	0.24128	0.27188	0.29533
94	095R	1	C	0.37234	0.34866	0.37549	0.35657
95	098R	1	C	0.29082	0.26533	0.29533	0.27846
96	124R	1	C	0.31915	0.31504	0.35795	0.37648
97	133L	1	2	0.30893	0.30580	0.26533	0.30999
98	133R	1	C	0.28301	0.26577	0.27610	0.28204
99	163R	1	C	0.31284	0.29222	0.32592	0.32287
100	181L	1	0	0.22179	0.24898	0.23639	0.28925
101	184L	1	0	0.20353	0.22887	0.22299	0.27715
102	190L	1	2	0.23679	0.23195	0.20770	0.23107
103	197R	1	C	0.22832	0.20445	0.23572	0.24149
104	199L	1	2	0.23241	0.23588	0.20756	0.24155
105	200R	1	C	0.24099	0.20771	0.21988	0.23136
106	203R	1	2	0.55883	0.55673	0.55258	0.57444

Table A.2: LOOCV results for coronal projection analysis (continuted).

Subjects	Patient	Truth	Predicted	Distance G0	Distance G1	Distance G2	Distance G3
107	204R	1	C	0.27161	0.24118	0.25680	0.25940
108	209R	1	3	0.23929	0.20219	0.20694	0.18891
109	210L	1	2	0.26898	0.24140	0.19935	0.19971
110	219L	1	2	0.25004	0.25772	0.23339	0.25626
111	507L	1	2	0.23235	0.21175	0.17066	0.19654
112	507R	1	C	0.24234	0.20512	0.21999	0.21594
113	509R	1	C	0.25562	0.22636	0.24390	0.25356
114	511R	1	C	0.21763	0.17643	0.18393	0.18087
115	512R	1	C	0.19852	0.18380	0.21527	0.23104
116	514L	1	2	0.24297	0.24775	0.22584	0.28544
117	515L	1	2	0.18930	0.18156	0.15271	0.18831
118	515R	1	C	0.21811	0.18043	0.20271	0.18689
119	516L	1	2	0.29719	0.28651	0.24374	0.27136
120	516R	1	C	0.25784	0.22311	0.24297	0.24154
121	517L	1	2	0.32981	0.32642	0.29699	0.32648
122	517R	1	C	0.22423	0.18929	0.20083	0.20342
123	521L	1	2	0.27068	0.27385	0.24407	0.30153
124	522R	1	C	0.23089	0.19827	0.21322	0.22996
125	523R	1	3	0.23350	0.19193	0.19580	0.18148
126	527L	1	2	0.34200	0.34476	0.32551	0.36378
127	527R	1	C	0.24030	0.21627	0.23207	0.25688
128	534L	1	2	0.43163	0.42075	0.40211	0.41239
129	539R	1	C	0.25889	0.23688	0.26034	0.25645
130	540L	1	2	0.21779	0.20317	0.18427	0.19182
131	541L	1	2	0.40456	0.40632	0.37313	0.40555
132	541R	1	C	0.23000	0.20074	0.21694	0.22215
133	543L	1	2	0.21939	0.21194	0.17260	0.22193
134	543R	1	C	0.22622	0.19944	0.21432	0.21016
135	574R	1	3	0.24496	0.22940	0.23177	0.21476
136	691L	1	2	0.26837	0.28096	0.25662	0.32155
137	691R	1	2	0.22643	0.21899	0.21607	0.24683
138	699R	1	C	0.18119	0.15832	0.17204	0.17910
139	700L	1	2	0.21302	0.20543	0.17332	0.19520
140	703R	1	C	0.26571	0.22884	0.24952	0.24286
141	704L	1	2	0.25693	0.25751	0.21925	0.27642
142	710R	1	C	0.23030	0.20112	0.21922	0.22196
143	711L	1	2	0.26791	0.25516	0.22992	0.25516
144	713L	1	2	0.26600	0.26958	0.23724	0.29337
145	713R	1	C	0.27683	0.24063	0.26589	0.26204
146	717R	1	C	0.20446	0.19254	0.20303	0.22407
147	002L	2	C	0.32194	0.30172	0.26795	0.28798
148	010L	2	3	0.42424	0.40086	0.37986	0.37099
149	026L	2	C	0.37841	0.37131	0.36196	0.37781
150	029L	2	0	0.40317	0.44295	0.47490	0.52342
151	065L	2	C	0.27996	0.27294	0.25190	0.29140
152	066L	2	C	0.24080	0.24369	0.22503	0.27253
153	189L	2	C	0.23295	0.21134	0.20870	0.22220
154	208L	2	C	0.36664	0.34942	0.32248	0.33377
155	214R	2	1	0.24106	0.21255	0.24496	0.23640
156	216L	2	C	0.23993	0.23914	0.22565	0.27907
157	219R	2	3	0.26933	0.24391	0.26548	0.24217
158	506L	2	C	0.24925	0.24591	0.22117	0.26169
159	509L	2	C	0.23581	0.22883	0.20439	0.24114
160	518L	2	C	0.22911	0.22268	0.19729	0.21184
161	518R	2	3	0.22723	0.20267	0.18545	0.17703

Table A.2: LOOCV results for coronal projection analysis (continuted).

Subjects	Patient	Truth	Predicted	Distance G0	Distance G1	Distance G2	Distance G3
162	520L	2	C	0.19537	0.18208	0.15387	0.18198
163	520R	2	1	0.24277	0.21660	0.22586	0.22856
164	522L	2	C	0.32899	0.31477	0.28734	0.31180
165	525L	2	3	0.29223	0.26556	0.23503	0.21834
166	526R	2	1	0.22360	0.17785	0.20423	0.18148
167	530R	2	1	0.31696	0.28700	0.30466	0.30091
168	532L	2	C	0.24446	0.23309	0.21162	0.22064
169	532R	2	3	0.29263	0.24451	0.24054	0.18731
170	533L	2	C	0.33257	0.31987	0.29529	0.32533
171	533R	2	3	0.27369	0.23694	0.25852	0.22984
172	536L	2	C	0.33485	0.33194	0.31178	0.35498
173	536R	2	1	0.27612	0.24001	0.25203	0.25520
174	537R	2	1	0.25468	0.21539	0.24321	0.24251
175	539L	2	C	0.21968	0.21581	0.18953	0.21732
176	546L	2	C	0.23064	0.23327	0.21240	0.25459
177	546R	2	1	0.22140	0.19761	0.21532	0.21955
178	689R	2	3	0.27471	0.23349	0.25797	0.23143
179	692L	2	C	0.38743	0.38623	0.38027	0.39683
180	694L	2	C	0.25253	0.24003	0.20935	0.21795
181	701R	2	3	0.34985	0.31102	0.32918	0.28647
182	177L	3	2	0.26895	0.24086	0.19675	0.21335
183	177R	3	C	0.36423	0.31984	0.31964	0.28488
184	206L	3	C	0.48563	0.46195	0.44714	0.44621
185	207R	3	1	0.29138	0.26867	0.28054	0.27936
186	212L	3	2	0.29769	0.26833	0.22672	0.23335
187	215L	3	2	0.29228	0.26047	0.21920	0.22737
188	215R	3	C	0.28942	0.23183	0.23340	0.18641
189	513L	3	2	0.27785	0.24903	0.21570	0.21809
190	513R	3	C	0.31024	0.26350	0.25735	0.22741
191	519L	3	2	0.25724	0.24101	0.21215	0.21871
192	519R	3	C	0.25903	0.21926	0.22186	0.20347
193	526L	3	2	0.25082	0.22155	0.18175	0.20186
194	52R	3	1	0.29574	0.26725	0.26729	0.27131
195	534R	3	C	0.27871	0.23297	0.23783	0.20117
196	538L	3	2	0.25154	0.22895	0.18967	0.19251
197	538R	3	C	0.21133	0.17354	0.17808	0.16782
198	547L	3	2	0.27061	0.25129	0.22003	0.23233
199	547R	3	C	0.35153	0.30134	0.30382	0.26768
200	549R	3	C	0.27608	0.23470	0.23291	0.19690
201	62R	3	C	0.44000	0.39975	0.39348	0.35983
202	697L	3	C	0.39748	0.35245	0.31675	0.27644
203	712L	3	C	0.28184	0.25145	0.21181	0.18948

A.3 LOOCV Results for the Y Component of the Surface Normal Analysis

Table A.3: LOOCV results for surface normal analysis.

Subjects	Patient	Truth	Predicted	Distance G0	Distance G1	Distance G2	Distance G3
1	003L	0	C	0.16513	0.18213	0.23739	0.30616
2	003R	0	C	0.19166	0.21855	0.28977	0.34729
3	005R	0	1	0.21654	0.19892	0.26120	0.29890
4	007L	0	C	0.29267	0.31553	0.32867	0.34625
5	007R	0	C	0.22674	0.25396	0.28688	0.31262
6	008R	0	C	0.34969	0.39963	0.42292	0.45092
7	009L	0	C	0.22689	0.26704	0.29365	0.36929
8	013R	0	C	0.17925	0.20367	0.27009	0.32077
9	016R	0	C	0.38761	0.43259	0.45181	0.47000
10	025L	0	C	0.32556	0.38047	0.40980	0.45849
11	029R	0	C	0.35274	0.35279	0.38657	0.45510
12	037L	0	C	0.25551	0.25746	0.27665	0.32360
13	037R	0	C	0.25902	0.27911	0.31897	0.35121
14	046L	0	C	0.21209	0.22944	0.25437	0.30176
15	046R	0	C	0.18171	0.21991	0.28179	0.33002
16	049L	0	C	0.22899	0.25418	0.30300	0.36405
17	053L	0	C	0.27641	0.32409	0.36794	0.42697
18	053R	0	C	0.26289	0.32623	0.36647	0.41650
19	055L	0	C	0.21455	0.27056	0.30893	0.36829
20	055R	0	C	0.26546	0.32799	0.37505	0.41714
21	067R	0	C	0.21204	0.26200	0.31553	0.35916
22	073R	0	C	0.37273	0.41881	0.44350	0.46784
23	076L	0	C	0.35515	0.38810	0.41985	0.49728
24	078L	0	C	0.35506	0.37553	0.40170	0.46980
25	079R	0	C	0.21584	0.21904	0.27133	0.31473
26	084L	0	C	0.24917	0.28892	0.33162	0.38287
27	084R	0	C	0.23525	0.26556	0.32269	0.38104
28	088R	0	C	0.24234	0.28178	0.35107	0.41088
29	089R	0	C	0.20436	0.20753	0.25923	0.30090
30	093L	0	C	0.22647	0.26816	0.31556	0.38814
31	096L	0	C	0.24560	0.24890	0.26914	0.32092
32	113R	0	C	0.20386	0.21217	0.27338	0.33210
33	131R	0	C	0.22895	0.27323	0.32601	0.38513
34	135R	0	C	0.28089	0.31320	0.38117	0.44001
35	154R	0	C	0.19246	0.21487	0.28760	0.34928
36	160L	0	2	0.28753	0.26630	0.25374	0.31625
37	175L	0	C	0.17570	0.21647	0.24127	0.30740
38	183L	0	C	0.27301	0.32309	0.35571	0.40579
39	186R	0	C	0.16894	0.18342	0.22537	0.28337
40	188R	0	C	0.22569	0.24715	0.29539	0.32409
41	192L	0	2	0.31481	0.31634	0.30914	0.36935
42	200L	0	C	0.29095	0.31575	0.31964	0.33986
43	201R	0	C	0.23085	0.26917	0.30298	0.33406
44	203L	0	C	0.30279	0.31516	0.32780	0.34993
45	204L	0	C	0.19353	0.20033	0.22175	0.26994
46	205L	0	C	0.25536	0.26920	0.31208	0.36727
47	205R	0	C	0.22458	0.24769	0.31460	0.35403
48	211R	0	C	0.26009	0.27071	0.28855	0.32249
49	217L	0	2	0.26167	0.24072	0.20895	0.21864

Table A.3: LOOCV results for surface normal analysis (continuted).

Subjects	Patient	Truth	Predicted	Distance G0	Distance G1	Distance G2	Distance G3
50	220L	0	1	0.36498	0.35531	0.37229	0.43640
51	220R	0	C	0.18457	0.21449	0.26814	0.33683
52	505L	0	C	0.25069	0.28536	0.31075	0.35446
53	505R	0	C	0.21581	0.24922	0.30193	0.36772
54	508R	0	1	0.23589	0.21097	0.27119	0.30735
55	511L	0	1	0.31294	0.29469	0.30726	0.35611
56	523L	0	C	0.21735	0.22497	0.26370	0.30850
57	528R	0	C	0.35993	0.37956	0.38292	0.38468
58	529L	0	C	0.22431	0.24340	0.29150	0.36399
59	529R	0	C	0.20706	0.22682	0.27657	0.32250
60	535L	0	C	0.22595	0.24799	0.27543	0.32396
61	535R	0	1	0.24781	0.23587	0.27964	0.32279
62	542L	0	C	0.29451	0.31842	0.32583	0.34248
63	542R	0	C	0.13243	0.15470	0.21575	0.27947
64	554L	0	2	0.22751	0.23250	0.21830	0.25704
65	554R	0	1	0.21261	0.20851	0.22237	0.27354
66	700R	0	1	0.20427	0.17955	0.23661	0.28741
67	702L	0	C	0.24081	0.26660	0.29051	0.32657
68	702R	0	C	0.21890	0.23493	0.29323	0.32854
69	704R	0	1	0.23472	0.22554	0.28661	0.33369
70	705L	0	1	0.22749	0.22189	0.25171	0.30142
71	710L	0	2	0.37262	0.34053	0.33244	0.37212
72	006L	1	0	0.22724	0.25010	0.27721	0.31163
73	012L	1	C	0.21190	0.18617	0.20418	0.25139
74	012R	1	C	0.21368	0.20735	0.26818	0.31052
75	018L	1	0	0.22895	0.26398	0.29601	0.34954
76	018R	1	0	0.32340	0.36965	0.38545	0.40548
77	022L	1	0	0.22554	0.26934	0.30996	0.36321
78	022R	1	0	0.26261	0.31457	0.36591	0.40104
79	023L	1	0	0.21353	0.25060	0.28420	0.33700
80	023R	1	0	0.23678	0.25579	0.31887	0.36004
81	027R	1	3	0.39302	0.32122	0.29790	0.26299
82	047L	1	2	0.35573	0.36904	0.34993	0.35224
83	047R	1	0	0.22581	0.26987	0.32019	0.36297
84	049R	1	0	0.25923	0.28873	0.35400	0.40059
85	056L	1	0	0.23281	0.26371	0.28813	0.31708
86	057R	1	C	0.20463	0.18671	0.21791	0.25843
87	060L	1	0	0.21165	0.21249	0.22662	0.29359
88	069R	1	0	0.19298	0.20286	0.25543	0.29171
89	070R	1	C	0.28980	0.24491	0.26308	0.30855
90	075R	1	C	0.27963	0.24645	0.25768	0.30193
91	082L	1	C	0.27977	0.26336	0.27498	0.32861
92	086L	1	0	0.25532	0.25995	0.25577	0.31214
93	094R	1	0	0.23047	0.27389	0.31379	0.34379
94	095R	1	0	0.40158	0.43194	0.42693	0.42683
95	098R	1	C	0.19806	0.18362	0.21778	0.25657
96	124R	1	0	0.22172	0.22684	0.28797	0.34530
97	133L	1	2	0.24257	0.23372	0.23187	0.24564
98	133R	1	3	0.36580	0.37615	0.37112	0.35846
99	163R	1	0	0.22457	0.24717	0.29367	0.33334
100	181L	1	0	0.19665	0.20689	0.24034	0.30718
101	184L	1	0	0.15934	0.18904	0.22393	0.28360
102	190L	1	2	0.19790	0.17040	0.15532	0.20400
103	197R	1	C	0.32918	0.27643	0.30359	0.33016
104	199L	1	C	0.23156	0.22100	0.23602	0.29230

Table A.3: LOOCV results for surface normal analysis (continuted).

Subjects	Patient	Truth	Predicted	Distance G0	Distance G1	Distance G2	Distance G3
105	200R	1	C	0.19930	0.18808	0.20231	0.23743
106	203R	1	C	0.24394	0.22550	0.26767	0.33240
107	204R	1	C	0.18589	0.18496	0.21525	0.24532
108	209R	1	2	0.43685	0.39841	0.37036	0.39507
109	210L	1	2	0.31027	0.26043	0.24187	0.24343
110	219L	1	C	0.22610	0.20849	0.22803	0.27443
111	507L	1	2	0.31593	0.28948	0.25502	0.29314
112	507R	1	C	0.30743	0.25605	0.25636	0.27107
113	509R	1	C	0.29451	0.25865	0.30144	0.31782
114	511R	1	C	0.22461	0.20105	0.24430	0.27554
115	512R	1	C	0.24566	0.21473	0.25931	0.31019
116	514L	1	0	0.22730	0.24864	0.26725	0.29750
117	515L	1	C	0.19426	0.18136	0.20634	0.25917
118	515R	1	C	0.21710	0.18298	0.22035	0.25273
119	516L	1	2	0.34341	0.31463	0.27928	0.30566
120	516R	1	C	0.31751	0.27860	0.29198	0.33049
121	517L	1	0	0.33086	0.33863	0.34036	0.34328
122	517R	1	C	0.32181	0.27188	0.27930	0.31088
123	521L	1	C	0.24467	0.23904	0.25659	0.29645
124	522R	1	C	0.19666	0.17112	0.19744	0.23187
125	523R	1	C	0.31768	0.26903	0.27011	0.29624
126	527L	1	0	0.33141	0.35656	0.35913	0.38275
127	527R	1	C	0.21963	0.19952	0.24688	0.27702
128	534L	1	3	0.36349	0.36948	0.35408	0.34748
129	539R	1	C	0.29174	0.25460	0.29188	0.34401
130	540L	1	3	0.35285	0.35242	0.34085	0.32920
131	541L	1	0	0.30774	0.31435	0.31314	0.31900
132	541R	1	C	0.32869	0.28120	0.28417	0.32126
133	543L	1	2	0.27863	0.23586	0.21323	0.23267
134	543R	1	2	0.31759	0.27231	0.27007	0.29543
135	574R	1	0	0.25525	0.28252	0.30434	0.31718
136	691L	1	C	0.23672	0.23571	0.25494	0.30870
137	691R	1	0	0.29021	0.29809	0.31858	0.31795
138	699R	1	C	0.17029	0.13727	0.16171	0.21332
139	700L	1	C	0.18500	0.17731	0.18859	0.22741
140	703R	1	C	0.25471	0.23303	0.26098	0.28169
141	704L	1	0	0.25209	0.25634	0.28803	0.32770
142	710R	1	C	0.31512	0.27126	0.28609	0.32782
143	711L	1	2	0.27220	0.26328	0.26207	0.26960
144	713L	1	0	0.23987	0.24693	0.27579	0.31445
145	713R	1	0	0.22518	0.23198	0.28290	0.30593
146	717R	1	0	0.19537	0.21781	0.26737	0.30583
147	002L	2	3	0.34668	0.30930	0.29590	0.27668
148	010L	2	3	0.46140	0.44607	0.42444	0.37029
149	026L	2	0	0.41846	0.43527	0.43304	0.42436
150	029L	2	3	0.43981	0.45304	0.44573	0.42527
151	065L	2	C	0.22606	0.20205	0.19730	0.24023
152	066L	2	C	0.22808	0.23116	0.21735	0.21995
153	189L	2	0	0.26676	0.26931	0.28009	0.28487
154	208L	2	3	0.43522	0.42527	0.41390	0.37992
155	214R	2	1	0.25979	0.21911	0.23716	0.26756
156	216L	2	1	0.27100	0.24931	0.26025	0.31746
157	219R	2	1	0.22419	0.17387	0.18408	0.20470
158	506L	2	1	0.27232	0.24853	0.25065	0.25887
159	509L	2	1	0.28348	0.26522	0.26959	0.31286

Table A.3: LOOCV results for surface normal analysis (continuted).

Subjects	Patient	Truth	Predicted	Distance G0	Distance G1	Distance G2	Distance G3
160	518L	2	C	0.31588	0.29451	0.27946	0.30709
161	518R	2	3	0.32623	0.29753	0.30660	0.27269
162	520L	2	C	0.28414	0.24948	0.21839	0.24602
163	520R	2	1	0.42482	0.40716	0.41035	0.43707
164	522L	2	3	0.29816	0.27672	0.26814	0.25401
165	525L	2	1	0.30593	0.29116	0.29798	0.29228
166	526R	2	1	0.29990	0.24010	0.24510	0.25851
167	530R	2	3	0.28159	0.26224	0.26100	0.23648
168	532L	2	1	0.26065	0.22257	0.22829	0.27163
169	532R	2	C	0.37564	0.31993	0.30711	0.30823
170	533L	2	1	0.30165	0.27385	0.27645	0.29151
171	533R	2	1	0.34448	0.28787	0.30716	0.32864
172	536L	2	1	0.26038	0.23078	0.23336	0.27561
173	536R	2	1	0.34739	0.29067	0.29340	0.31087
174	537R	2	1	0.29847	0.24342	0.26257	0.28096
175	539L	2	1	0.25653	0.25639	0.27812	0.29839
176	546L	2	1	0.25338	0.24007	0.24418	0.28975
177	546R	2	1	0.25586	0.21015	0.21774	0.23484
178	689R	2	1	0.29855	0.29085	0.31506	0.30234
179	692L	2	3	0.48266	0.50043	0.49347	0.47367
180	694L	2	C	0.37864	0.35419	0.35012	0.38352
181	701R	2	3	0.38112	0.36509	0.36593	0.32607
182	177L	3	C	0.29588	0.27484	0.25052	0.23883
183	177R	3	C	0.44442	0.42541	0.39742	0.36443
184	206L	3	C	0.54345	0.54103	0.50861	0.49511
185	207R	3	2	0.37147	0.31391	0.30669	0.32743
186	212L	3	C	0.33260	0.27229	0.22748	0.21436
187	215L	3	C	0.33385	0.27523	0.23398	0.22549
188	215R	3	C	0.35322	0.27999	0.26382	0.23526
189	513L	3	C	0.32337	0.28781	0.26817	0.25626
190	513R	3	C	0.37008	0.30803	0.28564	0.26307
191	519L	3	2	0.31689	0.26019	0.21046	0.23389
192	519R	3	2	0.26206	0.20736	0.20268	0.21409
193	526L	3	C	0.32739	0.28320	0.26015	0.25289
194	52R	3	C	0.49796	0.50636	0.48740	0.48076
195	534R	3	2	0.38819	0.33095	0.29952	0.31019
196	538L	3	2	0.31359	0.27808	0.24492	0.29099
197	538R	3	2	0.23454	0.19667	0.19133	0.21487
198	547L	3	2	0.40032	0.35836	0.30405	0.32853
199	547R	3	C	0.38193	0.32082	0.28983	0.23856
200	549R	3	C	0.29303	0.26794	0.27773	0.26646
201	62R	3	C	0.52379	0.50693	0.46756	0.42939
202	697L	3	C	0.43968	0.37383	0.32703	0.27987
203	712L	3	2	0.25560	0.21262	0.19672	0.20964

A.4 LOOCV Results for Combination of Gaussian Curvature and Coronal Projection

Table A.4: LOOCV results for Gaussian curvature and coronal projection.

Subjects	Patient	Truth	Predicted	Distance G0	Distance G1	Distance G2	Distance G3
1	003L	0	C	0.2901	0.2973	0.2986	0.3433
2	003R	0	C	0.3173	0.3208	0.3518	0.3859
3	005R	0	1	0.2978	0.2893	0.3021	0.3128
4	007L	0	1	0.3311	0.3229	0.3309	0.3487
5	007R	0	1	0.3215	0.3195	0.3300	0.3433
6	008R	0	C	0.3103	0.3210	0.3407	0.3757
7	009L	0	C	0.3937	0.4139	0.4221	0.4655
8	013R	0	C	0.2945	0.3051	0.3297	0.3537
9	016R	0	C	0.3273	0.3534	0.3661	0.3962
10	025L	0	C	0.3304	0.3630	0.3721	0.4242
11	029R	0	C	0.3467	0.3645	0.3904	0.4255
12	037L	0	2	0.3177	0.3201	0.3086	0.3478
13	037R	0	1	0.3548	0.3508	0.3712	0.3932
14	046L	0	2	0.2559	0.2552	0.2498	0.2901
15	046R	0	1	0.2688	0.2650	0.2896	0.3143
16	049L	0	C	0.2649	0.2725	0.2713	0.3290
17	053L	0	C	0.2709	0.3054	0.3124	0.3712
18	053R	0	C	0.2837	0.3295	0.3401	0.3986
19	055L	0	C	0.2562	0.2853	0.2848	0.3273
20	055R	0	C	0.3026	0.3320	0.3546	0.3909
21	067R	0	C	0.2168	0.2439	0.2637	0.3117
22	073R	0	1	0.3600	0.3513	0.3768	0.3947
23	076L	0	C	0.3968	0.4393	0.4389	0.4947
24	078L	0	C	0.3165	0.3484	0.3575	0.4022
25	079R	0	C	0.2528	0.2598	0.2905	0.3238
26	084L	0	2	0.2619	0.2636	0.2593	0.2938
27	084R	0	1	0.2735	0.2678	0.2867	0.3134
28	088R	0	C	0.2837	0.2952	0.3209	0.3571
29	089R	0	1	0.2869	0.2775	0.3048	0.3090
30	093L	0	C	0.2344	0.2717	0.2788	0.3413
31	096L	0	C	0.2503	0.2632	0.2634	0.3052
32	113R	0	C	0.2161	0.2201	0.2424	0.2705
33	131R	0	C	0.3011	0.3283	0.3580	0.3919
34	135R	0	C	0.3061	0.3250	0.3579	0.3912
35	154R	0	1	0.2458	0.2455	0.2803	0.3190
36	160L	0	2	0.2422	0.2300	0.2288	0.2577
37	175L	0	C	0.2606	0.2774	0.2673	0.3118
38	183L	0	C	0.2512	0.2752	0.2818	0.3456
39	186R	0	C	0.2522	0.2733	0.2936	0.3279
40	188R	0	1	0.2322	0.2054	0.2431	0.2531
41	192L	0	C	0.2413	0.2590	0.2610	0.3027
42	200L	0	2	0.3061	0.3050	0.3019	0.3316
43	201R	0	1	0.3448	0.3351	0.3539	0.3697
44	203L	0	2	0.3268	0.3241	0.3143	0.3498
45	204L	0	2	0.2482	0.2345	0.2145	0.2420
46	205L	0	2	0.2455	0.2482	0.2441	0.2894
47	205R	0	1	0.2380	0.2223	0.2485	0.2749
48	211R	0	1	0.3096	0.2863	0.2903	0.2966
49	217L	0	2	0.2729	0.2566	0.2422	0.2743
50	220L	0	C	0.2213	0.2433	0.2453	0.2897

Table A.4: LOOCV results for Gaussian curvature and coronal projection (continuted).

Subjects	Patient	Truth	Predicted	Distance G0	Distance G1	Distance G2	Distance G3
51	220R	0	C	0.2982	0.3064	0.3348	0.3709
52	505L	0	C	0.2980	0.3118	0.3109	0.3553
53	505R	0	C	0.2453	0.2674	0.2987	0.3388
54	508R	0	1	0.2498	0.2061	0.2274	0.2292
55	511L	0	2	0.2747	0.2432	0.2308	0.2432
56	523L	0	2	0.2516	0.2374	0.2263	0.2672
57	528R	0	1	0.2435	0.2301	0.2441	0.2693
58	529L	0	C	0.2702	0.2924	0.2944	0.3564
59	529R	0	C	0.2312	0.2590	0.2803	0.3246
60	535L	0	2	0.2821	0.2739	0.2623	0.3013
61	535R	0	1	0.2335	0.1999	0.2234	0.2335
62	542L	0	2	0.2478	0.2403	0.2350	0.2576
63	542R	0	1	0.2319	0.2313	0.2459	0.2817
64	554L	0	2	0.2618	0.2592	0.2545	0.2844
65	554R	0	1	0.2407	0.2255	0.2392	0.2409
66	700R	0	1	0.2312	0.2019	0.2170	0.2291
67	702L	0	1	0.2381	0.2359	0.2365	0.2719
68	702R	0	1	0.2277	0.2172	0.2255	0.2396
69	704R	0	1	0.2312	0.2020	0.2239	0.2361
70	705L	0	2	0.2470	0.2265	0.2218	0.2358
71	710L	0	2	0.2513	0.2097	0.2035	0.2088
72	006L	1	0	0.2665	0.2716	0.2698	0.3048
73	012L	1	2	0.3227	0.3262	0.3169	0.3467
74	012R	1	C	0.3048	0.3003	0.3149	0.3289
75	018L	1	0	0.3609	0.3825	0.3741	0.4199
76	018R	1	0	0.3489	0.3614	0.3841	0.4029
77	022L	1	0	0.3682	0.3830	0.3828	0.4245
78	022R	1	0	0.3175	0.3360	0.3570	0.3955
79	023L	1	0	0.3679	0.3849	0.3803	0.4247
80	023R	1	0	0.3701	0.3812	0.4070	0.4359
81	027R	1	3	0.3906	0.3778	0.3700	0.3540
82	047L	1	2	0.3094	0.3018	0.2944	0.3119
83	047R	1	C	0.3032	0.2916	0.3184	0.3473
84	049R	1	0	0.2582	0.2624	0.2931	0.3278
85	056L	1	2	0.1875	0.1788	0.1665	0.2157
86	057R	1	C	0.2306	0.1980	0.2103	0.2193
87	060L	1	0	0.2222	0.2306	0.2331	0.2644
88	069R	1	C	0.2948	0.2872	0.3121	0.3316
89	070R	1	C	0.2299	0.2040	0.2286	0.2392
90	075R	1	C	0.2192	0.2039	0.2243	0.2358
91	082L	1	0	0.2033	0.2035	0.2038	0.2389
92	086L	1	2	0.2452	0.2420	0.2280	0.2743
93	094R	1	C	0.2274	0.2194	0.2412	0.2702
94	095R	1	C	0.3225	0.3038	0.3195	0.3084
95	098R	1	C	0.2617	0.2436	0.2681	0.2660
96	124R	1	0	0.2958	0.2984	0.3302	0.3573
97	133L	1	2	0.2554	0.2435	0.2214	0.2511
98	133R	1	C	0.2511	0.2407	0.2514	0.2578
99	163R	1	C	0.2986	0.2829	0.3050	0.3149
100	181L	1	0	0.2462	0.2592	0.2595	0.2993
101	184L	1	0	0.2022	0.2168	0.2194	0.2713
102	190L	1	2	0.2313	0.2329	0.2311	0.2485
103	197R	1	C	0.2451	0.2189	0.2371	0.2524
104	199L	1	2	0.2236	0.2171	0.2071	0.2370
105	200R	1	C	0.2273	0.2050	0.2147	0.2247

Table A.4: LOOCV results for Gaussian curvature and coronal projection (continuted).

Subjects	Patient	Truth	Predicted	Distance G0	Distance G1	Distance G2	Distance G3
106	203R	1	C	0.4245	0.4228	0.4251	0.4501
107	204R	1	C	0.2585	0.2305	0.2375	0.2398
108	209R	1	3	0.2377	0.1903	0.1881	0.1738
109	210L	1	3	0.2776	0.2359	0.2113	0.1974
110	219L	1	2	0.2538	0.2469	0.2364	0.2549
111	507L	1	2	0.2501	0.2148	0.1881	0.2021
112	507R	1	3	0.2663	0.2193	0.2256	0.2188
113	509R	1	2	0.2871	0.2474	0.2472	0.2566
114	511R	1	C	0.2444	0.1925	0.2008	0.1946
115	512R	1	C	0.2185	0.1945	0.2146	0.2334
116	514L	1	2	0.2598	0.2413	0.2307	0.2636
117	515L	1	2	0.2376	0.2108	0.2056	0.2189
118	515R	1	C	0.2620	0.2177	0.2315	0.2208
119	516L	1	2	0.3041	0.2700	0.2357	0.2420
120	516R	1	C	0.2871	0.2421	0.2489	0.2482
121	517L	1	2	0.3297	0.3009	0.2751	0.2861
122	517R	1	3	0.2782	0.2300	0.2302	0.2300
123	521L	1	2	0.2519	0.2403	0.2283	0.2704
124	522R	1	C	0.2197	0.1941	0.2083	0.2247
125	523R	1	3	0.2550	0.2033	0.2037	0.1881
126	527L	1	2	0.3108	0.2984	0.2849	0.3136
127	527R	1	C	0.2377	0.2074	0.2198	0.2417
128	534L	1	2	0.3596	0.3393	0.3221	0.3257
129	539R	1	C	0.2408	0.2165	0.2379	0.2487
130	540L	1	3	0.2399	0.2116	0.1994	0.1951
131	541L	1	2	0.3446	0.3315	0.3111	0.3273
132	541R	1	C	0.2545	0.2175	0.2233	0.2317
133	543L	1	2	0.2423	0.2165	0.1919	0.2091
134	543R	1	C	0.2461	0.2156	0.2213	0.2167
135	574R	1	3	0.2409	0.2184	0.2288	0.2170
136	691L	1	2	0.2659	0.2638	0.2597	0.3075
137	691R	1	2	0.2432	0.2127	0.2100	0.2265
138	699R	1	C	0.2003	0.1747	0.1894	0.1961
139	700L	1	2	0.2371	0.2141	0.2037	0.2173
140	703R	1	C	0.2665	0.2277	0.2377	0.2370
141	704L	1	2	0.2558	0.2432	0.2216	0.2582
142	710R	1	C	0.2400	0.1977	0.2138	0.2172
143	711L	1	2	0.2986	0.2655	0.2504	0.2583
144	713L	1	2	0.2417	0.2286	0.2194	0.2593
145	713R	1	C	0.2543	0.2151	0.2366	0.2382
146	717R	1	C	0.2410	0.2205	0.2407	0.2510
147	002L	2	C	0.3657	0.3597	0.3464	0.3564
148	010L	2	3	0.4275	0.4172	0.4070	0.3953
149	026L	2	C	0.3448	0.3378	0.3362	0.3432
150	029L	2	0	0.4026	0.4512	0.4806	0.5335
151	065L	2	C	0.2492	0.2418	0.2368	0.2670
152	066L	2	0	0.3447	0.3546	0.3513	0.3780
153	189L	2	1	0.2439	0.2264	0.2343	0.2367
154	208L	2	3	0.3416	0.3035	0.2806	0.2692
155	214R	2	1	0.2418	0.2088	0.2239	0.2252
156	216L	2	C	0.2468	0.2384	0.2360	0.2750
157	219R	2	1	0.2479	0.2164	0.2314	0.2180
158	506L	2	C	0.2725	0.2456	0.2292	0.2451
159	509L	2	C	0.2852	0.2660	0.2529	0.2685
160	518L	2	C	0.2715	0.2444	0.2331	0.2388

Table A.4: LOOCV results for Gaussian curvature and coronal projection (continuted).

Subjects	Patient	Truth	Predicted	Distance G0	Distance G1	Distance G2	Distance G3
161	518R	2	3	0.2552	0.2093	0.1909	0.1747
162	520L	2	C	0.2329	0.2024	0.1829	0.1907
163	520R	2	1	0.2569	0.2200	0.2230	0.2294
164	522L	2	C	0.2907	0.2659	0.2516	0.2591
165	525L	2	3	0.3084	0.2601	0.2364	0.2102
166	526R	2	3	0.2441	0.1960	0.2000	0.1849
167	530R	2	3	0.2919	0.2592	0.2617	0.2532
168	532L	2	C	0.2316	0.2035	0.1968	0.2061
169	532R	2	3	0.3034	0.2455	0.2394	0.1936
170	533L	2	C	0.3108	0.2783	0.2574	0.2728
171	533R	2	3	0.2954	0.2517	0.2587	0.2400
172	536L	2	C	0.3019	0.2893	0.2834	0.3115
173	536R	2	1	0.2836	0.2394	0.2462	0.2396
174	537R	2	1	0.2407	0.1995	0.2170	0.2193
175	539L	2	C	0.2331	0.2114	0.1988	0.2196
176	546L	2	C	0.2336	0.2227	0.2160	0.2463
177	546R	2	1	0.2239	0.1946	0.2064	0.2084
178	689R	2	3	0.2827	0.2356	0.2484	0.2198
179	692L	2	C	0.3449	0.3229	0.3206	0.3250
180	694L	2	C	0.2589	0.2317	0.2176	0.2200
181	701R	2	3	0.3271	0.2751	0.2781	0.2372
182	177L	3	2	0.2632	0.2270	0.1921	0.1954
183	177R	3	C	0.3467	0.2945	0.2909	0.2477
184	206L	3	C	0.4136	0.3782	0.3569	0.3447
185	207R	3	C	0.2856	0.2559	0.2556	0.2554
186	212L	3	C	0.3001	0.2558	0.2229	0.2101
187	215L	3	C	0.2839	0.2390	0.2065	0.1940
188	215R	3	C	0.2821	0.2217	0.2079	0.1661
189	513L	3	C	0.2888	0.2434	0.2139	0.1988
190	513R	3	C	0.3226	0.2742	0.2571	0.2362
191	519L	3	2	0.2490	0.2333	0.2159	0.2195
192	519R	3	C	0.2350	0.2005	0.2037	0.1946
193	526L	3	C	0.2718	0.2318	0.1994	0.1953
194	52R	3	C	0.2853	0.2469	0.2393	0.2345
195	534R	3	C	0.2785	0.2302	0.2222	0.1954
196	538L	3	2	0.2614	0.2208	0.1949	0.1957
197	538R	3	C	0.2286	0.1742	0.1729	0.1676
198	547L	3	C	0.2862	0.2481	0.2253	0.2237
199	547R	3	C	0.3275	0.2728	0.2619	0.2243
200	549R	3	C	0.2673	0.2102	0.2034	0.1723
201	62R	3	C	0.3946	0.3512	0.3368	0.2958
202	697L	3	C	0.4037	0.3531	0.3228	0.2735
203	712L	3	C	0.2821	0.2399	0.2122	0.1923

A.5 LOOCV Results for Combination of Gaussian Curvature and the Y Component of the Surface Normal

Table A.5: LOOCV results for Gaussian curvature and surface normal.

Subjects	Patient	Truth	Predicted	Distance G0	Distance G1	Distance G2	Distance G3
1	003L	0	C	0.24162	0.25403	0.28942	0.33622
2	003R	0	C	0.25076	0.27996	0.32342	0.37627
3	005R	0	1	0.28771	0.28279	0.31696	0.34141
4	007L	0	C	0.35657	0.36142	0.37300	0.38500
5	007R	0	C	0.32453	0.33128	0.35130	0.36681
6	008R	0	C	0.32404	0.36049	0.38380	0.41215
7	009L	0	C	0.38837	0.41258	0.43036	0.48389
8	013R	0	C	0.27959	0.30135	0.33956	0.37777
9	016R	0	C	0.35834	0.40062	0.41791	0.44192
10	025L	0	C	0.33551	0.37949	0.40343	0.44902
11	029R	0	C	0.39008	0.40149	0.43117	0.48200
12	037L	0	C	0.29053	0.29668	0.30979	0.34644
13	037R	0	C	0.30984	0.32792	0.35348	0.38602
14	046L	0	C	0.23613	0.23865	0.25531	0.29129
15	046R	0	C	0.23325	0.24867	0.28631	0.32750
16	049L	0	C	0.23477	0.24963	0.28841	0.34281
17	053L	0	C	0.27075	0.31540	0.34839	0.40067
18	053R	0	C	0.28038	0.34077	0.36103	0.41672
19	055L	0	C	0.24185	0.28584	0.30616	0.35125
20	055R	0	C	0.31002	0.35848	0.38887	0.42405
21	067R	0	C	0.23142	0.27304	0.30729	0.35109
22	073R	0	C	0.31769	0.34729	0.36899	0.39799
23	076L	0	C	0.37818	0.42406	0.43745	0.50398
24	078L	0	C	0.34691	0.37609	0.39695	0.45001
25	079R	0	C	0.20988	0.23148	0.26471	0.31404
26	084L	0	C	0.27405	0.29022	0.31610	0.35211
27	084R	0	C	0.28774	0.29650	0.33179	0.37272
28	088R	0	C	0.28421	0.31064	0.35205	0.39966
29	089R	0	C	0.21754	0.22530	0.26157	0.29446
30	093L	0	C	0.22462	0.26475	0.30046	0.36159
31	096L	0	C	0.24009	0.24749	0.26923	0.30778
32	113R	0	C	0.21474	0.22687	0.26629	0.31191
33	131R	0	C	0.25427	0.30714	0.34046	0.39224
34	135R	0	C	0.28774	0.32598	0.37092	0.42158
35	154R	0	C	0.20408	0.22132	0.26961	0.32480
36	160L	0	1	0.25814	0.24171	0.24541	0.28391
37	175L	0	C	0.22992	0.25499	0.26566	0.31219
38	183L	0	C	0.23712	0.27554	0.30217	0.35522
39	186R	0	C	0.23813	0.25659	0.28038	0.32002
40	188R	0	1	0.23433	0.23082	0.27632	0.29790
41	192L	0	C	0.28005	0.28951	0.29395	0.34177
42	200L	0	C	0.24905	0.25683	0.26568	0.28418
43	201R	0	C	0.22444	0.24803	0.27299	0.30693
44	203L	0	C	0.27824	0.27838	0.28574	0.30719
45	204L	0	1	0.22215	0.20920	0.21480	0.24641
46	205L	0	C	0.25168	0.25535	0.28287	0.32583
47	205R	0	C	0.22586	0.23215	0.27832	0.31147
48	211R	0	1	0.26423	0.26207	0.26759	0.28843
49	217L	0	2	0.23769	0.20881	0.19354	0.20353
50	220L	0	C	0.29745	0.30542	0.31698	0.37317

Table A.5: LOOCV results for Gaussian curvature and surface normal (continuted).

Subjects	Patient	Truth	Predicted	Distance G0	Distance G1	Distance G2	Distance G3
51	220R	0	C	0.20159	0.23300	0.26959	0.32368
52	505L	0	C	0.26075	0.28398	0.30347	0.33944
53	505R	0	C	0.24414	0.27311	0.31320	0.36446
54	508R	0	1	0.25301	0.21432	0.25472	0.27795
55	511L	0	1	0.29208	0.25794	0.26781	0.30043
56	523L	0	1	0.22956	0.21384	0.24162	0.27141
57	528R	0	C	0.30586	0.30658	0.31608	0.32230
58	529L	0	C	0.26008	0.27605	0.30447	0.36367
59	529R	0	C	0.23213	0.25548	0.28865	0.32720
60	535L	0	1	0.22749	0.22705	0.24808	0.28289
61	535R	0	1	0.23532	0.21199	0.24762	0.27777
62	542L	0	C	0.26550	0.26923	0.28182	0.29218
63	542R	0	C	0.19291	0.19725	0.24013	0.28375
64	554L	0	2	0.24449	0.24459	0.24010	0.26308
65	554R	0	1	0.24242	0.23361	0.24308	0.26978
66	700R	0	1	0.23002	0.19777	0.24090	0.27118
67	702L	0	C	0.23465	0.24076	0.26529	0.29280
68	702R	0	C	0.22866	0.22955	0.27184	0.29431
69	704R	0	1	0.24361	0.22561	0.26472	0.29730
70	705L	0	1	0.24036	0.22804	0.25009	0.28090
71	710L	0	1	0.32543	0.28081	0.28164	0.30437
72	006L	1	0	0.27812	0.29099	0.30626	0.33507
73	012L	1	C	0.31146	0.30758	0.31319	0.34275
74	012R	1	0	0.30045	0.30273	0.33059	0.35841
75	018L	1	0	0.30923	0.33647	0.35464	0.39767
76	018R	1	0	0.35126	0.38742	0.40598	0.42655
77	022L	1	0	0.31724	0.34203	0.36880	0.40496
78	022R	1	0	0.32308	0.35686	0.39077	0.42417
79	023L	1	0	0.30389	0.32559	0.34899	0.38686
80	023R	1	0	0.30197	0.32823	0.36340	0.40682
81	027R	1	3	0.42670	0.40080	0.38160	0.37061
82	047L	1	2	0.29476	0.29616	0.28846	0.28978
83	047R	1	0	0.24432	0.25765	0.29174	0.33086
84	049R	1	0	0.25371	0.27589	0.32266	0.36973
85	056L	1	0	0.20455	0.21394	0.23011	0.26047
86	057R	1	C	0.20452	0.18242	0.19880	0.23274
87	060L	1	0	0.22219	0.22968	0.24652	0.28965
88	069R	1	0	0.21101	0.21774	0.25248	0.28368
89	070R	1	C	0.25396	0.21875	0.23462	0.26942
90	075R	1	C	0.24470	0.22755	0.24061	0.27492
91	082L	1	C	0.24790	0.23118	0.24371	0.28490
92	086L	1	C	0.23113	0.22664	0.22749	0.27567
93	094R	1	0	0.21615	0.23773	0.26544	0.29744
94	095R	1	0	0.33958	0.35330	0.35035	0.35020
95	098R	1	C	0.21404	0.20244	0.22804	0.25480
96	124R	1	0	0.24729	0.25526	0.29400	0.34119
97	133L	1	C	0.21667	0.19958	0.20175	0.21257
98	133R	1	0	0.29987	0.30552	0.30654	0.30155
99	163R	1	0	0.25587	0.26058	0.28812	0.32029
100	181L	1	0	0.23527	0.23996	0.26126	0.30808
101	184L	1	0	0.18128	0.19662	0.21992	0.27464
102	190L	1	C	0.21222	0.20461	0.20947	0.23631
103	197R	1	C	0.29700	0.25537	0.27301	0.29838
104	199L	1	C	0.22321	0.20908	0.22180	0.26399
105	200R	1	C	0.20608	0.19535	0.20586	0.22785

Table A.5: LOOCV results for Gaussian curvature and surface normal (continuted).

Subjects	Patient	Truth	Predicted	Distance G0	Distance G1	Distance G2	Distance G3
106	203R	1	C	0.23190	0.22189	0.25262	0.30465
107	204R	1	C	0.21732	0.20282	0.21588	0.23227
108	209R	1	2	0.35114	0.30848	0.28732	0.30064
109	210L	1	3	0.29835	0.24582	0.23244	0.22059
110	219L	1	C	0.24226	0.22247	0.23380	0.26416
111	507L	1	2	0.29231	0.25619	0.23096	0.25392
112	507R	1	2	0.29804	0.24463	0.24408	0.24758
113	509R	1	C	0.30517	0.26270	0.27715	0.29014
114	511R	1	C	0.24751	0.20425	0.23078	0.24390
115	512R	1	C	0.24123	0.20973	0.23766	0.27553
116	514L	1	C	0.25264	0.24177	0.25181	0.27015
117	515L	1	C	0.23958	0.21068	0.22779	0.25257
118	515R	1	C	0.26155	0.21880	0.23942	0.25144
119	516L	1	2	0.32757	0.28526	0.25461	0.26168
120	516R	1	C	0.31557	0.26930	0.27392	0.29501
121	517L	1	3	0.33023	0.30754	0.29920	0.29573
122	517R	1	2	0.32251	0.26826	0.26797	0.28380
123	521L	1	C	0.23820	0.22090	0.23502	0.26762
124	522R	1	C	0.20241	0.18075	0.20033	0.22569
125	523R	1	2	0.29702	0.24312	0.24252	0.25060
126	527L	1	2	0.30505	0.30522	0.30448	0.32466
127	527R	1	C	0.22753	0.19880	0.22777	0.25261
128	534L	1	3	0.31966	0.30796	0.29258	0.28535
129	539R	1	C	0.25886	0.22630	0.25551	0.29686
130	540L	1	3	0.30995	0.29366	0.28435	0.27176
131	541L	1	3	0.29025	0.27702	0.27608	0.27523
132	541R	1	2	0.30390	0.25825	0.25824	0.28395
133	543L	1	2	0.27107	0.22850	0.21129	0.21482
134	543R	1	2	0.29222	0.25229	0.24993	0.26179
135	574R	1	0	0.24620	0.24760	0.26795	0.27260
136	691L	1	C	0.25045	0.24067	0.25891	0.30082
137	691R	1	C	0.27501	0.25633	0.26737	0.26720
138	699R	1	C	0.19545	0.16558	0.18478	0.21250
139	700L	1	C	0.22504	0.20119	0.21035	0.23248
140	703R	1	C	0.26107	0.22985	0.24375	0.25756
141	704L	1	C	0.25338	0.24259	0.25800	0.28663
142	710R	1	C	0.28417	0.23589	0.25017	0.27620
143	711L	1	3	0.30052	0.26945	0.26568	0.26557
144	713L	1	C	0.22765	0.21539	0.24089	0.27139
145	713R	1	C	0.22740	0.21031	0.24625	0.26307
146	717R	1	C	0.23717	0.23197	0.27029	0.29101
147	002L	2	3	0.37683	0.36290	0.35759	0.35186
148	010L	2	3	0.44630	0.43954	0.42843	0.39493
149	026L	2	0	0.36717	0.37401	0.37587	0.36941
150	029L	2	0	0.42132	0.45620	0.46645	0.48792
151	065L	2	1	0.22009	0.20400	0.20927	0.24021
152	066L	2	0	0.34034	0.35038	0.34885	0.36045
153	189L	2	1	0.26063	0.25533	0.26893	0.26818
154	208L	2	3	0.37971	0.34854	0.33529	0.29820
155	214R	2	1	0.25129	0.21215	0.21964	0.24200
156	216L	2	1	0.26240	0.24360	0.25316	0.29510
157	219R	2	1	0.22427	0.17946	0.18781	0.19787
158	506L	2	3	0.28333	0.24690	0.24387	0.24364
159	509L	2	C	0.30615	0.28237	0.28178	0.30326
160	518L	2	C	0.31198	0.27983	0.27190	0.28593

Table A.5: LOOCV results for Gaussian curvature and surface normal (continuted).

Subjects	Patient	Truth	Predicted	Distance G0	Distance G1	Distance G2	Distance G3
161	518R	2	3	0.30418	0.25990	0.25742	0.22810
162	520L	2	C	0.27485	0.23561	0.21324	0.22377
163	520R	2	1	0.35606	0.32838	0.32928	0.34931
164	522L	2	3	0.27358	0.24379	0.24078	0.22538
165	525L	2	3	0.31496	0.27345	0.26952	0.25109
166	526R	2	C	0.28210	0.22673	0.22179	0.22609
167	530R	2	3	0.27322	0.24573	0.23692	0.21637
168	532L	2	1	0.24024	0.19753	0.20593	0.23458
169	532R	2	3	0.34610	0.28556	0.27482	0.25970
170	533L	2	C	0.29460	0.25255	0.24675	0.25299
171	533R	2	1	0.33037	0.27694	0.28407	0.29190
172	536L	2	1	0.26260	0.23499	0.24273	0.26838
173	536R	2	1	0.32041	0.26603	0.26815	0.27045
174	537R	2	1	0.26465	0.21505	0.22803	0.24112
175	539L	2	1	0.25125	0.23298	0.24540	0.26290
176	546L	2	1	0.24512	0.22629	0.23214	0.26497
177	546R	2	1	0.24160	0.20108	0.20765	0.21660
178	689R	2	3	0.29452	0.26557	0.27941	0.25931
179	692L	2	3	0.40043	0.39356	0.39018	0.37292
180	694L	2	C	0.32688	0.29598	0.29447	0.31339
181	701R	2	3	0.34415	0.30652	0.30015	0.26148
182	177L	3	C	0.27726	0.24556	0.22116	0.20965
183	177R	3	C	0.39065	0.35505	0.33546	0.29525
184	206L	3	C	0.44816	0.42741	0.39588	0.37662
185	207R	3	2	0.32878	0.28048	0.27023	0.28251
186	212L	3	C	0.31793	0.25787	0.22330	0.19972
187	215L	3	C	0.30593	0.24715	0.21448	0.19293
188	215R	3	C	0.31639	0.24797	0.22537	0.19462
189	513L	3	C	0.31155	0.26394	0.24177	0.22044
190	513R	3	C	0.35271	0.29653	0.27164	0.25406
191	519L	3	2	0.28129	0.24338	0.21507	0.22718
192	519R	3	2	0.23669	0.19410	0.19342	0.20018
193	526L	3	C	0.30988	0.26322	0.23892	0.22299
194	52R	3	C	0.40206	0.39170	0.37461	0.36574
195	534R	3	2	0.33776	0.28396	0.25680	0.25704
196	538L	3	2	0.29301	0.24742	0.22358	0.24919
197	538R	3	2	0.23967	0.18606	0.17982	0.19260
198	547L	3	2	0.35416	0.30694	0.26973	0.27753
199	547R	3	C	0.34408	0.28369	0.25381	0.20726
200	549R	3	C	0.27614	0.22923	0.22984	0.21405
201	62R	3	C	0.44284	0.41466	0.38122	0.33905
202	697L	3	C	0.42503	0.36390	0.32787	0.27519
203	712L	3	C	0.26927	0.22033	0.20484	0.20250

A.6 LOOCV Results for Combination of Coronal Projection and the Y Component of the Surface Normal

Table A.6: LOOCV results for coronal projection and surface normal.

Subjects	Patient	Truth	Predicted	Distance G0	Distance G1	Distance G2	Distance G3
1	003L	0	C	0.2304	0.2388	0.2485	0.3140
2	003R	0	1	0.2730	0.2689	0.3211	0.3577
3	005R	0	1	0.2298	0.2081	0.2430	0.2658
4	007L	0	C	0.2610	0.2706	0.2800	0.3054
5	007R	0	C	0.2224	0.2383	0.2603	0.2847
6	008R	0	C	0.3370	0.3644	0.3842	0.4179
7	009L	0	C	0.2360	0.2690	0.2814	0.3448
8	013R	0	C	0.2018	0.2091	0.2576	0.2921
9	016R	0	C	0.3591	0.3892	0.4044	0.4273
10	025L	0	C	0.3203	0.3641	0.3790	0.4342
11	029R	0	C	0.3041	0.3100	0.3405	0.3947
12	037L	0	2	0.2860	0.2842	0.2753	0.3251
13	037R	0	1	0.3114	0.3057	0.3385	0.3591
14	046L	0	C	0.2340	0.2466	0.2488	0.3006
15	046R	0	C	0.2255	0.2382	0.2851	0.3170
16	049L	0	C	0.2598	0.2766	0.2868	0.3511
17	053L	0	C	0.2766	0.3144	0.3340	0.3995
18	053R	0	C	0.2664	0.3144	0.3459	0.3984
19	055L	0	C	0.2307	0.2700	0.2878	0.3455
20	055R	0	C	0.2568	0.2988	0.3393	0.3833
21	067R	0	C	0.1960	0.2315	0.2733	0.3207
22	073R	0	C	0.4094	0.4221	0.4500	0.4650
23	076L	0	C	0.3749	0.4047	0.4214	0.4879
24	078L	0	C	0.3254	0.3478	0.3628	0.4242
25	079R	0	1	0.2578	0.2488	0.2966	0.3245
26	084L	0	C	0.2357	0.2622	0.2780	0.3301
27	084R	0	C	0.2176	0.2331	0.2761	0.3233
28	088R	0	C	0.2417	0.2646	0.3198	0.3696
29	089R	0	1	0.2770	0.2633	0.3028	0.3151
30	093L	0	C	0.2362	0.2750	0.2950	0.3693
31	096L	0	C	0.2556	0.2645	0.2633	0.3185
32	113R	0	1	0.2053	0.2049	0.2502	0.2935
33	131R	0	C	0.2800	0.2968	0.3442	0.3848
34	135R	0	C	0.2996	0.3122	0.3686	0.4110
35	154R	0	C	0.2363	0.2397	0.2976	0.3439
36	160L	0	2	0.2733	0.2557	0.2377	0.2929
37	175L	0	C	0.2143	0.2425	0.2431	0.3070
38	183L	0	C	0.2853	0.3228	0.3386	0.3974
39	186R	0	C	0.1882	0.2062	0.2416	0.2922
40	188R	0	C	0.2235	0.2236	0.2646	0.2834
41	192L	0	2	0.2809	0.2886	0.2780	0.3335
42	200L	0	C	0.3411	0.3561	0.3503	0.3804
43	201R	0	C	0.3490	0.3511	0.3775	0.3925
44	203L	0	C	0.3480	0.3562	0.3529	0.3878
45	204L	0	2	0.2229	0.2266	0.2215	0.2659
46	205L	0	C	0.2493	0.2624	0.2774	0.3354
47	205R	0	C	0.2368	0.2385	0.2885	0.3223
48	211R	0	1	0.3061	0.2942	0.3097	0.3298
49	217L	0	2	0.2940	0.2832	0.2547	0.2857

Table A.6: LOOCV results for coronal projection and surface normal (continutted).

Subjects	Patient	Truth	Predicted	Distance G0	Distance G1	Distance G2	Distance G3
50	220L	0	1	0.3061	0.3036	0.3135	0.3676
51	220R	0	C	0.2870	0.2926	0.3336	0.3824
52	505L	0	C	0.2892	0.3130	0.3180	0.3696
53	505R	0	C	0.2171	0.2429	0.2868	0.3423
54	508R	0	1	0.2324	0.2027	0.2457	0.2641
55	511L	0	2	0.2968	0.2819	0.2756	0.3093
56	523L	0	C	0.2405	0.2474	0.2497	0.3048
57	528R	0	C	0.3087	0.3210	0.3261	0.3415
58	529L	0	C	0.2360	0.2618	0.2810	0.3568
59	529R	0	C	0.2060	0.2308	0.2679	0.3199
60	535L	0	C	0.2809	0.2915	0.2883	0.3402
61	535R	0	1	0.2461	0.2251	0.2585	0.2856
62	542L	0	C	0.2787	0.2943	0.2863	0.3135
63	542R	0	C	0.1847	0.1963	0.2221	0.2774
64	554L	0	2	0.2460	0.2478	0.2340	0.2788
65	554R	0	1	0.2106	0.1994	0.2181	0.2451
66	700R	0	1	0.2056	0.1841	0.2122	0.2481
67	702L	0	C	0.2442	0.2622	0.2645	0.3080
68	702R	0	C	0.2179	0.2229	0.2509	0.2806
69	704R	0	1	0.2218	0.2019	0.2494	0.2806
70	705L	0	1	0.2345	0.2203	0.2236	0.2599
71	710L	0	2	0.3100	0.2848	0.2695	0.2991
72	006L	1	0	0.2129	0.2272	0.2364	0.2788
73	012L	1	2	0.2281	0.2155	0.2098	0.2567
74	012R	1	C	0.2197	0.2037	0.2486	0.2760
75	018L	1	0	0.2951	0.3206	0.3191	0.3746
76	018R	1	0	0.3208	0.3423	0.3624	0.3805
77	022L	1	0	0.2929	0.3197	0.3265	0.3849
78	022R	1	0	0.2557	0.2908	0.3297	0.3706
79	023L	1	0	0.2977	0.3240	0.3219	0.3799
80	023R	1	0	0.3191	0.3210	0.3678	0.3926
81	027R	1	3	0.3535	0.2921	0.2829	0.2391
82	047L	1	2	0.3680	0.3735	0.3548	0.3707
83	047R	1	0	0.2885	0.3025	0.3446	0.3781
84	049R	1	0	0.2637	0.2759	0.3273	0.3623
85	056L	1	0	0.2180	0.2361	0.2404	0.2814
86	057R	1	C	0.2307	0.2019	0.2285	0.2464
87	060L	1	0	0.2116	0.2135	0.2119	0.2687
88	069R	1	C	0.2821	0.2760	0.3145	0.3385
89	070R	1	C	0.2690	0.2319	0.2578	0.2825
90	075R	1	C	0.2576	0.2248	0.2426	0.2668
91	082L	1	C	0.2412	0.2394	0.2403	0.2896
92	086L	1	2	0.2681	0.2734	0.2562	0.3109
93	094R	1	0	0.2410	0.2581	0.2936	0.3205
94	095R	1	0	0.3872	0.3925	0.4020	0.3933
95	098R	1	C	0.2488	0.2282	0.2595	0.2677
96	124R	1	C	0.2748	0.2745	0.3249	0.3612
97	133L	1	2	0.2777	0.2722	0.2492	0.2797
98	133R	1	3	0.3270	0.3257	0.3271	0.3225
99	163R	1	C	0.2723	0.2706	0.3102	0.3281
100	181L	1	0	0.2096	0.2289	0.2384	0.2984
101	184L	1	0	0.1828	0.2099	0.2235	0.2804
102	190L	1	2	0.2182	0.2035	0.1834	0.2180
103	197R	1	C	0.2833	0.2431	0.2718	0.2892
104	199L	1	2	0.2320	0.2286	0.2222	0.2681

Table A.6: LOOCV results for coronal projection and surface normal (continuted).

Subjects	Patient	Truth	Predicted	Distance G0	Distance G1	Distance G2	Distance G3
105	200R	1	C	0.2211	0.1981	0.2113	0.2344
106	203R	1	C	0.4312	0.4247	0.4342	0.4693
107	204R	1	C	0.2327	0.2149	0.2369	0.2525
108	209R	1	2	0.3522	0.3159	0.3000	0.3096
109	210L	1	2	0.2904	0.2511	0.2216	0.2226
110	219L	1	2	0.2384	0.2344	0.2307	0.2655
111	507L	1	2	0.2773	0.2536	0.2170	0.2496
112	507R	1	C	0.2768	0.2320	0.2389	0.2451
113	509R	1	C	0.2758	0.2430	0.2742	0.2875
114	511R	1	C	0.2211	0.1891	0.2162	0.2331
115	512R	1	C	0.2233	0.1999	0.2383	0.2735
116	514L	1	0	0.2353	0.2482	0.2474	0.2915
117	515L	1	C	0.1918	0.1815	0.1815	0.2265
118	515R	1	C	0.2176	0.1817	0.2117	0.2223
119	516L	1	2	0.3211	0.3009	0.2621	0.2890
120	516R	1	C	0.2892	0.2524	0.2686	0.2895
121	517L	1	2	0.3303	0.3326	0.3194	0.3350
122	517R	1	C	0.2773	0.2343	0.2433	0.2627
123	521L	1	2	0.2580	0.2570	0.2504	0.2990
124	522R	1	C	0.2145	0.1852	0.2055	0.2309
125	523R	1	C	0.2788	0.2337	0.2359	0.2457
126	527L	1	0	0.3367	0.3507	0.3427	0.3734
127	527R	1	C	0.2302	0.2081	0.2396	0.2671
128	534L	1	2	0.3990	0.3959	0.3789	0.3813
129	539R	1	C	0.2758	0.2459	0.2766	0.3034
130	540L	1	3	0.2932	0.2876	0.2740	0.2694
131	541L	1	2	0.3594	0.3633	0.3444	0.3649
132	541R	1	C	0.2837	0.2443	0.2528	0.2762
133	543L	1	2	0.2508	0.2242	0.1940	0.2274
134	543R	1	C	0.2757	0.2387	0.2438	0.2564
135	574R	1	0	0.2502	0.2573	0.2705	0.2709
136	691L	1	0	0.2530	0.2593	0.2558	0.3152
137	691R	1	0	0.2603	0.2615	0.2722	0.2846
138	699R	1	C	0.1758	0.1482	0.1670	0.1970
139	700L	1	2	0.1995	0.1919	0.1811	0.2119
140	703R	1	C	0.2603	0.2309	0.2553	0.2630
141	704L	1	0	0.2545	0.2569	0.2560	0.3031
142	710R	1	C	0.2760	0.2388	0.2549	0.2799
143	711L	1	2	0.2701	0.2593	0.2465	0.2625
144	713L	1	0	0.2533	0.2585	0.2572	0.3041
145	713R	1	C	0.2523	0.2363	0.2745	0.2848
146	717R	1	0	0.2000	0.2056	0.2374	0.2681
147	002L	2	C	0.3345	0.3055	0.2823	0.2824
148	010L	2	3	0.4432	0.4241	0.4028	0.3706
149	026L	2	0	0.3989	0.4046	0.3991	0.4018
150	029L	2	0	0.4219	0.4480	0.4605	0.4769
151	065L	2	C	0.2544	0.2401	0.2263	0.2670
152	066L	2	C	0.2345	0.2375	0.2212	0.2476
153	189L	2	1	0.2504	0.2421	0.2470	0.2555
154	208L	2	3	0.4024	0.3892	0.3710	0.3576
155	214R	2	1	0.2506	0.2159	0.2411	0.2525
156	216L	2	C	0.2559	0.2443	0.2436	0.2989
157	219R	2	1	0.2478	0.2118	0.2284	0.2242
158	506L	2	C	0.2610	0.2472	0.2364	0.2603
159	509L	2	C	0.2607	0.2477	0.2392	0.2793

Table A.6: LOOCV results for coronal projection and surface normal (continuted).

Subjects	Patient	Truth	Predicted	Distance G0	Distance G1	Distance G2	Distance G3
160	518L	2	C	0.2759	0.2611	0.2419	0.2638
161	518R	2	3	0.2811	0.2546	0.2534	0.2299
162	520L	2	C	0.2438	0.2184	0.1889	0.2164
163	520R	2	1	0.3460	0.3261	0.3312	0.3488
164	522L	2	C	0.3140	0.2964	0.2779	0.2844
165	525L	2	3	0.2992	0.2787	0.2684	0.2580
166	526R	2	1	0.2645	0.2113	0.2256	0.2233
167	530R	2	3	0.2998	0.2749	0.2837	0.2706
168	532L	2	C	0.2527	0.2279	0.2201	0.2475
169	532R	2	3	0.3367	0.2847	0.2758	0.2550
170	533L	2	C	0.3175	0.2978	0.2860	0.3089
171	533R	2	1	0.3111	0.2636	0.2839	0.2836
172	536L	2	C	0.2999	0.2859	0.2754	0.3178
173	536R	2	1	0.3138	0.2665	0.2735	0.2844
174	537R	2	1	0.2774	0.2298	0.2531	0.2624
175	539L	2	1	0.2388	0.2370	0.2380	0.2610
176	546L	2	C	0.2423	0.2367	0.2288	0.2727
177	546R	2	1	0.2393	0.2040	0.2165	0.2273
178	689R	2	1	0.2869	0.2637	0.2879	0.2692
179	692L	2	3	0.4376	0.4470	0.4405	0.4369
180	694L	2	C	0.3218	0.3025	0.2885	0.3119
181	701R	2	3	0.3658	0.3391	0.3480	0.3069
182	177L	3	2	0.2827	0.2584	0.2252	0.2264
183	177R	3	C	0.4063	0.3763	0.3606	0.3271
184	206L	3	C	0.5153	0.5030	0.4789	0.4713
185	207R	3	1	0.3338	0.2922	0.2939	0.3043
186	212L	3	C	0.3156	0.2703	0.2271	0.2241
187	215L	3	C	0.3138	0.2680	0.2267	0.2264
188	215R	3	C	0.3229	0.2570	0.2491	0.2122
189	513L	3	C	0.3015	0.2691	0.2433	0.2379
190	513R	3	C	0.3415	0.2866	0.2719	0.2459
191	519L	3	2	0.2886	0.2508	0.2113	0.2264
192	519R	3	C	0.2605	0.2134	0.2125	0.2089
193	526L	3	2	0.2916	0.2542	0.2244	0.2288
194	52R	3	C	0.4095	0.4049	0.3931	0.3903
195	534R	3	C	0.3379	0.2862	0.2704	0.2614
196	538L	3	2	0.2843	0.2547	0.2190	0.2467
197	538R	3	2	0.2232	0.1855	0.1848	0.1928
198	547L	3	2	0.3417	0.3095	0.2654	0.2845
199	547R	3	C	0.3670	0.3112	0.2969	0.2535
200	549R	3	C	0.2847	0.2519	0.2563	0.2343
201	62R	3	C	0.4837	0.4565	0.4321	0.3961
202	697L	3	C	0.4191	0.3633	0.3219	0.2782
203	712L	3	C	0.2690	0.2328	0.2044	0.1998

Table A.6: LOOCV Results for combination of coronal projection and surface normal analysis

A.7 LOOCV Results for Combination of All the Three 3D Features

Table A.7: LOOCV results for combination of all the three 3D features.

Subjects	Patient	Truth	Predicted	Distance G0	Distance G1	Distance G2	Distance G3
1	003L	0	C	0.25537	0.26454	0.27971	0.33140
2	003R	0	C	0.28171	0.29073	0.33241	0.37347
3	005R	0	1	0.27345	0.26268	0.28911	0.30824
4	007L	0	C	0.31880	0.32046	0.33014	0.34788
5	007R	0	C	0.29334	0.29922	0.31625	0.33338
6	008R	0	C	0.32397	0.34921	0.37013	0.40233
7	009L	0	C	0.34716	0.37143	0.38409	0.43580
8	013R	0	C	0.26181	0.27545	0.31113	0.34310
9	016R	0	C	0.34856	0.38160	0.39674	0.42226
10	025L	0	C	0.32879	0.36894	0.38505	0.43594
11	029R	0	C	0.34871	0.36064	0.38914	0.43556
12	037L	0	2	0.29842	0.30070	0.29834	0.33994
13	037R	0	C	0.32598	0.32866	0.35466	0.37973
14	046L	0	C	0.24221	0.24690	0.25131	0.29401
15	046R	0	C	0.24326	0.25087	0.28703	0.31965
16	049L	0	C	0.25348	0.26651	0.28227	0.34111
17	053L	0	C	0.27277	0.31178	0.33194	0.39068
18	053R	0	C	0.27692	0.32839	0.34910	0.40465
19	055L	0	C	0.24315	0.28050	0.29309	0.34150
20	055R	0	C	0.29077	0.33068	0.36151	0.39981
21	067R	0	C	0.21525	0.25007	0.28206	0.32826
22	073R	0	C	0.36427	0.37515	0.40025	0.42049
23	076L	0	C	0.38344	0.42291	0.43266	0.49557
24	078L	0	C	0.32986	0.35767	0.37284	0.42593
25	079R	0	C	0.24111	0.24699	0.28426	0.32082
26	084L	0	C	0.25772	0.27232	0.28543	0.32623
27	084R	0	C	0.26137	0.26705	0.29916	0.33748
28	088R	0	C	0.27062	0.29077	0.33127	0.37588
29	089R	0	1	0.26228	0.25633	0.29039	0.30631
30	093L	0	C	0.23179	0.27049	0.29159	0.35762
31	096L	0	C	0.24875	0.25851	0.26531	0.31056
32	113R	0	C	0.21210	0.21746	0.25317	0.29246
33	131R	0	C	0.27912	0.31101	0.34763	0.38968
34	135R	0	C	0.29791	0.32113	0.36585	0.40814
35	154R	0	C	0.22941	0.23575	0.28273	0.32940
36	160L	0	2	0.25822	0.24271	0.23740	0.27858
37	175L	0	C	0.23573	0.25869	0.25893	0.31035
38	183L	0	C	0.25869	0.29201	0.30842	0.36678
39	186R	0	C	0.22783	0.24702	0.27277	0.31376
40	188R	0	1	0.23008	0.22021	0.26171	0.27877
41	192L	0	C	0.26808	0.27940	0.27795	0.32643
42	200L	0	C	0.30115	0.30864	0.30792	0.33440
43	201R	0	C	0.31151	0.31468	0.33776	0.35819
44	203L	0	2	0.31901	0.32117	0.31883	0.34981
45	204L	0	2	0.23139	0.22368	0.21696	0.25165
46	205L	0	C	0.24882	0.25537	0.26865	0.31750
47	205R	0	1	0.23364	0.23107	0.27232	0.30355
48	211R	0	1	0.29403	0.28121	0.28970	0.30545
49	217L	0	2	0.26921	0.25145	0.23168	0.25709
50	220L	0	C	0.27760	0.28557	0.29377	0.34557
51	220R	0	C	0.26581	0.27917	0.31412	0.35987
52	505L	0	C	0.28309	0.30322	0.31083	0.35500

Table A.7: LOOCV results for combination of all the three 3D features (continuted).

Subjects	Patient	Truth	Predicted	Distance G0	Distance G1	Distance G2	Distance G3
53	505R	0	C	0.23589	0.26145	0.29977	0.34868
54	508R	0	1	0.24523	0.20777	0.24287	0.25790
55	511L	0	2	0.28804	0.26148	0.25882	0.28582
56	523L	0	1	0.24071	0.23330	0.23942	0.28164
57	528R	0	C	0.28759	0.28865	0.29768	0.31252
58	529L	0	C	0.25585	0.27702	0.29347	0.35897
59	529R	0	C	0.22342	0.24875	0.27908	0.32392
60	535L	0	C	0.26475	0.26553	0.26678	0.30904
61	535R	0	1	0.23835	0.21258	0.24360	0.26662
62	542L	0	C	0.26430	0.26886	0.26868	0.28867
63	542R	0	C	0.20423	0.20892	0.23625	0.28096
64	554L	0	2	0.25088	0.25059	0.24303	0.27556
65	554R	0	1	0.23169	0.21999	0.23372	0.25225
66	700R	0	1	0.22259	0.19476	0.22372	0.25008
67	702L	0	C	0.23900	0.24654	0.25578	0.29129
68	702R	0	1	0.22478	0.22327	0.25013	0.27247
69	704R	0	1	0.23239	0.21015	0.24656	0.27256
70	705L	0	1	0.24065	0.22497	0.23219	0.25951
71	710L	0	2	0.29729	0.26072	0.25388	0.27427
72	006L	1	0	0.25409	0.26462	0.27232	0.30709
73	012L	1	2	0.29048	0.28719	0.28432	0.31811
74	012R	1	C	0.27774	0.27282	0.30012	0.32290
75	018L	1	0	0.32300	0.34752	0.35004	0.39781
76	018R	1	0	0.34061	0.36418	0.38457	0.40376
77	022L	1	0	0.32759	0.34922	0.36015	0.40511
78	022R	1	0	0.30031	0.32904	0.36002	0.39734
79	023L	1	0	0.32472	0.34598	0.35123	0.39765
80	023R	1	0	0.33165	0.34451	0.37992	0.41216
81	027R	1	3	0.39141	0.35995	0.34765	0.32651
82	047L	1	2	0.32558	0.32574	0.31399	0.32591
83	047R	1	0	0.27982	0.28456	0.31899	0.35263
84	049R	1	0	0.25857	0.27148	0.31472	0.35373
85	056L	1	0	0.20373	0.21095	0.21481	0.25401
86	057R	1	C	0.22229	0.19429	0.21287	0.23306
87	060L	1	0	0.21872	0.22474	0.23096	0.27448
88	069R	1	C	0.26521	0.26209	0.29444	0.31887
89	070R	1	C	0.25147	0.21851	0.24067	0.26432
90	075R	1	C	0.24101	0.21902	0.23598	0.25971
91	082L	1	C	0.23163	0.22521	0.22996	0.27209
92	086L	1	2	0.24863	0.24811	0.23759	0.28744
93	094R	1	0	0.22842	0.23892	0.26760	0.29674
94	095R	1	0	0.35084	0.35176	0.35892	0.35234
95	098R	1	C	0.24235	0.22536	0.25247	0.26292
96	124R	1	0	0.27335	0.27663	0.31676	0.35335
97	133L	1	2	0.25122	0.24026	0.22495	0.24931
98	133R	1	C	0.29435	0.29287	0.29674	0.29519
99	163R	1	C	0.27617	0.27154	0.30125	0.32115
100	181L	1	0	0.23086	0.24301	0.25324	0.30193
101	184L	1	0	0.18899	0.20793	0.22095	0.27548
102	190L	1	2	0.22072	0.21411	0.20888	0.23458
103	197R	1	C	0.27601	0.23960	0.26117	0.28070
104	199L	1	2	0.22631	0.21838	0.21716	0.25673
105	200R	1	C	0.21833	0.19955	0.21063	0.22902
106	203R	1	C	0.37411	0.36898	0.37991	0.41458
107	204R	1	C	0.23681	0.21636	0.23033	0.24165

Table A.7: LOOCV results for combination of all the three 3D features (continuted).

Subjects	Patient	Truth	Predicted	Distance G0	Distance G1	Distance G2	Distance G3
108	209R	1	2	0.31825	0.27760	0.26327	0.26861
109	210L	1	3	0.28889	0.24436	0.22196	0.21385
110	219L	1	2	0.24488	0.23481	0.23367	0.26155
111	507L	1	2	0.27378	0.24228	0.21276	0.23635
112	507R	1	C	0.28071	0.23221	0.23632	0.23750
113	509R	1	C	0.28960	0.25117	0.26653	0.27848
114	511R	1	C	0.23797	0.19542	0.21629	0.22486
115	512R	1	C	0.22788	0.20145	0.23044	0.26154
116	514L	1	2	0.24946	0.24378	0.24346	0.27534
117	515L	1	C	0.22408	0.20145	0.20583	0.23312
118	515R	1	C	0.24792	0.20680	0.22784	0.23193
119	516L	1	2	0.31776	0.28567	0.25104	0.26494
120	516R	1	C	0.29757	0.25483	0.26401	0.27833
121	517L	1	2	0.33009	0.31396	0.29846	0.30633
122	517R	1	C	0.29343	0.24478	0.24762	0.25979
123	521L	1	2	0.24950	0.23985	0.23808	0.27938
124	522R	1	C	0.21233	0.18678	0.20472	0.22713
125	523R	1	C	0.27747	0.22734	0.22801	0.22988
126	527L	1	2	0.31785	0.31894	0.31165	0.33820
127	527R	1	C	0.23186	0.20479	0.22921	0.25404
128	534L	1	2	0.36087	0.34963	0.33312	0.33313
129	539R	1	C	0.25887	0.22988	0.25713	0.28403
130	540L	1	3	0.28258	0.26692	0.25538	0.24799
131	541L	1	2	0.33275	0.32587	0.31181	0.32454
132	541R	1	C	0.28143	0.24061	0.24524	0.26495
133	543L	1	2	0.25500	0.22312	0.19923	0.21721
134	543R	1	C	0.27201	0.23600	0.23865	0.24579
135	574R	1	C	0.24579	0.24169	0.25646	0.25478
136	691L	1	C	0.25656	0.25481	0.25814	0.30789
137	691R	1	C	0.25983	0.24451	0.25143	0.26058
138	699R	1	C	0.19081	0.16319	0.18063	0.20198
139	700L	1	2	0.22110	0.20261	0.19877	0.22075
140	703R	1	C	0.26263	0.22951	0.24569	0.25276
141	704L	1	2	0.25457	0.24766	0.24576	0.28327
142	710R	1	C	0.26742	0.22490	0.24030	0.25938
143	711L	1	2	0.29006	0.26477	0.25432	0.26215
144	713L	1	C	0.24112	0.23485	0.23968	0.27891
145	713R	1	C	0.24499	0.22088	0.25297	0.26273
146	717R	1	C	0.22679	0.21961	0.24989	0.27054
147	002L	2	C	0.35946	0.34372	0.33042	0.33194
148	010L	2	3	0.43907	0.42703	0.41287	0.38712
149	026L	2	0	0.37095	0.37311	0.37129	0.37223
150	029L	2	0	0.41536	0.45183	0.46929	0.50003
151	065L	2	C	0.24170	0.22929	0.22438	0.25840
152	066L	2	0	0.31072	0.31880	0.31306	0.33372
153	189L	2	1	0.25174	0.24156	0.25047	0.25378
154	208L	2	3	0.37540	0.34883	0.33107	0.31051
155	214R	2	1	0.24793	0.21228	0.22839	0.24014
156	216L	2	1	0.25513	0.24212	0.24434	0.28985
157	219R	2	1	0.24023	0.20323	0.21681	0.21366
158	506L	2	C	0.27245	0.24657	0.23655	0.24980
159	509L	2	C	0.28464	0.26572	0.25857	0.28406
160	518L	2	C	0.28703	0.26216	0.24952	0.26356
161	518R	2	3	0.28088	0.24233	0.23589	0.21244
162	520L	2	C	0.25117	0.21923	0.19546	0.21076

Table A.7: LOOCV results for combination of all the three 3D features (continuted).

Subjects	Patient	Truth	Predicted	Distance G0	Distance G1	Distance G2	Distance G3
163	520R	2	1	0.32274	0.29584	0.29881	0.31425
164	522L	2	C	0.29322	0.26954	0.25724	0.25743
165	525L	2	3	0.30757	0.27084	0.25853	0.24067
166	526R	2	1	0.26404	0.21169	0.21610	0.21227
167	530R	2	3	0.28854	0.26022	0.26146	0.24778
168	532L	2	C	0.24165	0.21006	0.20784	0.23003
169	532R	2	3	0.32924	0.27257	0.26389	0.23803
170	533L	2	C	0.30778	0.27682	0.26392	0.27920
171	533R	2	1	0.31262	0.26428	0.27582	0.27278
172	536L	2	C	0.28870	0.27118	0.26774	0.30004
173	536R	2	1	0.30636	0.25765	0.26289	0.26547
174	537R	2	1	0.26137	0.21516	0.23320	0.24159
175	539L	2	1	0.24119	0.22740	0.22830	0.24863
176	546L	2	C	0.24039	0.22864	0.22575	0.26156
177	546R	2	1	0.23506	0.19993	0.21024	0.21759
178	689R	2	3	0.28806	0.25533	0.27245	0.25036
179	692L	2	3	0.39615	0.39113	0.38691	0.38106
180	694L	2	C	0.30412	0.27858	0.26911	0.28514
181	701R	2	3	0.34606	0.30803	0.31013	0.27007
182	177L	3	C	0.27452	0.24400	0.21333	0.21089
183	177R	3	C	0.38204	0.34372	0.33027	0.29184
184	206L	3	C	0.46099	0.43923	0.41367	0.40116
185	207R	3	2	0.31680	0.27660	0.27371	0.28146
186	212L	3	C	0.31133	0.26140	0.22445	0.21152
187	215L	3	C	0.30145	0.25167	0.21607	0.20506
188	215R	3	C	0.30766	0.24271	0.22808	0.19192
189	513L	3	C	0.30074	0.25907	0.23340	0.21966
190	513R	3	C	0.33915	0.28594	0.26696	0.24550
191	519L	3	2	0.27351	0.24259	0.21410	0.22439
192	519R	3	C	0.24436	0.20284	0.20335	0.20129
193	526L	3	C	0.29152	0.25010	0.22151	0.21618
194	52R	3	C	0.37003	0.35510	0.34259	0.33722
195	534R	3	C	0.31929	0.26804	0.25064	0.23986
196	538L	3	2	0.27987	0.24142	0.21288	0.23184
197	538R	3	2	0.23061	0.18198	0.17924	0.18471
198	547L	3	2	0.32868	0.28958	0.25425	0.26333
199	547R	3	C	0.34658	0.28969	0.27150	0.22917
200	549R	3	C	0.27612	0.23107	0.23087	0.20849
201	62R	3	C	0.44190	0.40975	0.38535	0.34611
202	697L	3	C	0.41605	0.36013	0.32421	0.27561
203	712L	3	C	0.27352	0.23117	0.20719	0.19826

Appendix B

Subjective Rating

B.1 Subjective Rating for Grade 0

Table B.1: Subjective rating for grade 0

Patient No.	Surgeon 1	Surgeon 2	Patient No.	Surgeon 1	Surgeon 2
003L	0	0	175L	0	0
003R	0	0	183L	0	1
005R	0	1	186R	0	2
007L	0	0	188R	0	1
007R	0	0	192L	0	2
008R	0	1	200L	0	0
009L	0	0	201R	0	0
013R	0	0	203L	0	2
016R	0	0	204L	0	0
025L	0	0	205L	0	1
029R	0	0	205R	0	1
037L	0	0	211R	0	1
037R	0	0	217L	0	1
046L	0	1	220L	0	2
046R	0	1	220R	0	2
049L	0	1	505L	0	0
053L	0	0	505R	0	0
053R	0	0	508R	0	1
055L	0	0	511L	0	1
055R	0	0	523L	0	1
067R	0	0	528R	0	1
073R	0	0	529L	0	0
076L	0	0	529R	0	0
078L	0	0	535L	0	0
079R	0	2	535R	0	0
084L	0	0	542L	0	0
084R	0	0	542R	0	0
088R	0	1	554L	0	0
089R	0	1	554R	0	0
093L	0	1	700R	0	1
096L	0	2	702L	0	0
113R	0	0	702R	0	0
131R	0	0	704R	0	1
135R	0	0	705L	0	0
154R	0	1	710L	0	2
160L	0	2			

B.2 Subjective Rating for Grade 1

Table B.2: Subjective rating for grade 1.

Patient No.	Surgeon 1	Surgeon 2	Patient No.	Surgeon 1	Surgeon 2
006L	1	1	219L	1	1
012L	1	1	507L	1	2
012R	1	1	507R	1	2
018L	1	0	509R	1	3
018R	1	1	511R	1	1
022L	1	1	512R	1	2
022R	1	1	514L	1	2
023L	1	2	515L	1	1
023R	1	2	515R	1	1
027R	1	2	516L	1	3
047L	1	2	516R	1	3
047R	1	2	517L	1	2
049R	1	1	517R	1	2
056L	1	2	521L	1	2
057R	1	2	522R	1	2
060L	1	1	523R	1	2
069R	1	2	527L	1	2
070R	1	2	527R	1	2
075R	1	2	534L	1	2
082L	1	2	539R	1	2
086L	1	2	540L	1	2
094R	1	2	541L	1	2
095R	1	0	541R	1	3
098R	1	3	543L	1	2
124R	1	2	543R	1	2
133L	1	2	574R	1	1
133R	1	2	691L	1	2
163R	1	2	691R	1	2
181L	1	2	699R	1	2
184L	1	2	700L	1	1
190L	1	2	703R	1	2
197R	1	2	704L	1	1
199L	1	1	710R	1	2
200R	1	0	711L	1	2
203R	1	2	713L	1	1
204R	1	0	713R	1	1
209R	1	2	717R	1	1
210L	1	2			

B.3 Subjective Rating for Grade 2

Table B.3: Subjective rating for grade 2.

Patient No.	Surgeon 1	Surgeon 2	Patient No.	Surgeon 1	Surgeon 2
002L	2	1	525L	2	3
010L	2	1	526R	2	2
026L	2	2	530R	2	3
029L	2	1	532L	2	2
065L	2	3	532R	2	3
066L	2	3	533L	2	3
189L	2	3	533R	2	3
208L	2	3	536L	2	2
214R	2	2	536R	2	3
216L	2	2	537R	2	2
219R	2	2	539L	2	2
506L	2	2	546L	2	2
509L	2	3	546R	2	2
518L	2	2	689R	2	3
518R	2	2	692L	2	2
520L	2	3	694L	2	1
520R	2	3	701R	2	3
522L	2	2			

B.4 Subjective Rating for Grade 3

Table B.4: Subjective rating for grade 3.

Patient No.	Surgeon 1	Surgeon 2	Patient No.	Surgeon 1	Surgeon 2
177R	3	3	52R	3	3
206L	3	3	534R	3	3
207R	3	3	538L	3	3
212L	3	3	538R	3	3
215L	3	3	547L	3	3
215R	3	3	547R	3	3
513L	3	3	549R	3	3
513R	3	3	62R	3	3
519L	3	3	697L	3	3
519R	3	3	712L	3	3

Appendix C
Distance Measurements

Table C.1: Distance measurements on Grade 0.

Patient	N	I	s	v	s-i	s-n	s-i/s-n	round	M-1	p1	n-v	i-v	n-v/i-v	r2	M-2	p2	n-i	p3
205L	-8.61	-50.4	176.43	-76.05	226.83	185.04	1.2258	1.0000	1.0512	1	67.44	25.65	2.6292	1.0000	0.9531	1	4.179	0
205R	-15.9	-37.81	176.43	-82.13	214.24	192.33	1.1139	1.0000	1.0512	1	66.23	44.32	1.4944	1.0000	0.9531	1	2.191	0
211R	41.04	7.66	224.33	-15.28	216.67	183.29	1.1821	1.0000	1.0512	1	56.32	22.94	2.4551	1.0000	0.9531	1	3.338	0
217L	70.26	40.35	228.83	15.89	188.48	158.57	1.1886	1.0000	1.0512	1	54.37	24.46	2.2228	1.0000	0.9531	1	2.991	0
220L	14.81	-16.78	199.26	-69.3	216.04	184.45	1.1713	1.0000	1.0512	1	84.11	52.52	1.6015	1.0000	0.9531	1	3.159	0
220R	25.06	-25.79	199.26	-68.52	225.05	174.2	1.2919	1.0000	1.0512	1	93.58	42.73	2.1900	1.0000	0.9531	1	5.085	0
505L	45.93	-27.11	167.33	-57.85	194.44	121.4	1.6016	1.0000	1.0512	1	103.78	30.74	3.3761	1.0000	0.9531	1	7.304	0
505R	41.71	-38.69	167.33	-58.03	206.02	125.62	1.6400	1.0000	1.0512	1	99.74	19.34	5.1572	1.0000	0.9531	1	8.04	0
508R	86.62	51.7	263.71	29.57	212.01	177.09	1.1972	1.0000	1.0512	1	57.05	22.13	2.5779	1.0000	0.9531	1	3.492	0
511L	226.02	202.31	393.12	152.88	190.81	167.1	1.1419	1.0000	1.0512	1	73.14	49.43	1.4797	1.0000	0.9531	1	2.371	0
523L	-21.36	-65.28	197.02	-99.67	262.3	218.38	1.2011	1.0000	1.0512	1	78.31	34.39	2.2771	1.0000	0.9531	1	4.392	0
528R	6.25	6.23	196.5	-31.39	190.27	190.25	1.0001	1.0000	1.0512	1	37.64	37.62	1.0005	1.0000	0.9531	1	0.002	0
529L	60.27	41.06	211.05	-4.43	169.99	150.78	1.1274	1.0000	1.0512	1	64.7	45.49	1.4223	1.0000	0.9531	1	1.921	0
529R	73.32	55.99	211.05	0.64	155.06	137.73	1.1258	1.0000	1.0512	1	72.68	55.35	1.3131	1.0000	0.9531	1	1.733	0
535L	185.61	149.41	323.47	111.45	174.06	137.86	1.2626	1.0000	1.0512	1	74.16	37.96	1.9536	1.0000	0.9531	1	3.62	0
535R	160.07	143.99	323.47	101.86	179.48	163.4	1.0984	1.0000	1.0512	1	58.21	42.13	1.3817	1.0000	0.9531	1	1.608	0
542L	96.75	76.72	273.06	42.58	196.34	176.31	1.1136	1.0000	1.0512	1	54.17	34.14	1.5867	1.0000	0.9531	1	2.003	0
542R	72.67	84.49	273.06	-2.46	188.57	200.39	0.9410	0.9410	1.5871	2	75.13	86.95	0.8641	0.8641	1.4878	1	-1.182	2
554L	-99.82	-84.95	82.89	-138.29	167.84	182.71	0.9186	0.9186	1.7907	2	38.47	53.34	0.7212	0.7212	2.0496	2	-1.487	2
554R	-74.7	-65.82	82.89	-115.49	148.71	157.59	0.9437	0.9437	1.5632	2	40.79	49.67	0.8212	0.8212	1.6563	2	-0.888	1
700R	85.05	98.33	322.24	2.34	223.91	237.19	0.9440	0.9440	1.5599	2	82.71	95.99	0.8617	0.8617	1.4973	1	-1.328	2
702L	147.32	159.99	293.98	83.12	133.99	146.66	0.9136	0.9136	1.8361	2	64.2	76.87	0.8352	0.8352	1.6014	2	-1.267	2
702R	136.79	152.15	293.98	78.06	141.83	157.19	0.9023	0.9023	1.9390	2	58.73	74.09	0.7927	0.7927	1.7685	2	-1.536	2
704R	24.09	32.57	191.32	-38.7	158.75	167.23	0.9493	0.9493	1.5119	2	62.79	71.27	0.8810	0.8810	1.4211	1	-0.848	1
705L	42.38	51.71	193.46	-15.46	141.75	151.08	0.9382	0.9382	1.6123	2	57.84	67.17	0.8611	0.8611	1.4994	1	-0.933	1
710L	107.94	117.88	284.79	42.36	166.91	176.85	0.9438	0.9438	1.5619	2	65.58	75.52	0.8684	0.8684	1.4708	1	-0.994	1

Table C.2: Distance measurements on Grade 1.

Patient	N	I	s	v	s-i	s-n	s-i/s-n	round	M-1	p1	n-v	i-v	n-v/i-v	r2	M-2	p2	n-i	p3
006L	-17.35	-8.23	165.48	-67.87	173.71	182.83	0.9501	0.9501	1.5044	2	50.52	59.64	0.8471	0.8471	1.5546	2	-0.912	1
012L	-63.66	-86.05	11.45	-110.12	97.5	75.11	1.2981	1.0000	1.0512	1	46.46	24.07	1.9302	1.0000	0.9531	1	2.239	0
012R	-57.52	-80.1	11.45	-109.62	91.55	68.97	1.3274	1.0000	1.0512	1	52.1	29.52	1.7649	1.0000	0.9531	1	2.258	0
018L	32.27	11.48	212.65	-34.06	201.17	180.38	1.1153	1.0000	1.0512	1	66.33	45.54	1.4565	1.0000	0.9531	1	2.079	0
018R	32.65	16.13	212.65	-32.97	196.52	180	1.0918	1.0000	1.0512	1	65.62	49.1	1.3365	1.0000	0.9531	1	1.652	0
022L	69.74	79.85	251.09	13.54	171.24	181.35	0.9443	0.9443	1.5577	2	56.2	66.31	0.8475	0.8475	1.5528	2	-1.011	2
022R	85.87	40.61	251.09	27.63	210.48	165.22	1.2739	1.0000	1.0512	1	58.24	12.98	4.4869	1.0000	0.9531	1	4.526	0
023L	68.74	79.85	251.09	13.54	171.24	182.35	0.9391	0.9391	1.6048	2	55.2	66.31	0.8325	0.8325	1.6121	2	-1.111	2
023R	85.87	40.61	251.09	27.63	210.48	165.22	1.2739	1.0000	1.0512	1	58.24	12.98	4.4869	1.0000	0.9531	1	4.526	0
027R	34.18	49.7	269.32	4.42	219.62	235.14	0.9340	0.9340	1.6509	2	29.76	45.28	0.6572	0.6572	2.3013	2	-1.552	2
047L	-19.27	-5.76	214.05	-68.41	219.81	233.32	0.9421	0.9421	1.5773	2	49.14	62.65	0.7844	0.7844	1.8013	2	-1.351	2
047R	1.17	12.13	214.05	-64.97	201.92	212.88	0.9485	0.9485	1.5190	2	66.14	77.1	0.8578	0.8578	1.5122	2	-1.096	2
049R	62.06	47.7	214.19	9.56	166.49	152.13	1.0944	1.0000	1.0512	1	52.5	38.14	1.3765	1.0000	0.9531	1	1.436	0
056L	52.22	92.22	299.54	-10.41	207.32	247.32	0.8383	0.8383	2.5207	3	62.63	102.63	0.6103	0.6103	2.4861	2	-4	3
057R	-1.47	24.5	245.44	-45.32	220.94	246.91	0.8948	0.8948	2.0068	2	43.85	69.82	0.6280	0.6280	2.4161	2	-2.597	2
060L	1.26	15.95	231.57	-48.48	215.62	230.31	0.9362	0.9362	1.6307	2	49.74	64.43	0.7720	0.7720	1.8499	2	-1.469	2
069R	53.91	63.56	241.23	-1.75	177.67	187.32	0.9485	0.9485	1.5193	2	55.66	65.31	0.8522	0.8522	1.5343	2	-0.965	1
070R	-11.73	7.41	214.45	-56.2	207.04	226.18	0.9154	0.9154	1.8201	2	44.47	63.61	0.6991	0.6991	2.1366	2	-1.914	2
075R	-7.86	9.59	241.96	-53.05	232.37	249.82	0.9301	0.9301	1.6858	2	45.19	62.64	0.7214	0.7214	2.0488	2	-1.745	2
082L	-24.6	-10.12	176.79	-72.21	186.91	201.39	0.9281	0.9281	1.7045	2	47.61	62.09	0.7668	0.7668	1.8704	2	-1.448	2
086L	-10.59	4.39	246.75	-61.76	242.36	257.34	0.9418	0.9418	1.5801	2	51.17	66.15	0.7735	0.7735	1.8438	2	-1.498	2
094R	27.45	63.18	241.84	-38.54	178.66	214.39	0.8333	0.8333	2.5654	3	65.99	101.72	0.6487	0.6487	2.3347	2	-3.573	3
095R	82.33	92.34	275.06	41.77	182.72	192.73	0.9481	0.9481	1.5231	2	40.56	50.57	0.8021	0.8021	1.7317	2	-1.001	2
098R	26.77	37.2	217.46	-31.03	180.26	190.69	0.9453	0.9453	1.5482	2	57.8	68.23	0.8471	0.8471	1.5544	2	-1.043	2
124R	102.88	53.33	256.85	23.38	203.52	153.97	1.3218	1.0000	1.0512	1	79.5	29.95	2.6544	1.0000	0.9531	1	4.955	0
133L	12.95	24.81	244.52	-28.03	219.71	231.57	0.9488	0.9488	1.5165	2	40.98	52.84	0.7755	0.7755	1.8359	2	-1.186	2
133R	21.61	33.87	244.52	-22.2	210.65	222.91	0.9450	0.9450	1.5509	2	43.81	56.07	0.7813	0.7813	1.8131	2	-1.226	2
163R	9.79	-6.89	192.04	60.11	198.93	182.25	1.0915	1.0000	1.0512	1	-50.32	-67	0.7510	0.7510	1.9323	2	1.668	0
181L	53.97	21.64	235.01	-15.2	213.37	181.04	1.1786	1.0000	1.0512	1	69.17	36.84	1.8776	1.0000	0.9531	1	3.233	0
184L	85.08	96.42	314.57	17.93	218.15	229.49	0.9506	0.9506	1.5002	2	67.15	78.49	0.8555	0.8555	1.5214	2	-1.134	2
190L	15.68	25.71	209.98	-29.24	184.27	194.3	0.9484	0.9484	1.5202	2	44.92	54.95	0.8175	0.8175	1.6710	2	-1.003	2
197R	2.51	-22.38	196.81	-52.2	219.19	194.3	1.1281	1.0000	1.0512	1	54.71	29.82	1.8347	1.0000	0.9531	1	2.489	0
199L	-23.55	-11.04	172.01	-69.17	183.05	195.56	0.9360	0.9360	1.6324	2	45.62	58.13	0.7848	0.7848	1.7996	2	-1.251	2
200R	120.03	131.98	283.89	73.13	151.91	163.86	0.9271	0.9271	1.7138	2	46.9	58.85	0.7969	0.7969	1.7518	2	-1.195	2
203R	-85.92	-67.79	122.94	-144.81	190.73	208.86	0.9132	0.9132	1.8399	2	58.89	77.02	0.7646	0.7646	1.8790	2	-1.813	2
204R	76.02	58.93	276	10.29	217.07	199.98	1.0855	1.0000	1.0512	1	65.73	48.64	1.3514	1.0000	0.9531	1	1.709	0
209R	-35.87	-23.24	164.05	-90.12	187.29	199.92	0.9368	0.9368	1.6252	2	54.25	66.88	0.8112	0.8112	1.6959	2	-1.263	2
210L	78.53	89.26	287.49	39.39	198.23	208.96	0.9487	0.9487	1.5178	2	39.14	49.87	0.7848	0.7848	1.7994	2	-1.073	2

Table C.3: Distance measurements on Grade 1 (continued).

Patient	N	I	s	v	s-i	s-n	s-i/s-n	round	M-1	p1	n-v	i-v	n-v/i-v	r2	M-2	p2	n-i	p3
219L	-79.4	-65.81	143.52	-126.97	209.33	222.92	0.9390	0.9390	1.6051	2	47.57	61.16	0.7778	0.7778	1.8271	2	-1.359	2
507L	-7.06	15.76	203.71	-68.66	187.95	210.77	0.8917	0.8917	2.0349	2	61.6	84.42	0.7297	0.7297	2.0163	2	-2.282	2
507R	-20.05	-39.77	203.71	91.69	243.48	223.76	1.0881	1.0000	1.0512	1	-111.74	-131.46	0.8500	0.8500	1.5431	2	1.972	0
509R	-193.43	-176.43	117.53	-230.56	293.96	310.96	0.9453	0.9453	1.5479	2	37.13	54.13	0.6859	0.6859	2.1884	2	-1.7	2
511R	220.71	202.47	393.12	154	190.65	172.41	1.1058	1.0000	1.0512	1	66.71	48.47	1.3763	1.0000	0.9531	1	1.824	0
512R	-89.88	-102.08	95.18	-139.07	197.26	185.06	1.0659	1.0000	1.0512	1	49.19	36.99	1.3298	1.0000	0.9531	1	1.22	0
514L	-76.06	-114.8	92.63	-143.51	207.43	168.69	1.2297	1.0000	1.0512	1	67.45	28.71	2.3494	1.0000	0.9531	1	3.874	0
515L	120.16	105.33	291.06	-72.35	185.73	170.9	1.0868	1.0000	1.0512	1	192.51	177.68	1.0835	1.0000	0.9531	1	1.483	0
515R	97.05	109.23	291.06	53.96	181.83	194.01	0.9372	0.9372	1.6216	2	43.09	55.27	0.7796	0.7796	1.8199	2	-1.218	2
516L	-21.93	-45.04	201.83	-89.16	246.87	223.76	1.1033	1.0000	1.0512	1	67.23	44.12	1.5238	1.0000	0.9531	1	2.311	0
516R	-33.06	-20.14	201.83	-73.59	221.97	234.89	0.9450	0.9450	1.5510	2	40.53	53.45	0.7583	0.7583	1.9039	2	-1.292	2
517L	-7.1	-60.29	183.9	-105.51	244.19	191	1.2785	1.0000	1.0512	1	98.41	45.22	2.1762	1.0000	0.9531	1	5.319	0
517R	-2.19	-50.04	183.9	-100.96	233.94	186.09	1.2571	1.0000	1.0512	1	98.77	50.92	1.9397	1.0000	0.9531	1	4.785	0
521L	-78.41	-98.92	87.84	-130.86	186.76	166.25	1.1234	1.0000	1.0512	1	52.45	31.94	1.6421	1.0000	0.9531	1	2.051	0
522R	25.92	37.13	212.62	-9.37	175.49	186.7	0.9400	0.9400	1.5967	2	35.29	46.5	0.7589	0.7589	1.9013	2	-1.121	2
523R	-73.58	-59.75	197.02	-121.27	256.77	270.6	0.9489	0.9489	1.5156	2	47.69	61.52	0.7752	0.7752	1.8373	2	-1.383	2
527L	188.45	109.09	310.51	55.75	201.42	122.06	1.6502	1.0000	1.0512	1	132.7	53.34	2.4878	1.0000	0.9531	1	7.936	0
527R	94.54	121.42	310.51	43.52	189.09	215.97	0.8755	0.8755	2.1820	2	51.02	77.9	0.6549	0.6549	2.3103	2	-2.688	2
534L	-119.78	-144.03	90.07	-175.18	234.1	209.85	1.1156	1.0000	1.0512	1	55.4	31.15	1.7785	1.0000	0.9531	1	2.425	0
539R	50.43	55.06	241.23	40.75	186.17	190.8	0.9757	0.9757	1.2717	1	9.68	14.31	0.6765	0.6765	2.2257	2	-0.463	1
540L	-8.56	5.75	204.94	-43.15	199.19	213.5	0.9330	0.9330	1.6602	2	34.59	48.9	0.7074	0.7074	2.1041	2	-1.431	2
541L	-19.56	-42.46	151.18	-74.97	193.64	170.74	1.1341	1.0000	1.0512	1	55.41	32.51	1.7044	1.0000	0.9531	1	2.29	0
541R	-58.79	-81.44	151.18	-112.15	232.62	209.97	1.1079	1.0000	1.0512	1	53.36	30.71	1.7375	1.0000	0.9531	1	2.265	0
543L	-63.39	-50.22	130.64	-111.4	180.86	194.03	0.9321	0.9321	1.6679	2	48.01	61.18	0.7847	0.7847	1.7998	2	-1.317	2
543R	-35.12	-22.1	130.64	-88.4	152.74	165.76	0.9215	0.9215	1.7649	2	53.28	66.3	0.8036	0.8036	1.7255	2	-1.302	2
574R	-72.69	-135.13	315.37	118.47	450.5	388.06	1.1609	1.0000	1.0512	1	-191.16	-253.6	0.7538	0.7538	1.9215	2	6.244	0
691L	115.68	66.56	261.95	36.44	195.39	146.27	1.3358	1.0000	1.0512	1	79.24	30.12	2.6308	1.0000	0.9531	1	4.912	0
691R	97.03	48.56	261.95	26.3	213.39	164.92	1.2939	1.0000	1.0512	1	70.73	22.26	3.1774	1.0000	0.9531	1	4.847	0
699R	44.47	24.65	225.67	-18.31	201.02	181.2	1.1094	1.0000	1.0512	1	62.78	42.96	1.4614	1.0000	0.9531	1	1.982	0
700L	139.98	105.69	322.24	80.96	216.55	182.26	1.1881	1.0000	1.0512	1	59.02	24.73	2.3866	1.0000	0.9531	1	3.429	0
703R	79.4	39.98	297.85	23.72	257.87	218.45	1.1805	1.0000	1.0512	1	55.68	16.26	3.4244	1.0000	0.9531	1	3.942	0
704L	26.81	-17.65	191.32	-33.35	208.97	164.51	1.2703	1.0000	1.0512	1	60.16	15.7	3.8318	1.0000	0.9531	1	4.446	0
710R	109.21	83.02	284.79	56.69	201.77	175.58	1.1492	1.0000	1.0512	1	52.52	26.33	1.9947	1.0000	0.9531	1	2.619	0
711L	58.42	14.22	244.89	-3.1	230.67	186.47	1.2370	1.0000	1.0512	1	61.52	17.32	3.5520	1.0000	0.9531	1	4.42	0
713L	88.88	54.5	277.46	26.9	222.96	188.58	1.1823	1.0000	1.0512	1	61.98	27.6	2.2457	1.0000	0.9531	1	3.438	0
713R	89.35	60.23	277.46	17.01	217.23	188.11	1.1548	1.0000	1.0512	1	72.34	43.22	1.6738	1.0000	0.9531	1	2.912	0
717R	85.83	45.24	258.03	23.87	212.79	172.2	1.2357	1.0000	1.0512	1	61.96	21.37	2.8994	1.0000	0.9531	1	4.059	0

Table C.4: Distance measurements on Grade 2.

Patient	N	I	s	v	s-i	s-n	s-i/s-n	round	M-1	p1	n-v	i-v	n-v/i-v	r2	M-2	p2	n-i	p3
002L	-85.61	-59.91	170.04	-113	229.95	255.65	0.8995	0.8995	1.9646	2	27.39	53.09	0.5159	0.5159	2.8571	3	-2.57	2
010L	-103.78	-90.1	163.83	-131.05	253.93	267.61	0.9489	0.9489	1.5157	2	27.27	40.95	0.6659	0.6659	2.2671	2	-1.368	2
026L	-29.43	4.9	236.56	-77.66	231.66	265.99	0.8709	0.8709	2.2239	2	48.23	82.56	0.5842	0.5842	2.5886	3	-3.433	3
029L	-3.35	6.46	182.72	-37.15	176.26	186.07	0.9473	0.9473	1.5302	2	33.8	43.61	0.7751	0.7751	1.8379	2	-0.981	1
065L	-42.22	-15.78	220.3	-85.93	236.08	262.52	0.8993	0.8993	1.9663	2	43.71	70.15	0.6231	0.6231	2.4356	2	-2.644	2
066L	48.29	71.56	286.16	11.2	214.6	237.87	0.9022	0.9022	1.9400	2	37.09	60.36	0.6145	0.6145	2.4695	2	-2.327	2
189L	52.37	66.52	252.67	-5.38	186.15	200.3	0.9294	0.9294	1.6931	2	57.75	71.9	0.8032	0.8032	1.7272	2	-1.415	2
208L	-40.62	-55.33	164.05	-99.01	219.38	204.67	1.0719	1.0000	1.0512	1	58.39	43.68	1.3368	1.0000	0.9531	1	1.471	0
214R	-39.89	-28.08	184.39	-90.87	212.47	224.28	0.9473	0.9473	1.5296	2	50.98	62.79	0.8119	0.8119	1.6929	2	-1.181	2
216L	-19.27	-37.13	157.39	-69.62	194.52	176.66	1.1011	1.0000	1.0512	1	50.35	32.49	1.5497	1.0000	0.9531	1	1.786	0
219R	-96.71	-80.56	143.52	-141.84	224.08	240.23	0.9328	0.9328	1.6620	2	45.13	61.28	0.7365	0.7365	1.9897	2	-1.615	2
506L	-109.28	-90.47	117.32	-152.31	207.79	226.6	0.9170	0.9170	1.8054	2	43.03	61.84	0.6958	0.6958	2.1495	2	-1.881	2
509L	-141.16	-127.25	117.53	-199.32	244.78	258.69	0.9462	0.9462	1.5398	2	58.16	72.07	0.8070	0.8070	1.7123	2	-1.391	2
518L	-56.57	-89.1	104.84	-109.23	193.94	161.41	1.2015	1.0000	1.0512	1	52.66	20.13	2.6160	1.0000	0.9531	1	3.253	0
518R	-64.92	-105.86	104.84	-123.86	210.7	169.76	1.2412	1.0000	1.0512	1	58.94	18	3.2744	1.0000	0.9531	1	4.094	0
520L	-159.35	-126.9	99.96	-196.24	226.86	259.31	0.8749	0.8749	2.1882	2	36.89	69.34	0.5320	0.5320	2.7938	3	-3.245	3
520R	-149.55	-113.59	99.96	-196.64	213.55	249.51	0.8559	0.8559	2.3607	2	47.09	83.05	0.5670	0.5670	2.6562	3	-3.596	3
522L	10.38	26.22	212.62	-22.36	186.4	202.24	0.9217	0.9217	1.7628	2	32.74	48.58	0.6739	0.6739	2.2356	2	-1.584	2
525L	-44.72	-21.07	251.24	-110.12	272.31	295.96	0.9201	0.9201	1.7772	2	65.4	89.05	0.7344	0.7344	1.9977	2	-2.365	2
526R	-135.07	-97.86	129.61	-188.5	227.47	264.68	0.8594	0.8594	2.3285	2	53.43	90.64	0.5895	0.5895	2.5678	3	-3.721	3
530R	-133.39	-115.64	112.88	-192.05	228.52	246.27	0.9279	0.9279	1.7061	2	58.66	76.41	0.7677	0.7677	1.8668	2	-1.775	2
532L	31.78	43.9	270.17	-7.1	226.27	238.39	0.9492	0.9492	1.5131	2	38.88	51	0.7624	0.7624	1.8878	2	-1.212	2
532R	8.73	39.68	270.17	-14.78	230.49	261.44	0.8816	0.8816	2.1268	2	23.51	54.46	0.4317	0.4317	3.1884	3	-3.095	3
533L	-75.83	-60.95	139.25	-139.74	200.2	215.08	0.9308	0.9308	1.6798	2	63.91	78.79	0.8111	0.8111	1.6959	2	-1.488	2
533R	-98.52	-119.96	139.25	-161.72	259.21	237.77	1.0902	1.0000	1.0512	1	63.2	41.76	1.5134	1.0000	0.9531	1	2.144	0
536L	-82	-109.01	106.45	-139.35	215.46	188.45	1.1433	1.0000	1.0512	1	57.35	30.34	1.8902	1.0000	0.9531	1	2.701	0
536R	-100.02	-132.78	106.45	-152.89	239.23	206.47	1.1587	1.0000	1.0512	1	52.87	20.11	2.6290	1.0000	0.9531	1	3.276	0
537R	107.7	91.23	264.47	56.29	173.24	156.77	1.1051	1.0000	1.0512	1	51.41	34.94	1.4714	1.0000	0.9531	1	1.647	0
539L	44.42	59.01	241.23	-4.56	182.22	196.81	0.9259	0.9259	1.7248	2	48.98	63.57	0.7705	0.7705	1.8558	2	-1.459	2
546L	57.41	69.22	248.49	10.24	179.27	191.08	0.9382	0.9382	1.6128	2	47.17	58.98	0.7998	0.7998	1.7407	2	-1.181	2
546R	28.59	46.46	248.49	-4.47	202.03	219.9	0.9187	0.9187	1.7896	2	33.06	50.93	0.6491	0.6491	2.3332	2	-1.787	2
689R	10.32	-15.22	220.97	-44.87	236.19	210.65	1.1212	1.0000	1.0512	1	55.19	29.65	1.8614	1.0000	0.9531	1	2.554	0
692L	79.82	89.71	266.33	33.45	176.62	186.51	0.9470	0.9470	1.5330	2	46.37	56.26	0.8242	0.8242	1.6445	2	-0.989	1
694L	57.4	31.61	209.42	7.45	177.81	152.02	1.1696	1.0000	1.0512	1	49.95	24.16	2.0675	1.0000	0.9531	1	2.579	0
701R	118.62	62.28	311.2	36.05	248.92	192.58	1.2926	1.0000	1.0512	1	82.57	26.23	3.1479	1.0000	0.9531	1	5.634	0

Table C.5: Distance measurements on Grade 3.

Patient	N	I	s	v	s-i	s-n	s-i/s-n	round	M-1	p1	n-v	i-v	n-v/i-v	r2	M-2	p2	n-i	p3
177L	53.29	71.56	286.16	11.2	214.6	232.87	0.9215	0.9215	1.7640	2	42.09	60.36	0.6973	0.6973	2.1436	2	-1.827	2
177R	64.28	75.01	286.16	-3.01	211.15	221.88	0.9516	0.9516	1.4906	1	67.29	78.02	0.8625	0.8625	1.4940	1	-1.073	2
206L	-12.1	20.8	244.83	-71.81	224.03	256.93	0.8719	0.8719	2.2146	2	59.71	92.61	0.6447	0.6447	2.3504	2	-3.29	3
207L	-52.94	13.57	199.56	-48.4	185.99	252.5	0.7366	0.7366	3.4445	3	-4.54	61.97	-0.0733	-0.0733	5.1746	3	-6.651	3
212L	-96.99	-65.5	119.2	-153.87	184.7	216.19	0.8543	0.8543	2.3746	2	56.88	88.37	0.6437	0.6437	2.3547	2	-3.149	3
215L	-78.93	-75.79	137.34	-105.1	213.13	216.27	0.9855	0.9855	1.1831	1	26.17	29.31	0.8929	0.8929	1.3745	1	-0.314	1
215R	-66.64	-66.32	137.34	-101.64	203.66	203.98	0.9984	0.9984	1.0655	1	35	35.32	0.9909	0.9909	0.9887	1	-0.032	1
513L	-149.12	-118.29	128.32	-220.95	246.61	277.44	0.8889	0.8889	2.0608	2	71.83	102.66	0.6997	0.6997	2.1343	2	-3.083	3
513R	-105.75	-85.78	128.32	-146.37	214.1	234.07	0.9147	0.9147	1.8264	2	40.62	60.59	0.6704	0.6704	2.2495	2	-1.997	2
519L	-176.23	-160.78	33.71	-210.87	194.49	209.94	0.9264	0.9264	1.7198	2	34.64	50.09	0.6916	0.6916	2.1663	2	-1.545	2
519R	-181.8	-169.06	33.71	-211.18	202.77	215.51	0.9409	0.9409	1.5883	2	29.38	42.12	0.6975	0.6975	2.1428	2	-1.274	2
526L	-19.33	-88.73	129.61	-229.47	218.34	148.94	1.4660	1.0000	1.0512	1	210.14	140.74	1.4931	1.0000	0.9531	1	6.94	0
52R	-97.23	15.04	297.57	-99.76	282.53	394.8	0.7156	0.7156	3.6349	3	2.53	114.8	0.0220	0.0220	4.7997	3	-11.227	3
534R	-162.73	-134.59	90.07	-206.36	224.66	252.8	0.8887	0.8887	2.0626	2	43.63	71.77	0.6079	0.6079	2.4953	2	-2.814	2
538L	70.67	102	322.85	20.38	220.85	252.18	0.8758	0.8758	2.1800	2	50.29	81.62	0.6161	0.6161	2.4629	2	-3.133	3
538R	69.58	52.19	322.85	36.26	270.66	253.27	1.0687	1.0000	1.0512	1	33.32	15.93	2.0917	1.0000	0.9531	1	1.739	0
547L	-111.21	-110.01	105.95	-149.91	215.96	217.16	0.9945	0.9945	1.1014	1	38.7	39.9	0.9699	0.9699	1.0714	1	-0.12	1
547R	-104.58	-97.86	105.95	-141.44	203.81	210.53	0.9681	0.9681	1.3412	1	36.86	43.58	0.8458	0.8458	1.5596	2	-0.672	1
549R	-53.58	2.29	200.93	-79.07	198.64	254.51	0.7805	0.7805	3.0457	3	25.49	81.36	0.3133	0.3133	3.6541	3	-5.587	3
62R	-72.68	-26.07	212.51	-98.94	238.58	285.19	0.8366	0.8366	2.5361	3	26.26	72.87	0.3604	0.3604	3.4690	3	-4.661	3
697L	-76.6	-68.85	210.85	-128.49	279.7	287.45	0.9730	0.9730	1.2962	1	51.89	59.64	0.8701	0.8701	1.4642	1	-0.775	1
712L	-53.33	-42.87	208.97	-78	251.84	262.3	0.9601	0.9601	1.4135	1	24.67	35.13	0.7022	0.7022	2.1242	2	-1.046	2

Table C.6: Distance measurements.

Grade	Patient	n	i	s	v	s-i	s-n	s-i/s-n	M1	n-v	i-v	n-v/i-v	M2
0	kit-r	243.31	148.77	342.22	120.36	191	164	1.1646	1.0000	122.95	28.41	4.3277	1.0000
0	kit-l	237.74	145.51	342.22	120.36	196.71	104.48	1.8828	1.0000	117.38	25.15	4.6672	1.0000
0	model-03 r	58.36	-15.89	141.21	-20.11	157.1	82.85	1.8962	1.0000	78.47	4.22	18.5948	1.0000
0	model-03 l	60	-18.36	141.21	-20.11	159.57	81.21	1.9649	1.0000	80.11	1.75	45.7771	1.0000
0	p134-r	83.14	57.25	270.5	8.14	213.25	187.36	1.1382	1.0000	75	49.11	1.5272	1.0000
0	p140-l	41	57.92	192.09	-2.16	134.17	151.09	0.8880	0.8880	43.16	60.08	0.7184	0.7184
0	p148-r	71.36	45.99	248.94	5.05	202.95	177.58	1.1429	1.0000	66.31	40.94	1.6197	1.0000
0	p148-l	89.52	63.88	248.94	17.97	185.06	159.42	1.1608	1.0000	71.55	45.91	1.5585	1.0000
0	p161-r	11.08	26.42	220	-14.09	193.58	208.92	0.9266	0.9266	25.17	40.51	0.6213	0.6213
0	p156-l	25.66	-2.33	200.29	-39.52	202.62	174.63	1.1603	1.0000	65.18	37.19	1.7526	1.0000
0	p173-r	50.56	44.93	219.11	13.74	174.18	168.55	1.0334	1.0000	36.82	31.19	1.1805	1.0000
0	p173-l	55.91	55.51	219.11	16.51	163.6	163.2	1.0025	1.0000	39.4	39	1.0103	1.0000
0	p126-r	22.86	32.64	218.08	8.13	185.44	195.22	0.9499	0.9499	14.73	24.51	0.6010	0.6010
0	p126-l	8.22	27.57	218.08	-8.51	190.51	209.86	0.9078	0.9078	16.73	36.08	0.4637	0.4637
0	p145-l	-68.1	-68.98	189.21	-45.94	258.19	257.31	1.0034	1.0000	-22.16	-23.04	0.9618	1.0000
0	p146-l	24.72	22.76	218.44	24.14	195.68	193.72	1.0101	1.0000	0.58	-1.38	1.4203	1.0000
1	model-01-l	101.53	44.68	199.34	-61.83	154.66	97.81	1.5812	1.0000	163.36	106.51	1.5338	1.0000
1	model-02-l	31.72	-18.5	142.25	-59.24	160.75	110.53	1.4544	1.0000	90.96	40.74	2.2327	1.0000
1	model-04-r	29.87	-27.44	193.86	-53.68	221.3	163.99	1.3495	1.0000	83.55	26.24	3.1841	1.0000
1	p117-r	-41.46	-26.44	214.54	-6.2	240.98	256	0.9413	0.9413	-35.26	-20.24	0.9135	0.9135
1	p119-l	9.58	67.5	250.6	23.17	183.1	241.02	0.7597	0.7597	-13.59	44.33	0.7835	0.7835
1	p119-r	-10.84	29.33	250.6	-2.97	221.27	261.44	0.8464	0.8464	-7.87	32.3	0.8248	0.8248
1	p120-r	23.03	47.68	261.39	34.66	213.71	238.36	0.8966	0.8966	-11.63	13.02	0.9005	0.9005
1	p125-r	7.29	35.9	243.06	-3.08	207.16	235.77	0.8787	0.8787	10.37	38.98	0.8787	0.8787
1	p127-l	-20.63	9.47	252.67	29.65	243.2	273.3	0.8899	0.8899	-50.28	-20.18	0.8563	0.8563
1	p127-r	-17.7	15.83	252.67	42.5	236.84	270.37	0.8760	0.8760	-60.2	-26.67	0.8446	0.8446
1	p128-l	-113.43	-84.43	175.97	-96.31	260.4	289.4	0.8998	0.8998	-17.12	11.88	0.7491	0.7491
1	p128-r	-112.68	-81.17	175.97	-98.95	257.14	288.65	0.8908	0.8908	-13.73	17.78	0.7348	0.7348
1	p104-r	-10.82	28.7	233.43	-8.8	204.73	244.25	0.8382	0.8382	-2.02	37.5	0.8272	0.8272
1	p105-r	-20.03	17.15	228.88	-8.4	211.73	248.91	0.8506	0.8506	-11.63	25.55	0.8288	0.8288
1	p110-l	-87.78	-45.8	176.68	-54.84	222.48	264.46	0.8413	0.8413	-32.94	9.04	0.7278	0.7278

Table C.7: Distance measurements (continued).

Grade	Patient	n	i	s	v	s-i	s-n	s-i/s-n	M1	n-v	i-v	n-v/i-v	M2
2	107-l	-63.23	-13.06	195.38	-58.53	208.44	258.61	0.8060	0.8060	-4.7	45.47	0.7316	0.7316
2	155-r	-52.13	22.87	200.68	-65.66	177.81	252.81	0.7033	0.7033	13.53	88.53	0.6635	0.6635
2	157-l	-12.15	29.64	214.11	13.09	184.47	226.26	0.8153	0.8153	-25.24	16.55	0.8180	0.8180
2	158-l	-26.79	37.78	234.3	-25.94	196.52	261.09	0.7527	0.7527	-0.85	63.72	0.7284	0.7284
2	176-l	-44.03	27.74	238.95	-44.74	211.21	282.98	0.7464	0.7464	0.71	-183.47	0.6849	0.6849
2	176-r	-57.14	13.78	238.95	-55.54	225.17	296.09	0.7605	0.7605	-12.4	58.52	0.6683	0.6683
2	179-r	-37.58	35.26	265.33	-14.47	230.07	302.91	0.7595	0.7595	17.96	90.8	0.6904	0.6904
2	525-l	-78.69	-63.97	218.55	-130.44	282.52	297.24	0.9505	0.9505	51.75	66.47	0.8918	0.8918
2	689-r	10.32	-15.22	220.97	-44.87	236.19	210.65	1.1212	1.0000	55.19	29.65	1.8614	1.0000
2	692-l	82.83	79.57	322.43	65.7	242.86	239.6	1.0136	1.0000	17.13	13.87	1.2350	1.0000
2	694-l	60.17	57.85	196.77	7.45	138.92	136.6	1.0170	1.0000	52.72	50.4	1.0460	1.0000
2	701-r	118.62	62.28	311.2	36.05	248.92	192.58	1.2926	1.0000	82.57	26.23	3.1479	1.0000
2	105-l	21.34	59.35	228.88	-23.36	169.53	207.54	0.8169	0.8169	44.7	82.71	0.8534	0.8534
2	model01-r	-37.08	-14.72	199.34	-61.83	214.06	236.42	0.9054	0.9054	24.75	47.11	0.8793	0.8793
2	model02-r	-41.16	-32.03	142.25	-59.24	174.28	183.41	0.9502	0.9502	18.08	27.21	0.9456	0.9456
2	model04-l	-24.62	-10.49	193.86	-53.68	204.35	218.48	0.9353	0.9353	29.06	43.19	0.9254	0.9254
3	108-l	-111.56	17.24	244.69	-78.04	227.45	356.25	0.6385	0.6385	38.78	95.28	0.4071	0.4071

Appendix D

Patient Information

Table D.1: Patient information.

Patient	Age	Race	Ethnicity	BMI
2	n.a.	White	Not_Hispanic_Latino	28
3	55	White	n.a.	22.5
5	53	White	n.a.	32.5
6	39	White	n.a.	n.a.
7	54	White	n.a.	21.5
8	56	White	n.a.	27.5
9	38	White	n.a.	24.3
10	53	White	n.a.	37.1
12	56	White	Hispanic_Latino	27.3
13	40	White	n.a.	20.4
16	47	White	n.a.	20.7
18	64	White	Hispanic_Latino	25.1
22	51	Black_AfricanAmerican	n.a.	29.5
23	40	Asian	n.a.	26.1
25	41	White	n.a.	22.2
26	53	White	n.a.	30.5
27	47	White	n.a.	33.6
29	42	White	n.a.	22.7
37	56	White	NotHispanic_Latino	27.3
46	36	White	NotHispanic_Latino	24.7
47	53	White	NotHispanic_Latino	35.3
49	42	White	Hispanic_Latino	27.5
52	n.a.	n.a.	n.a.	21.5
53	53	White	NotHispanic_Latino	23.1
55	53	White	NotHispanic_Latino	22
56	54	White	NotHispanic_Latino	25.9
57	63	White	NotHispanic_Latino	24.8
60	54	White	NotHispanic_Latino	32.1
62	n.a.	n.a.	n.a.	n.a.
65	53	White	Not_Hispanic_Latino	31
66	66	White	Not_Hispanic_Latino	27.6
67	50	White	Hispanic_Latino	23.4
69	50	White	NotHispanic_Latino	25.5
70	52	White	NotHispanic_Latino	39.6
73	41	White	NotHispanic_Latino	20.5
75	68	White	NotHispanic_Latino	33.5
76	43	White	Hispanic_Latino	20.6
78	40	White	NotHispanic_Latino	21.9
79	73	White	NotHispanic_Latino	28.9
82	59	White	NotHispanic_Latino	31.6
84	27	White	NotHispanic_Latino	23.4
86	53	White	NotHispanic_Latino	32.9
88	38	White	NotHispanic_Latino	33.1
89	66	White	NotHispanic_Latino	21.9
93	51	White	NotHispanic_Latino	22.2
94	48	White	NotHispanic_Latino	27.5
95	46	White	NotHispanic_Latino	25.2
96	37	Black_AfricanAmerican	NotHispanic_Latino	31.4
98	55	White	NotHispanic_Latino	30.6

Table D.1: Patient information (contínuted).

Patient	Age	Race	Ethnicity	BMI
113	54	White	NotHispanic_Latino	35.2
124	54	n.a.	n.a.	36.4
131	51	n.a.	NotHispanic_Latino	20.4
133	46	White	NotHispanic_Latino	34.4
135	51	White	NotHispanic_Latino	20.6
154	55	White	NotHispanic_Latino	30
160	n.a.	n.a.	n.a.	27.3
163	37	White	NotHispanic_Latino	26.2
175	37	White	NotHispanic_Latino	24.9
177	n.a.	n.a.	n.a.	n.a.
181	47	White	Hispanic_Latino	28.5
183	42	White	Hispanic_Latino	23.2
184	59	White	NotHispanic_Latino	28.7
186	48	Black_AfricanAmerican	n.a.	35.3
188	56	White	NotHispanic_Latino	34.5
189	n.a.	White	Hispanic_Latino	27.8
190	53	White	NotHispanic_Latino	27.6
192	46	White	NotHispanic_Latino	32.4
197	52	White	Hispanic_Latino	33.6
199	41	n.a.	n.a.	24.8
200	51	White	NotHispanic_Latino	21.7
201	38	n.a.	NotHispanic_Latino	19
203	55	White	NotHispanic_Latino	30.8
204	50	White	NotHispanic_Latino	25.9
205	57	White	NotHispanic_Latino	29
206	58	White	NotHispanic_Latino	n.a.
207	42	White	NotHispanic_Latino	n.a.
208	n.a.	n.a.	n.a.	n.a.
209	34	White	NotHispanic_Latino	n.a.
210	52	n.a.	n.a.	n.a.
211	53	Black_AfricanAmerican	NotHispanic_Latino	25.7
212	52	Black_AfricanAmerican	n.a.	38.4
214	40	White	Not_Hispanic_Latino	33.1
215	49	n.a.	Hispanic_Latino	n.a.
216	n.a.	n.a.	n.a.	n.a.
217	49	White	NotHispanic_Latino	28.2
219	50	White	NotHispanic_Latino	n.a.
220	52	White	NotHispanic_Latino	22.5
505	n.a.	n.a.	n.a.	24.2
506	n.a.	n.a.	n.a.	26
507	n.a.	n.a.	n.a.	n.a.
508	n.a.	n.a.	n.a.	n.a.
509	n.a.	n.a.	n.a.	n.a.
511	n.a.	n.a.	n.a.	n.a.
512	n.a.	n.a.	n.a.	n.a.
513	n.a.	n.a.	n.a.	n.a.
514	n.a.	n.a.	n.a.	n.a.
515	n.a.	n.a.	n.a.	n.a.
516	n.a.	n.a.	n.a.	n.a.
517	n.a.	n.a.	n.a.	n.a.
518	n.a.	n.a.	n.a.	31.2
519	n.a.	n.a.	n.a.	n.a.
520	n.a.	n.a.	n.a.	38.1
521	n.a.	n.a.	n.a.	n.a.
522	n.a.	n.a.	n.a.	n.a.

Table D.1: Patient information (continuted).

Patient	Age	Race	Ethnicity	BMI
523	n.a.	n.a.	n.a.	n.a.
525	n.a.	n.a.	n.a.	n.a.
526	n.a.	n.a.	n.a.	32.4
527	n.a.	n.a.	n.a.	n.a.
528	n.a.	n.a.	n.a.	22.4
529	n.a.	n.a.	n.a.	22.3
530	n.a.	n.a.	n.a.	30.6
532	n.a.	n.a.	n.a.	30.9
533	n.a.	n.a.	n.a.	31.8
534	n.a.	n.a.	n.a.	n.a.
535	n.a.	n.a.	n.a.	n.a.
536	n.a.	n.a.	n.a.	25.9
537	n.a.	n.a.	n.a.	34.6
538	n.a.	n.a.	n.a.	n.a.
539	n.a.	n.a.	n.a.	n.a.
540	n.a.	n.a.	n.a.	n.a.
541	n.a.	n.a.	n.a.	n.a.
542	n.a.	n.a.	n.a.	n.a.
543	n.a.	n.a.	n.a.	n.a.
546	n.a.	n.a.	n.a.	26.9
547	n.a.	n.a.	n.a.	n.a.
549	n.a.	n.a.	n.a.	40.3
554	n.a.	n.a.	n.a.	n.a.
574	n.a.	n.a.	n.a.	n.a.
689	n.a.	n.a.	n.a.	n.a.
691	n.a.	n.a.	n.a.	n.a.
692	n.a.	n.a.	n.a.	20.3
694	n.a.	n.a.	n.a.	28.2
697	n.a.	n.a.	n.a.	n.a.
699	n.a.	n.a.	n.a.	n.a.
700	n.a.	n.a.	n.a.	20.9
701	n.a.	n.a.	n.a.	n.a.
702	n.a.	n.a.	n.a.	n.a.
703	n.a.	n.a.	n.a.	n.a.
704	n.a.	n.a.	n.a.	n.a.
705	n.a.	n.a.	n.a.	n.a.
710	n.a.	n.a.	n.a.	n.a.
711	n.a.	n.a.	n.a.	n.a.
712	n.a.	n.a.	n.a.	n.a.
713	n.a.	n.a.	n.a.	n.a.
717	n.a.	n.a.	n.a.	n.a.